ISAS - INTERNATIONAL SCHOOL FOR ADVANCED STUDIES

Auxiliary Variables in Classical and Quantum Liquids

Thesis submitted for the degree of

"Doctor Philosophiæ"

CANDIDATE

Andrea Ferrante

SUPERVISORS

Prof. Stefano Fantoni

Prof. Mario P. Tosi

November 1992

TRIESTE

SISSA - SCUOLA INTERNAZIONALE SUPERIORE STUDI AVANZATI

TRIESTE

Strada Costiera 11

SISSA ISAS
SCUOLA INTERNAZIONALE SUPERIORE DI STUDI AVANZATI
INTERNATIONAL SCHOOL FOR ADVANCED STUDIES

Auxiliary Variables in Classical and Quantum Liquids

Thesis submitted for the degree of

"Doctor Philosophiæ"

CANDIDATE

Andrea Ferrante

SUPERVISORS

Prof. Stefano Fantoni

Prof. Mario P. Tosi

November 1992

Index

INTRODUCTION

This thesis consists of two parts: in the first a Bond Particle Model for the structural properties of group IV and III-V melts is presented and discussed; the second part deals with some properties of a variational wave function, the Shadow wave function, recently proposed to describe the ground state of ^{4}He both in the liquid and the solid phase, and describes some attempt to generalize it. The common theme between these apparently unrelated arguments consist in the usage of auxiliary degrees of freedom or "fictitious particles", employed as adiabatic variables to model a non simple classical liquid in the former case or integrated out in the construction of a wave function for a quantum system in the latter case. In both cases one aims to describe the solid and the liquid phases within the same framework (model or variational wavefunction); moreover one makes also use of the additional degrees of freedom to build up effective angular dependent many body-forces, in the former case, or to reproduce many body-correlations between He atoms without introducing them explicitly in the wave function in the latter. The physical meaning attached to these degrees of freedom is different in the two cases.

For group IV and III-V melts one wants to represent in a semiclassical way the process of "localization of electrons" in bonds(*)

with a "primitive model", in analogy to models developed for describing the lattice dynamics of the corresponding solids, and aims to model the effects of

(*) for a precise definition of the covalent bond in terms of charge density properties and for the quantitative meaning of phrases like "localization of electron pairs in covalent bond" the reader is referred to chap. 7 in R. F. W. Bader: *Atoms in Molecules* (Oxford University Press, Oxford (1990), pag. 332.

covalent bonding and the consequent association in the melts. The Bond Charge or Bond Particle represents that part of the valence charge density, residing in the region of a chemical bond, that can't be attached to any individual atom (and in a pictorial way represents pair of electrons in bonds although it is not only due to a defined electron pair [*]).

In the quantum case one obtains a pictorial representation of the shadow particles by the analogy with path integral simulations on ^4He, where the quantum particle is represented by a flexible ring made of classical beads and springs, and the shadow particle can be viewed as describing the center of mass for the beads distribution.

Extending the similarity between the two cases one can say that like Bond Particles represent in some sense the fermi hole attached to valence electrons (interaction between them being consequence of the fermi principle), and their localization in some region of space (different from an atom) is the signal of formation of chemical bond [*] with covalent character, in a similar manner Shadow Particles represent a sort of quantum correlation hole due to excluded volume effects, their position being the centre of an average excluded volume region for the quantum particles, due to the strong short range repulsion of the potential in the hamiltonian, and their localization in space on a regular lattice signalls the formation of a solid crystal.

For the reader's convenience we present here two short abstracts of content for the two parts, leaving the detailed exposition of the motivation of each work to the introduction of each part.

In the first part we studied by means of the integral equations of the theory of liquids the structural properties of a Bond Charge Model applied to liquid ger-

manium as a prototype case, and tested the accuracy of various approximations by comparison with the results of Monte Carlo simulations. In particular from the simulation we examined the angular correlations induced between Germanium Atoms, which we found in agreement with those obtained from ab-initio simulations. The HNC approximation, improved with the introduction of a suitable approximation for the elementary diagrams, is fairly accurate for the liquid region, and the structure resulting for the model is in semi-quantitative agreement with the experimental diffraction pattern for liquid Germanium near freezing. However this integral equations scheme fails in giving accurate results for the supercooled region, explored in connection to the structure of the amorphous phase.

In the second part we explore by means of Variational Monte Carlo simulations some issues related to a class of variational wave functions, the Shadow Wave Function of Kalos and Vitiello, namely to what extent this wave function reproduces three body-correlations between helium atoms, and the possibility of parametrizing the wave function in such a way to describe liquid-solid interfaces, without the need to fix by hand a one-body density profile or the shadow parameter b_s different in the two part of the interface. We present also integral equations for this class of wavefunctions.

Some generalizations of this wave function have also been explored. First, following a suggestion of Ceperley and Schmidt, we explored the effects of triplet correlations in the shadow part, finding that they don't contribute in a significant way to improve the wavefunction. On the other hand we generalized the original wave function in a different way, allowing each Helium atom to be correlated to any shadow, and we wrote down integral equations and Euler equations for the correlations. As optimization seemed to be difficult to perform through this way,

we tested this wave function in Variational Monte Carlo simulations, which didn' t gave us significant improvements, at least with the functional forms tried until now for the correlations. The problem of Shadow Wave Functions optimization in Monte Carlo simulations using correlated sampling (with and without reweighting) and variance reduction methods is also discussed.

PART ONE:

Bond Charge Models for

Semiconductor melts

Chapter 1

Introduction and overview

Simple models of interatomic forces have had an important role in advancing qualitative and quantitative understanding of condensed matter. In relation to properties of the liquid state, the fluids of neutral and charged hard spheres, the classical one-component plasma and the Lennard-Jones fluid have played such a role under two main aspects. Not only do they mimic classes of real fluids, but also provide simple test models for progress in statistical mechanics through joint theoretical and computer simulation studies.

Bond directionality and association are qualitative features of many real systems which are missing in the models mentioned above. It would be interesting to have a model of the same simplicity for describing structural properties of covalently bonded liquids and amorphous solids. We present in this work a simple primitive model showing both strong directional interactions and a variable degree of association in the liquid phase, model which is relevant for the study of the disordered phases of IV group elemental and III-V compound semiconductors.

Increasing attention has been given in recent years to the structure of covalently bonded systems in disordered states, from both the theoretical and the experimental point of view. A first class of systems extensively investigated is represented by a number of ionic or semiconducting compound materials of type AX_2 that share the common properties to be well-known glass formers: among them[1,2] BeF_2, $ZnCl_2$, GeO_2, SiO_2, $GeSe_2$, $SiSe_2$. On cooling from the melt at relatively moderate quench-rates, they can form a network-glass, that is an open

structure with tetrahedral local coordination around the A atom, which is stabilized by the presence of strong directional interactions. As a matter of fact all these compounds are known to form covalent bonds of more or less ionic character, that lead in the crystalline state to the formation of tetrahedral units of X atoms coordinated to one A atom. Such fourfold coordination can successfully be distinguished from others in the crystal structure classification built by Andreoni[3] for AX_2 compounds on the basis of quantal parameters of the component elements. The tetrahedral units can form an extended structure by connecting either by corner sharing or by edge sharing. This leads in the crystal state to the formation of 1D, 2D, or 3D regular networks respectively in the case of $SiSe_2$ (pure edge sharing), $GeSe_2$ (mixed edge and corner sharing), SiO_2 (pure corner sharing), and various allotropic crystalline forms distinguished by their medium range topology may also exist for a given compound (i.e. SiO_2). The glassy structure can be viewed as a disordered network of distorted tetrahedra, and an important point for its characterization is to understand how this units connect together to form an extended network, and what is the medium range topology that arises by their correlation. Interesting structural questions thus concern, the relative weight of corner and edge sharing, the "ring" statistics, and the presence of residual traces of low network dimensionality. From the experimental point of view the structure of the vitreous or amorphous state is reflected not only in static properties determined by elastic scattering experiments, but also in inelastic neutron scattering spectra[4], as well as in Raman scattering spectra[5]. As the information is not sufficient to fully characterize the structure as in the crystal states, models have been used to translate experimental results in structural terms.

The medium range order in these glasses is characterized by the presence of a first sharp diffraction peak (FSDP) in the total $S(k)$[2] in the range from 1.0 to 1.5

$\mathring{A}^{-1}$, peak due mainly to A-A correlations[6], and arising from the connectivity of tetrahedral units in the network. The FSDP is present, for some compounds, also in the Bathia-Thornton concentration-concentration structure factor $S_{cc}(k)$[7].

The corresponding liquids near melting (and in the supercooled states preceding the glass transition) are also thought to show a "network-like" structure, in the sense that quite a high degree of association between A and X atom is present, due to strong directional interactions, leading naturally to the picture of a percolating network of bonds, yet non-rigid, subjected to continuous bond breaking and bond forming processes. For compounds studied by scattering experiments in both the glassy and liquid state, as $ZnCl_2$[8,1] and $GeSe_2$[9,4,6], the diffraction pattern for the liquid phase clearly shows the same features as for the low temperature glass, including the FSDP that remains almost unchanged, while the other features show the expected thermal broadening.

A second class of covalent systems of current interest is represented by the amorphous phases of IV group and III-V compound semiconductors; they don't show any glass formation process when cooled from their melts at ordinary cooling rates and are currently prepared by various kind of deposition techniques[10]. The diffraction pattern of the liquid phase near freezing shows clear differences from that of their amorphous state; indeed melting at standard pressure brings elemental and polar III-V semiconductors from tetrahedrally coordinated open structures into metallic liquids having higher density than the solid and first-neighbour coordination number close to seven[11,12]. Their liquid structure is nevertheless quite distinct from that of other liquid metals[13]. Specifically a first-neighbour coordination number of order seven is still relatively low and the second shell of neighbours is closer to the first shell, in a region of interatomic separations where the pair distribution function g(r) has its main minimum for other liquid metals. Similarly

the liquid structure factor S(k) shows a distinctive shoulder on the large k-side of its main peak, merging into a single asymmetric broad peak with increasing temperature in the liquid phase. The FSDP observed in the amorphous state is no longer evident in the melt. Similar structural features have been observed in the total diffraction pattern from molten $GaAs$[14].

Like the systems in the previous class, these elements show in the liquid phase local density fluctuations around tetrahedral order, due to the tendency of atoms to associate in the melt through the formation of covalent bonds. The existence of these kind of fluctuations, with the persistence of some covalent bonding effect in metallic system like liquid Germanium or Silicon, was shown by a recent first-principles molecular dynamic simulation made on liquid Silicon[15], by means of the Car-Parrinello method that allows the simultaneous determination of structure and electronic properties. This simulation shows, from the analysis of charge density distributions, that temporary covalent bonds can indeed form in the liquid, the lifetime of the covalent bond being comparable to the characteristic time scale of lattice oscillations. Moreover it was observed that this process of forming and breaking bonds is characterized by a well defined tendency of density fluctuations towards local tetrahedral order.

A number of theoretical approaches have been presented in the recent literature to deal with the disordered states of the above mentioned systems. The basic approach represented by the Car-Parrinello method, combining density functional theory for the valence electrons with molecular dynamics for the ionic cores, has been applied to silicon[15], $GaAs$[16], and liquid carbon[17]. The metallic melts of elemental semiconductors have also been investigated by means of the conventional pseudo-atom approach used in the theory of metals[18,19].

A number of empirical approaches that include three-atom contributions in

the potential energy functions in addition to pair potentials have been proposed since the work of Stillinger and Weber on Silicon, (see ref.[20] and references therein) among which we mention that of Vashista on molten and glassy $GeSe_2$ and SiO_2[21], and that of Tersoff on Si and Ge[22]. These model potentials are tailored to describe a specific system by fitting their free parameters to properties of a specific phase, by means of MD test runs, and their success depend, on a certain extent, on the number of properties fitted and on which phase the fit was made.

Models of a certain simplicity that can be relevant to our subject arose in another context, in the statistical mechanical modelling of fluids with association, mainly in the treatment of network-like liquids. Wertheim developed an approach[23] to such fluids, modelling the elementary units as hard spheres with a fixed number of attraction sites attached on them. The directional interaction is mediated by forces between near-peripheral sites, that can interact only if the elementary units have the right relative orientation. This model was investigated mainly by means of Monte Carlo simulations[24]. Another model that has been used in studies of hydrogen bonding in water and methanol is due to Smith and Nezbeda[25], and is similar to Wertheim's scheme, with the variant that the near-peripheral sites now act attracting the center of another unit, not another site.

In this work we shall present a model able to take into account the peculiar density fluctuations towards local tetrahedral order that characterize the class of materials discussed above and distinguish their behaviour from simple liquid's one. We considered an extension to the melts of III - V and IV group semiconductors of the bond charge model adopted by Phillips[26] to give a picture of the non uniform charge density distribution in crystalline semiconductors and employed by Martin[27] and Weber[28,29] as a simple empirical model to account for the dynam-

ical properties of these materials. A primitive pseudoclassical model for the melt can be constructed by regarding it as a mixture of hard sphere atoms and pointlike bond particles, with mutual attractive interactions which can induce localization of bond particles between pairs of atoms under steric constraints limiting the coordination of an atom by bond particles to a maximum of four in tetrahedral configuration. The above model involves only pair potentials between components and thus it can be studied by means of the approximate integral equations of liquid state theory. A particular realization of this model has been examined in relation to liquid germanium, for which very accurate neutron scattering data are available[12]; we shall show that indeed it gives a semi-quantitative description of liquid germanium's structure near melting, and shows the correct trends of structural features on varying temperature[30]. Equilibrium supercooled states of the model were also investigated in this context, and their structure, as obtained by integral equations techniques, was contrasted with the results of diffraction experiments on amorphous germanium. The model presented here has also been employed by Badirkhan et al.[31] to study the freezing of liquid germanium in the framework of the density functional theory of freezing. We shall present here some empirical melting criteria for III - V semiconductors.

A considerable effort was devoted to test the accuracy of the integral equations techniques employed for the determination of the pair correlation functions for liquid and supercooled states, by comparison with accurate Monte Carlo simulations. The HNC approximation is insufficient for a reliable determination of the A-A correlations below the freezing temperature, and it was replaced by an improved scheme in which a crossover approximation to the elementary diagrams is employed. The short range part of these functions is described with an "universal" hard-sphere like behaviour, while the medium range part deviates from it.

This scheme requires the computation of the first elementary diagrams from the HNC pair correlation functions. The accuracy, the thermodynamic consistency of this scheme and the self consistency in the determined pair correlation functions were checked. This scheme is reliable in the region of model's parameter corresponding to the liquid phase, but become worse for the supercooled liquid, in which strong association takes place. Namely for temperature just below the melting point more effort is needed in determining the elementary diagrams, in that one uses the improved pair correlation functions to compute again the elementary diagrams and the pair correlation functions themselves, until self consistency is reached. Nonetheless the obtained structure is not in full agreement with the simulation and the situation is even worse for lower temperature were the self consistency in the determination of the elementary diagrams could not be obtained.

Chapter 2

Bond Charge Models

With the advent of density functional theory the one-body charge density plays a fundamental role in modern solid state physics and in chemistry. The energy and other properties of a many-body system, like a crystalline solid or a molecule, in its ground state can be determined in principle from the knowledge of its charge density distribution. Apart from ab-initio determination of this quantity, there are some approximate semi-empirical theories based on modelling the charge density of the system under study. Bond Charge Models (BCM)[26], which are based on the partition of the valence charge density into two parts, around atoms and in the bond region, have been employed in chemistry to study covalent bonds in molecules (see ref.[32] for references) and in solid state physics for modelling the lattice dynamics of semiconductors.

The electron density distribution in these materials is neither simply the superposition of spherical charge densities centered on the atoms as in purely ionic materials, nor almost uniformly distributed like in simple metals, but a certain amount of charge is accumulated in the covalent bond between adjacent atoms. This can be clearly seen from charge density plots of valence electrons for Ge and for $GaAs$ displayed in fig. 2.1, taken from band structure's calculation of Walter and Cohen[33]. Differential plots, in which the charge density of an "isolated" atom at each site is subtracted from the total charge density, clearly show that the bond charge is due to chemical bonding and not to simple superposition of individual charge densities[34]. This pileup of charge in bonds is responsible for

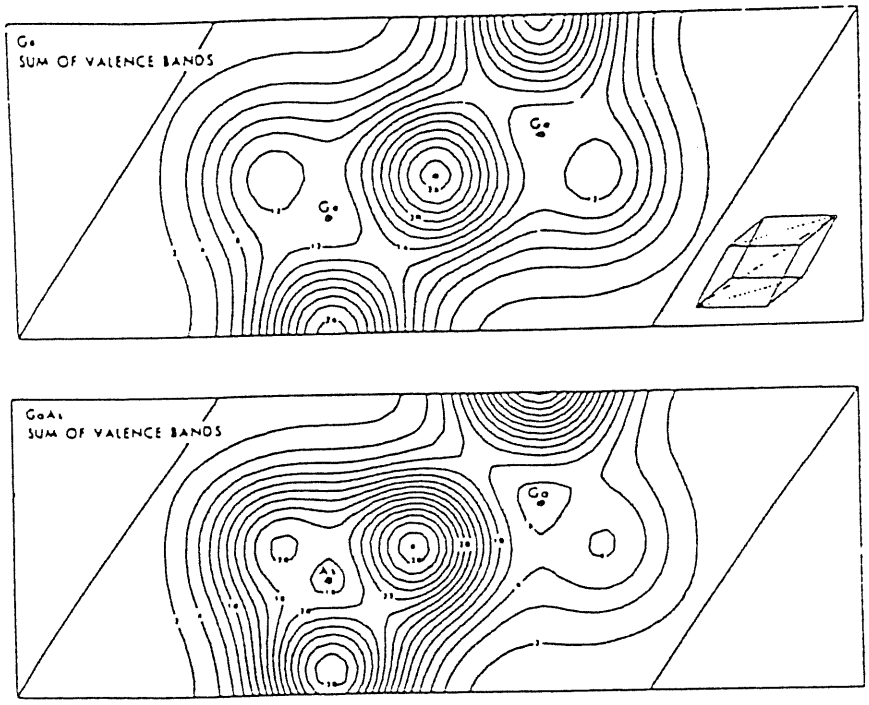

Figure 2.1
Total valence electron charge density (in units of the electronic charge, e) in the $(1\bar{1}0)$ plane, for crystalline Germanium (upper figure) and Gallium Arsenide (lower figure). The insert shows the direction of the plane in the unit cell. From Walter and Cohen, ref.[33].

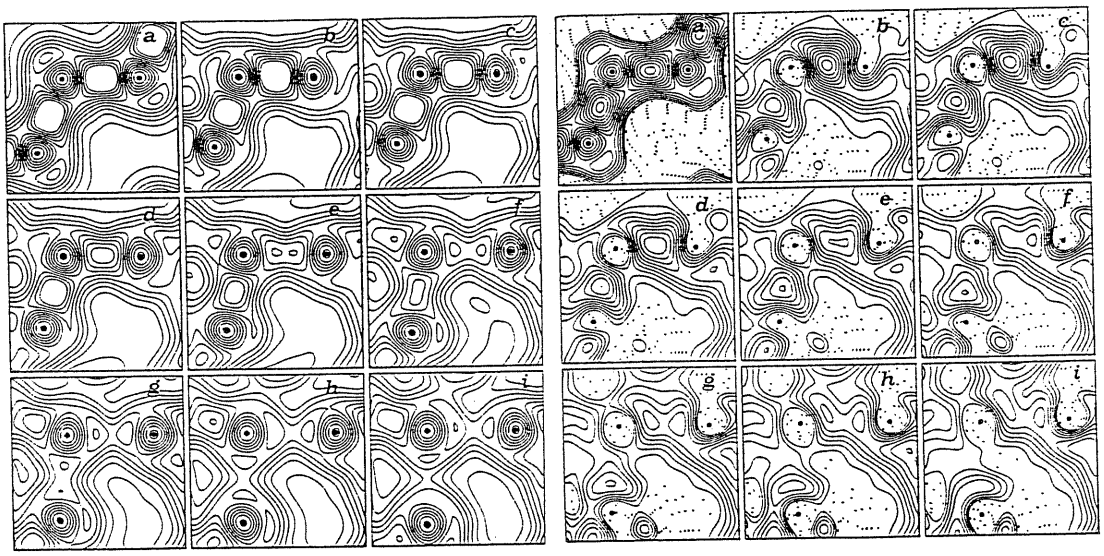

Figure 2.2
Contour plots of the valence electronic charge density $\rho_e(\mathbf{r})$ (left part) and difference charge density $\Delta\rho_e(\mathbf{r})$ between the self consistent density and the superposition of free atomic densities (right part). (a) c-Si in the (110) plane. (b)-(i) evolution in l-Si at time intervals of 5.5 10^{-3} psec, from the Car-Parrinello simulation of Stich et al., ref.[15].

the "forbidden" reflections observed, for instance, in X-ray scattering experiments on Si[35].

The bonding properties of liquid silicon near freezing were analyzed in ab-initio Car-Parrinello simulations by Stich[15], who found evidence that covalent bonding effects are present even in the melt. In figure 2.2, taken from ref.[15], we show contour plots of the valence electronic charge density (left part) and differential plots (as defined above, right part) which illustrate the evolution (b-f) of the electronic density for configurations in the liquid phase, taken in the MD-simulation at interval of 5.5 $10^{-}3$ ps; the crystalline configuration is also reproduced in (a) for reference. These plots clearly show the existence of transitory covalent bonds and local tetrahedral order in l-Si. Assigning a bond particle to each maximum in the electronic density, the authors also analyzed the pair correlations BP-BP and Si-BP. Persistence of transitory covalent bonding effects in the metallic liquid phase of Ge was also suggested by Ashcroft[19], on the basis of qualitative theoretical arguments.

In the first section of this chapter we review the application of BCM to the lattice dynamics of semiconductors. The next step in modelling has been to give bond charges the status of additional degrees of freedom, for the description of dynamical properties. The further step, described in the second section, was to extend the model to the liquid state for describing the process of "localization" of electron pairs in bonds. The last section deals about melting criteria for semiconductors.

2.1 BCM IN THE LATTICE DYNAMICS OF SEMICONDUCTORS

Phillip's idea at the basis of the BCM consists in parting the valence charge density of crystalline semiconductors in two contributions, a spherical charge density located at the atomic sites, and a point like charge located at the bond, halfway between nearest neighbour atoms in homopolar compounds. Figure 2.3 shows the diamond-type structure of crystalline Germanium after decoration of covalent bonds by bond particles.

As the band structure of Si and Ge is nearly-free-electron like, the bare ion-ion forces are expected to be screened by the charge distribution of valence electrons, and this screening is represented by the diagonal elements of the inverse dielectric matrix $\epsilon^{-1}(\mathbf{q}+\mathbf{G},\mathbf{q}+\mathbf{G}')$. But because of the finite gap between valence and conduction bands, the screening, unlike in metals, is incomplete giving rise to a finite but quite high value for the static dielectric constant ϵ_0 (16 for Ge and 12 for Si), and as a result there remains a residual screened charge of value $+4|e|/\epsilon_0$ at each ion. In order to preserve the charge neutrality, Phillips introduces charges of magnitude $-2|e|/\epsilon_0$ at the bond sites. These bond charges just represent the effect of the off diagonal elements of the inverse dielectric matrix[27,36]. The extension of this picture to III-V semiconductors, in which the bond has a partial ionic character, is straightforward. The partial charge transfer from less to more electronegative atom is reflected in a shift of the bond charge towards the latter, as could be seen in fig. 2.1, and so the equilibrium position of the bond charge in the model should be displaced in such a way to divide the bond length in the proportion 5 : 3.

These concepts where exploited by Martin[27] in a study of the lattice dynamics of Silicon. He pointed out that the diagonal (metallic-like) part of the screening, which gives rise to pair potentials between silicon atoms, is not able to account for the stability of the open tetrahedral structure, the instability against

shear modes being signalled by imaginary frequencies of TA modes. The introduction of bond charges constrained to remain at the midpoint of a bond even when atoms are moving, provides a bond-bending force through their Coulomb repulsion, thus giving rise to an effective non central interaction between ions which stabilizes the structure. Martin found an overall satisfactory agreement with the experimental phonon dispersion curves, being able to reproduce at least partially the characteristic flattening of TA modes along the [100] and [111] directions in the Brillouin zone, and the values of elastic constants. He also used a simple two parameter model to account for the main features of the dispersion relations, allowing Coulomb interactions between ion-ion, ion-BC and BC-BC and introducing a short range force between nearest-neighbour ions only, to account for the deviation from the Coulomb force due to the diagonal screening, which reaches the asymptotic value for distances of the order of the atomic spacing.

These ideas where developed by Weber who proposed a simple empirical model with few parameters, the Adiabatic Bond Charge Model, that reproduces in a satisfactory way describes the lattice dynamics of group IV elements[28] (C- diamond, Ge, Si, $\alpha - Tin$) and III-V semiconductors[29], and has the same importance for the lattice dynamics of semiconductors as the shell model[37] for the lattice dynamics of ionic systems.

Weber removed the constraint that B. C. should follow the atomic motion instantaneously, allowing them to move adiabatically like the electronic shells in the shell model, by providing an appropriate ion-B.C. force to fix their equilibrium position at the midpoint of the bond. The four kind of interactions allowed in the model are, as sketched in fig. 2.4:

- Coulomb forces between charges, with coupling parameter $\gamma_{ij} = Z_i Z_j / \epsilon_0$.
- Short range forces between nearest-neighbours

(a) ion - ion central interaction

(b) ion - B. C. central interaction

(c) B. C. - B. C. non-central interaction

As previously stated, forces of type (a) account for the effects of diagonal screening in semiconductors, while interactions of type (b) and (c) are characteristic of the covalent bond, representing respectively the strength of the bond and the interaction between neighbouring bonds, due to variation in the s-p hybridization when the angle between bonds changes. There are only 4 parameters, related to the couplings of the different interactions involved, that could be fitted matching an equal number of relations. These are derived requiring that the observed frequencies are reproduced at some high symmetry points in the Brillouin zone. In the extension to III-V semiconductors 6 parameters are necessary, being present now one interaction of type (b) and (c) for each type of ion (the charges of the two ions are set equal, so still one parameter is necessary for Coulomb coupling). The good agreement with the observed dispersion relations and elastic constants obtained by the model is shown in fig. 2.5 for the case of *Ge*.

Weber examined also the importance of Coulomb interactions in his model, considering the case in which they are dropped by setting $\gamma = 0$, and found that the overall agreement remains good, meaning that their effect is marginal. The dispersion relations of this uncharged model are compared in fig. 2.6 to that of the full model, already shown in fig. 2.5. He showed also that the characteristic flattening of TA modes depends on the relative importance of the ion-bc and bc-bc coupling. When the former is weaker than the latter, atoms vibrate in a rigid lattice of bond charges as almost decoupled oscillators with small force constant, and only in the long wavelenght limit, when atoms and b.c. move in phase, the rigidity is transferred also to the atomic motion. The variation of this ratio can

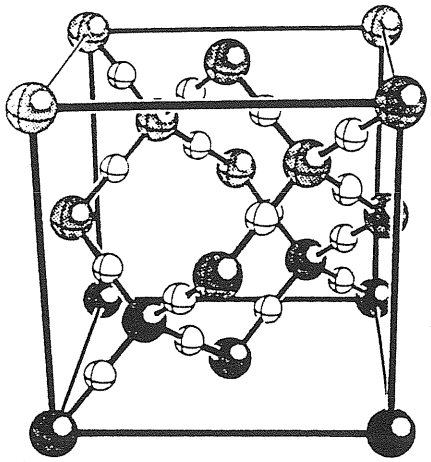

Figure 2.3
Cubic cell of crystalline Germanium showing decoration of interatomic bonds by bond particles. In crystallography this decorated structure is known as the ideal β crystobalite structure for SiO_2.

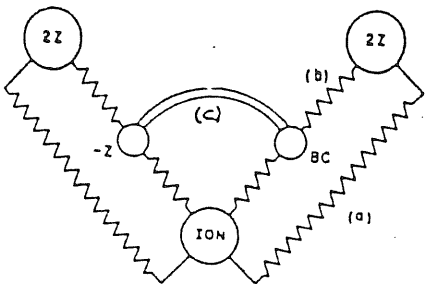

Figure 2.4
Schematic presentation of the short ranged interactions used in the Adiabatic Bond Charge Model by Weber. (a) ion-ion central interactions; (b) ion-BC (central); (c) BC-BC (non central). From Weber, ref.[28].

thus account for the trend in TA mode flattening, which is more pronounced in less covalent systems as $\alpha - Tin$, decreases going from Ge to Si and is not present in diamond. In a recent study, Fleszar and Resta[38] have shown that the BCM gives also correct values for the real space force constants, and for the interplanar force constants as compared with the results of first-principles calculations, and that the presence of BC with their interactions accounts for an effective atom-atom coupling up to the 13th neighbour.

Recently another work appeared in the literature[39] (inspired by Generalized Valence Bond calculations on silicon clusters), in which "electron pairs" in bonds are viewed as auxiliary degrees of freedom, or classical effective particles, and used in MD simulations of silicon clusters and surfaces. Like the model we are going to present in the next section it employes only central pair interactions and was tested with good results on the lattice dynamics of silicon and the prevision of small clusters structure, but it fails to account for elastic constants or the correct reconstruction of silicon surfaces, as the potentials employed favours too short bond lenghts. Another model employing Bond Particles as auxiliary degrees of freedom and only pair potentials has been analyzed by Ackland[40] to describe bonding in Silicon clusters.

No attempt to use it for modelling also the disordered phases has been reported by the authors of these papers.

It must be mentioned that Weber's BCM has been also used in modelling amorphous Si and Ge in a study (see ref.[41]) in which a crystalline sample was disordered by the introduction of a certain amount of defects, then relaxed in a Monte Carlo simulation at room temperature, with energies determined according to the BC Model.

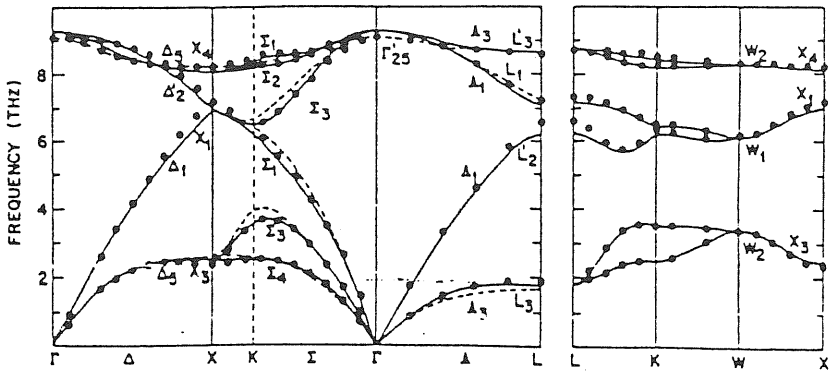

Figure 2.5
Phonon dispersion curves for Germanium. Solid lines show Weber's results with the Adiabatic Bond Charge Model compared with experimental values (points). From Weber, ref.[28].

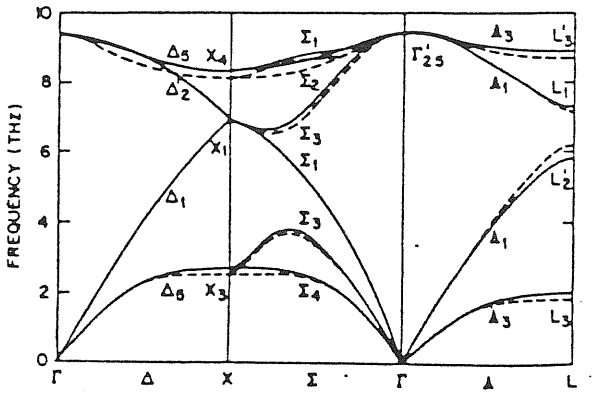

Figure 2.6
Phonon dispersion curves for Germanium as calculated from Weber's BCM with short range forces only (solid lines) in comparison with the results showed in fig 2.4 for the full model (dashed lines). From Weber, ref.[28].

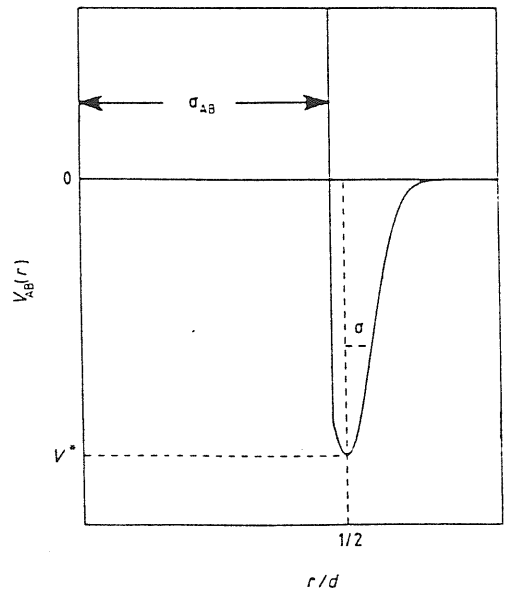

Figure 2.7
Atom - Bond Particle interaction potential in the LAM.

The adiabatic bond charge model found recent application to the lattice dynamics of polar semiconductor superlattices[42], of the polymorphic phases of Si and Ge[43], to the study of the surface phonons of the reconstructed $Si(111)$ 2×1 and of the $Si(111) + H$ 1×1 surfaces[44].

2.2 BCM FOR SEMICONDUCTOR MELTS

As we have seen in the preceding section, the success of the BCM in reproducing the lattice dynamics of semiconductors relies upon the simple physical representation that it gives for the forces due to the covalent bond, namely the introduction of bond charges as centers of forces to account for the directional interactions between atoms involved in chemical bonding. We want to extend this simple picture to treat interatomic forces in the melts of IV group and III - V semiconductors. The underling physical assumption for this extension is that, even if these systems show metal-like conductivity[45] in the molten state, the formation and breaking of covalent bonds in the melt play still an important role, driving the system towards density fluctuation of local tetrahedral order. It was shown by a recent first-principle simulation on molten Silicon by the Car-Parrinello method[15] that this is indeed the case.

In the spirit of BCM we examined a primitive model for the melt[30] regarding it as a mixture of atoms and Bond Particles, in which the atom-atom interaction is represented at the most elementary level by hard sphere repulsion, and an appropriate ion-BP interaction provides a stable equilibrium position for the Bond Particles, which are now free to leave the bond. This attractive interaction can induce localization of bond particles between pair of atoms, constituting a "bond" between them; the directionality in the interaction between atoms is accounted

for by the steric restriction that at most four BP can localize in tetrahedral configuration around one atom. The main aim in examining the model as formulated above is to follow the structural evolution of both the atomic and BP component as the temperature is lowered from hot liquid states to strongly supercooled states. Directionality of effective atom-atom interaction and angular interatomic correlations are progressively built into the model as localization of BP sets in and grows. In the liquid state this amounts in the presence of a fluctuating network of bonds, with the occurrence of fluctuations that lead to the temporary formation of tetrahedral open units of four atoms "bonded" to a central one. One can follow the increasing correlation between such units on lowering the temperature, ending eventually in the formation of a permanent network with stable bonds.

A Model for Liquid Germanium

We consider a two-component fluid of hard spheres, with component A (*Ge* atoms) and B (Bond Particles) having number density n_A and $n_B = 2n_A$ at temperature T. The hard-sphere interactions are characterized by three distances of closest approach (σ_{AA}, σ_{AB} and σ_{BB}, say). In the problem at hand the relevant values of the hard-sphere contact distances are asked to satisfy the approximate relations

$$\sigma_{AA} \simeq 2\sigma_{AB} \leq \mathrm{d} \qquad\qquad \sigma_{BB} \sim \sqrt{\frac{2}{3}}\,\mathrm{d} \tag{2.1}$$

where d represents the bond-length. These relations imply that, even though the B component is essentially point-like compared with the A component, no more than four B particles can be found in immediate contact with any A particle. This feature of the model (non-additivity in excluded volume effect) is to be contrasted with the primitive model of a liquid alloy as a mixture of hard spheres[46,47], in which additivity of hard-spheres diameters is imposed by setting

$\sigma_{AB} = (\sigma_{AA} + \sigma_{BB})/2$.

We next introduce interactions which lead to strong relative ordering of the two components in the liquid, considering two alternative cases. The first choice (Localized Attraction Model- LAM) is similar in spirit to the Weber BCM and introduces an attractive interaction between A and B particles in the form of a narrow potential well centered at the distance d/2 from the centre of each A particle and uniformly spread over its surface (see fig. 2.7). The well is taken to have a gaussian shape of half-width σ and depth V, with $\sigma \simeq d/2 - \sigma_{AB}$ is chosen narrow so that there is a well defined bond- length d. We may explicitly note here that the role played in Weber's model by bond bending non-central forces between Bond Particles is taken up in our model for the liquid, at appreciable values of the A-B coupling strength, by the simple requirement made on the distances of closest approach between them.

The well depth enters the model only in units of the thermal energy k_BT, yielding a coupling strength parameter $V^* = V/k_BT$ which will be allowed to increase continuously from zero in order to follow the process of localization of bond particles. For liquid germanium near freezing, estimating V from the valence-conduction band gap of the crystal ($V \simeq 0.7eV$), we anticipate $V^* = 6$.

The second alternative that we had explored[30] for the origin of relative order of the components of the liquid is closer to Phillips' original BCM. The hard-spheres are assigned charges in amounts $Z_A|e|$ and Z_Be respectively, with $Z_B = 1/2Z_A$.

The A-B coupling strength is now measured by the 'plasma parameter' $\Gamma = Z_B^2e^2/(ak_BT)$, the length a being related to the liquid density by $a = (4\pi n_A)^{-1/3}$. Again this parameter will be allowed to increase continuously

from zero. Phillips' original estimate was $|Z_B| \simeq 0.5$ corresponding to two electronic charges screened by the dielectric constant of the material, while fits in the BCM of Martin and Weber gives respectively values of 0.65 and 0.40. The corresponding value for Γ appropriate to Germanium near freezing is in the range 50-20.

A combination of short range attraction and Coulomb forces is also possible, but relying on Weber's analysis of his model, we think that also in the liquid near freezing only short range forces are determinant for structural features.

The calculations reported in Chap. 4 refer to two choices of the liquid density taken from experiments. We expected the average bond-length to be different in the melt from the value found in the solid, and this was indeed observed in the ab-initio simulation[15]. In our primitive model d is a parameter to be fixed,since the narrow well considered by us doesn't allow the bond length d to vary on temperature, it is a parameter to be fixed; then we chose two different values for d one for the liquid phase and one for the solid, taken from the $Ge - Ge$ first- neighbour distance in neutron scattering experiments.
For liquid Germanium at $T = 1253\ K$, which is above the freezing point at atmospheric pressure ($1210\ K$), one has $n_A = 0.0461 \mathring{A}^{-3}$ from rif. [45] and d $= 2.63 \mathring{A}$ from the neutron diffraction experiment of Gabathuler and Steeb[48]. In amorphous Germanium, on the other hand, the density depends on the film deposition rate and on film thickness, being at most equal to 97% of the crystalline density (see for instance ref. [49]). We have considered such a value of density as our second choice, in combination with the value d $= 2.46 \mathring{A}$ from the diffraction experiment of Etherington *et al.*[50] on amorphous Germanium at room temperature. This value of the bond-length is practically the same as in crystalline germanium. Finally the various choices that we shall illustrate for the hard spheres contact

distances and the well half-width, are collected for convenience in table 2.1. We shall comment later on these specific choices as the opportunity arises.

TABLE 2.1 Sets of model parameters used in the calculations

	$n_A(\AA^{-3})$	d (Å)	σ_{AA}/d	σ_{AB}/d	σ_{BB}/d	σ/d
Set 1	0.0461	2.63	0.94	0.475	0.80	0.050
Set 2	0.0429	2.46	0.95	0.475	0.76	0.050
Set 3	0.0429	2.46	0.98	0.475	0.81	0.050
Set 4	0.0429	2.46	0.98	0.500	0.81	—

Extension to III - V Semiconductors

Let us consider here as an example a straightforward extension of the LAM model to the description of III-V semiconductors. We shall adopt now a three component fluid composed by two kind of atoms, A1 and A2, and one kind bond particles B, so that six close contact distances $\sigma_{\alpha\beta}$ have to be chosen. In the case of Germanium only one of these distances, namely σ_{AA}, is an independent parameter, and it has been slightly adjusted in our calculations to give agreement with the height of the first peak in S(k) in diffraction experiments, while σ_{BB} and σ_{AB} were fixed by the relation (2.1). In III-V compounds the BP divides the bond length d in two parts d_{A1}, d_{A2} with $d_{A1}/d_{A2} = 3/5$, is the ratio between the number of valence electron in each atom. It should be noticed that the equilibrium position of BP is given by the location of the minimum in the A-B well, while σ_{AB} essentially represents the repulsive part of the A-B potential. The distances $\sigma_{B\alpha}$,

gaussian well can be used, centered at d_{A1} for A1 atoms and at d_{A2} for A2 atoms, with the depth fixed again from the value of the gap.

As there is evidence that a small amount of wrong-bonds between like elements may occur both in the liquid and amorphous state[16], it might be necessary to introduce two other different wells of suitable depth to account for A1-A1 and A2-A2 bonding, and their influence on the structure might systematically be studied. This kind of bonding should certainly be accounted for in studies of $Si - Ge$ systems, or other mixtures of IV group elements. Maybe the case that also for such systems the equilibrium position for BP in unlike bonds should be shifted towards the most electronegative atom.

Another point that can be explored by this model is whether the partial ionicity of these compounds is completely accounted for in this scheme by the shift in the equilibrium position of the BP in an uncharged system, or it should be necessary to place ionic charges of different sign on atoms of different kind. One can thus study to what extent this choice influences the structural properties.

2.3 MELTING CRITERIA

The liquid structure for the models considered here shows, as we shall see in Chap. 4, the same qualitative structure of liquid Ge when values of the coupling strength parameters assume approximatively values of $V^* \simeq 7.5$ for the LAM and $\Gamma \simeq 24$ in the other BCM. We notice that these values are close to those anticipated in Sec. 2.1 from the observed band-gap E_g in the crystal and from the estimated value of -2 for the bare bond charge, in the Phillip's scheme, that leads to a coupling $4/\epsilon_0$ between them.

We now ask whether there is any generality to these results. Namely, we ask whether for semiconductors which melts with a break-up of chemical bonding, one can formulate empirical melting criteria in the forms

$$\frac{E_g}{k_B T_m} \simeq constant \tag{2.3}$$

or

$$\frac{4e^2}{\epsilon_0 a k_B T_m} \simeq constant \tag{2.4}$$

at the melting temperature T_m. First we looked for linear correlations between T_m and E_g or T_m and $n^{1/3}/\epsilon_0$ where n is the number of atoms per unit volume.

Figure 2.8 shows that there is an approximate linear relation in both cases. Data for T_m, E_g, ϵ_0 used in the figures were taken from *Landolt-Börnstein* tables[54]. The constants of proportionality are approximately equal to 10 for (2.3) and 20 for (2.4), and are essentially in agreement with the values obtained in our model. We note also that criteria (2.4) is well satisfied, being almost all the values on the same line, and this line goes through the origin. In the other case the values are more scattered around a line, and the value for $E_g = 0$ lays at $T_m \simeq 740K$; being the value $740/k_B T$ of order unity at the melting temperature involved, we can still say that the criteria (2.3) is approximatively satisfied.

The melting criteria involving the bandgap was not unexpected, and a melting criterion relating the melting temperature to the band gap was already proposed by Godefroy and Aigrain[55]. Recently a similar criterion was proposed again by Aniya[56], on the basis of a tight binding analysis of cohesive energies[57], and extended to a wide range of binary compounds from insulators, including alkali halides and alkaline-earth halides to semiconductors and ferroelectrics. The melting criterion based on the bond charge concept is less obvious and its empirical verification give additional support to the qualitative usefulness of Phillip's ideas.

We now ask whether there is any generality to these results. Namely, we ask whether for semiconductors which melts with a break-up of chemical bonding, one can formulate empirical melting criteria in the forms

$$\frac{E_g}{k_B T_m} \simeq constant \tag{2.3}$$

or

$$\frac{4e^2}{\epsilon_0 a k_B T_m} \simeq constant \tag{2.4}$$

at the melting temperature T_m. First we looked for linear correlations between T_m and E_g or T_m and $n^{1/3}/\epsilon_0$ where n is the number of atoms per unit volume.

Figure 2.8 shows that there is an approximate linear relation in both cases. Data for T_m, E_g, ϵ_0 used in the figures were taken from *Landolt-Börnstein* tables[54]. The constants of proportionality are approximately equal to 10 for (2.3) and 20 for (2.4), and are essentially in agreement with the values obtained in our model. We note also that criteria (2.4) is well satisfied, being almost all the values on the same line, and this line goes through the origin. In the other case the values are more scattered around a line, and the value for $E_g = 0$ lays at $T_m \simeq 740K$; being the value $740/k_B T$ of order unity at the melting temperature involved, we can still say that the criteria (2.3) is approximatively satisfied.

The melting criteria involving the bandgap was not unexpected, and a melting criterion relating the melting temperature to the band gap was already proposed by Godefroy and Aigrain[55]. Recently a similar criterion was proposed again by Aniya[56], on the basis of a tight binding analysis of cohesive energies[57], and extended to a wide range of binary compounds from insulators, including alkali halides and alkaline-earth halides to semiconductors and ferroelectrics. The melting criterion based on the bond charge concept is less obvious and its empirical verification give additional support to the qualitative usefulness of Phillip's ideas.

The freezing properties of the BCM presented in sect 2.2 have been studied in detail by means of the density functional theory of freezing for binary mixtures by Bahdirkhan et al.[31], who found that this model liquid freezes indeed in a open tetrahedral structure.

Figure 2.8
Correlation of the melting temperature T_m of elemental semiconductors and III-V compounds with the valence conduction band-gap E_g (left) and with the quantity $n^{1/3}/\epsilon_0$ (right), where n is the number of atoms per unit volume and ϵ_0 the static dielectric constant of the crystal.

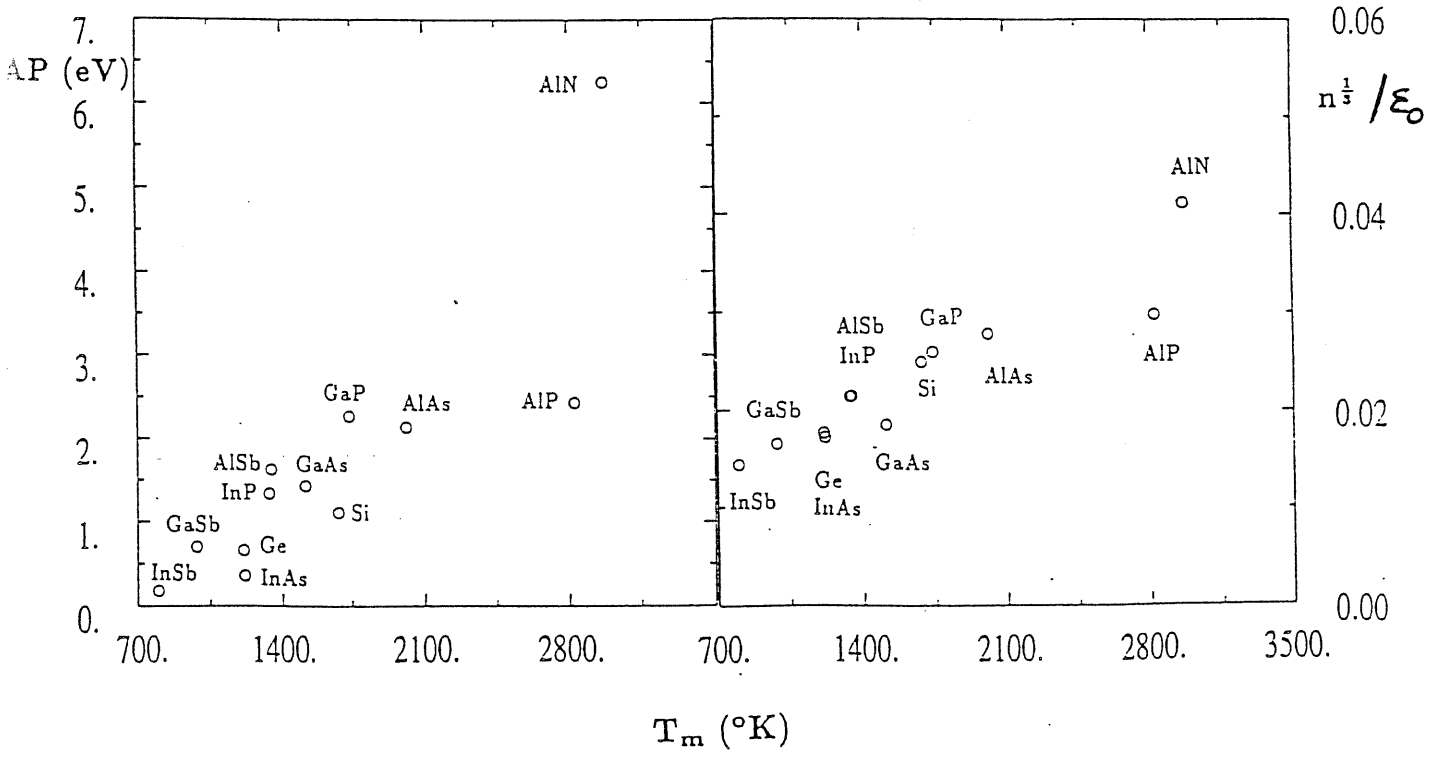

Chapter 3

Methods for the Study of the Model

We present here a summary of concepts from the theory of liquids, including the definitions of the relevant structural quantities (i.e. pair correlation functions and structure factors), and a description of the statistical mechanical methods we employed in the study of our model, namely integral equations and Monte Carlo simulations. In order to make the presentation of results in the following chapters as simple as possible, we include here for later reference all the technical details about numerical calculations. A general reference for this chapter is the book by Hansen and McDonald[58], for liquid state theory, and the book of Allen and Tildesley[59] for Monte Carlo Simulations.

3.1 DEFINITIONS

Notations for the Fourier Transforms

We shall adopt the following notation to indicate the 3D-Fourier transform for a function of a vector

$$\tilde{f}(\mathrm{k}) = \int f(\mathrm{r})\, e^{-i\ \mathrm{k}\cdot\mathrm{r}}\, \mathrm{dr} \qquad (3.1a)$$

If f depends only on the modulus of $\mathbf{r}$, one can write the integral in polar coordi-

nates as

$$\tilde{f}(k) = \int_0^{2\pi} \mathrm{d}\phi \int_0^{\infty} \mathrm{d}r \int_{-1}^{1} \mathrm{d}\cos\theta \; r^2 f(r) \; e^{-ikr\cos\theta} \quad = \\ = \frac{4\pi}{k} \int_0^{\infty} r f(r) \sin kr \; \mathrm{d}r \tag{3.1b}$$

In the same way we can express the inverse fourier transform when f depends only on the modulus of $\mathbf{k}$

$$f(\mathbf{r}) = \frac{1}{(2\pi)^3} \int \tilde{f}(\mathbf{k}) \; e^{i\,\mathbf{k}\cdot\mathbf{r}} \; \mathrm{dk} = \frac{1}{2\pi^2 r} \int_0^{\infty} k\tilde{f}(k) \sin kr \; \mathrm{d}k \tag{3.2}$$

Number Density

In what follows we shall always denote with n the **number density** of an homogeneous system, that is the number of atoms per unit volume measured in $\mathring{A}^{-3}$. On the contrary the mass density, i.e. mass per unit volume will be denoted with ρ. Dealing with m-component systems, n is the **total** number density, while n_α ($\alpha = 1, 2, ..., m$) are the **partial** number densities, and $x_\alpha = n_\alpha / n$ are the molar fractions or relative concentrations for the component of type α.

Pair Correlation Functions and Structure Factors

At present the only structural quantities directly measurable by experiment for disordered homogeneous systems like a liquid, a glass or an amorphous solid are the static pair correlation function (or radial distribution function) $g(r)$ and the static structure factor $S(k)$. They are related in the former system to the average (time average) equilibrium local fluctuations of density, and to the correlations between the positions of particles, averaged over the sample, in the latter. These functions give some information about the spatial correlations of pairs of particles in the range of few (from 0 to 10-12) Ångstrom.

In a X-ray scattering experiment, and in a neutron scattering experiment under certain conditions, the coherent scattered intensity at a given angle is proportional to $S(k)$, k being the transferred momentum in the scattering process. In Statistical Mechanics the structure factor describes the correlation between density fluctuations of wavelenght $\lambda = \frac{2\pi}{k}$ in two different points at equal time

$$S(\mathrm{k}) = \frac{1}{N} \left\langle \sum_{i=1}^{N} \sum_{j=1}^{N} e^{i\ \mathrm{k} \cdot (\mathrm{r}_i - \mathrm{r}_j)} \right\rangle$$

where the brackets indicate a statistical average over a canonical ensemble of N particles.

The pair correlation function for an homogeneous system can be defined as the probability distribution function for finding any particle around any other particle at a distance r. It describes at a pair level the average local arrangement of atoms in the system. It's useful to introduce another function, called also pair correlation function or total correlation function $h(r) = g(r) - 1$, describing the spatial deviation from the uniform mean density.

The link between the pair correlation function and the density-density autocorrelation function at equal time $G(r, t = 0)$, describing spatial density fluctuations is given by

$$G(\mathrm{r}, t) = \frac{1}{N} \left\langle \sum_{i=1}^{N} \sum_{j=1}^{N} \int \delta[\mathrm{r}' + \mathrm{r} - \mathrm{r}_i(t)]\ \delta[\mathrm{r} - \mathrm{r}_j(0)]\ \mathrm{dr}' \right\rangle \tag{3.3}$$

$$G(\mathrm{r}, 0) = ng(\mathrm{r}) + \delta(\mathrm{r})$$

The structure factor is related to the pair correlation function by a fourier transform, giving for $\mathrm{k} \neq 0$ the relation

$$S(\mathrm{k}) = 1 + n\tilde{h}(\mathrm{k}) \tag{3.4}$$

Dealing with a multi-component system we need more than one pair distribution function to describe its structure; for a two component fluid with particles of type

3.2 INTEGRAL EQUATIONS

Integral equation theories of liquids provide a simple way for determining the structure, at the level of pair correlations, and the thermodynamic properties for the equilibrium states of fluids. In the simplest version we shall sketch here, the theory apply to model fluids composed by "simple" particles, regarded as isotropic, structureless objects (i.e. "atomic" or "ionic" liquids), interacting with pair potentials only. Generalizations also exists to deal with molecular fluids[58] and fluids with association[23] or with polymers[60], nonspherical objects[61], or to obtain the three body correlations functions[62,63]; however in general they are more demanding from the computational point of view.

For studying our model we are interested in the case of a two component system of particles interacting with pair potentials only, that is a system whose potential energy V is factorizable as a sum of pair interaction $v_{\alpha\beta}(r_{ij})$.
We have two sets of equations connecting the unknown functions $g_{\alpha\beta}$ and $c_{\alpha\beta}$ with the pair interactions $v_{\alpha\beta}$.

– one is the set of integral equations (3.10)relating $c_{\alpha\beta}$ and $h_{\alpha\beta}$, which generalizes the O.Z. equation $c_{\alpha\beta}$ and $h_{\alpha\beta}$

– the other is an exact relation, called closure relation

$$g_{\alpha\beta}(r) = e^{-\Phi_{\alpha\beta}(r) + h_{\alpha\beta}(r) - c_{\alpha\beta}(r) - B_{\alpha\beta}(r)} \tag{3.12}$$

where $\Phi_{\alpha\beta}(r) = \beta v_{\alpha\beta}(r)$ is the pair potential in thermal units. This relation has originally been derived by diagrammatic methods[64] (see also ref.[65]), from the formal series expansions of g and c in powers of the density, but it can be derived also by means of a density functional formalism[66][67][68]. The functions $B_{\alpha\beta}(r)$ are expressed in the diagrammatic derivation as the sum of the so called "elementary diagrams" or "bridge diagrams", which have a precise topological characterization

(see ref.[58]); on the other hand also in the density functional derivation the bridge functions can be expressed by means of a series

$$B_{\alpha\beta}(r) = \sum_{\nu=4}^{\infty} B_{\alpha\beta}^{(\nu)}(r) \tag{3.13}$$

For a one-component system, the generic term in this sum takes the expression

$$B^{(\nu)}(r) = B^{(k+2)}(r) = -\frac{n^k}{k!} \int c^{(k+1)}(\mathbf{r}, \mathbf{r_1}...\mathbf{r_k}) h(\mathbf{r_1})...h(\mathbf{r_k})\ \mathbf{dr_1}...\mathbf{dr_k} \tag{3.14}$$

the first term of the series being

$$B^{(4)}(r) = -\frac{n^2}{2} \int c^{(3)}(\mathbf{r}, \mathbf{r_1}, \mathbf{r_2}) h(\mathbf{r_1}) h(\mathbf{r_2})\ \mathbf{dr_1 dr_2} \tag{3.15}$$

We shall deal extensively with the bridge functions in a later section. The two sets of equations (3.10) and (3.12) constitute a closed set of three coupled nonlinear integral equations, usually expressed in the unknown functions $\gamma_{\alpha\beta}(r) = h_{\alpha\beta}(r) - c_{\alpha\beta}(r)$, that can be solved from the knowledge of the potential $\Phi_{\alpha\beta}(r)$, provided that we have chosen a suitable analytical expression or an approximation for the bridge functions. The advantage in casting the equations in terms of $\gamma_{\alpha\beta}(r)$ is that these functions are smooth even for discontinuous potentials, like the hard-sphere one, while both $g_{\alpha\beta}(r)$ and $c_{\alpha\beta}(r)$ are discontinuous at the points of discontinuity in the potential (see ref.[58]).

Different kinds of approximate integral equations can be obtained assigning to $B_{\alpha\beta}(r)$ a specific functional form in terms of $\gamma_{\alpha\beta}(r)$. We present here a list of approximate closure relations that are relevant for our work, classifying them from the functional form that they show for the bridge functions.

HNC EQUATIONS – the simplest choice for the bridge functions, i.e. neglecting completely the contribution of the elementary diagrams, by setting $B_{\alpha\beta}(r) = 0$, gives rise to the Hyper-Netted-Chains equations

$$g_{\alpha\beta}(r) = e^{-\Phi_{\alpha\beta}(r) + h_{\alpha\beta}(r) - c_{\alpha\beta}(r)} \tag{3.16}$$

It is superior to other closures in the treatment of charged systems, where it is accurate for a wide range of parameters, as this approximation maintains some sum rules, involving correlation functions, that ensure the overall charge neutrality of the system[69] (for extensive refs. on this closure see the review article of Ichimaru[68]).

MSA APPROXIMATION – The Mean Spherical Approximation deals with system of hard-spheres plus a potential tail and corresponds to the choice

$$B_{\alpha\beta}(r) = \begin{cases} -\ln\left(h_{\alpha\beta}(r)+1\right) + h_{\alpha\beta}(r) & if \quad r > \sigma_{\alpha\beta}(r) \\ +\infty & otherwise. \end{cases} \tag{3.17a}$$

that substituted in (3.12) gives a more familiar relation

$$\begin{cases} g_{\alpha\beta}(r) = 0 & if \quad r < \sigma_{\alpha\beta}(r); \\ \Phi_{\alpha\beta}(r) = -c_{\alpha\beta}(r) & otherwise. \end{cases} \tag{3.17b}$$

that is motivated on the physical ground by the requirement of excluded volume effect and correct asymptotic behaviour of $c_{\alpha\beta}(r)$. It found extensive applications as in many cases it can be solved analytically. It can be generalized to soft repulsive potentials plus an attractive part (Soft MSA).

PY EQUATIONS – The Percus-Yevick closure (PY) corresponds to the choice

$$B_{\alpha\beta}(r) = \gamma_{\alpha\beta}(r) - ln[1+\gamma_{\alpha\beta}(r)] \tag{3.18a}$$

that when substituted into eq. (3.12) gives

$$g_{\alpha\beta}(r) = [1+\gamma_{\alpha\beta}(r)]e^{-\Phi_{\alpha\beta}(r)} \tag{3.18b}$$

or alternatively

$$c_{\alpha\beta}(r) = g_{\alpha\beta}(r)\left(1 - e^{\Phi_{\alpha\beta}(r)}\right) \tag{3.18c}$$

It was derived by diagrammatic methods by neglecting a particular class of bridge diagrams, and resumming the remainder. It is superior to other closures in the case

of hard spheres, for which it reduces to the MSA, and it is analytically solvable for one-component hard-sphere and two component additive hard-spheres systems. As the $g_{\alpha\beta}(r)$ are not positive definite in this approximation, they can show negative values at the position of deep minima for attractive potentials at strong coupling strength.

As a consequence of the approximations made on the bridge functions, one obtains an approximate theory for the structure that can be still accurate over a wide range of parameters for a certain class of systems, but one as to check the limits of validity of the chosen approximations contrasting its predictions with "exact" results provided by computer simulations. The exploration of the accuracy of various approximate closures in the case of the LAM is reported in the following chapter. Another consequence of the approximations is a certain amount of thermodynamic inconsistency, due to the violation of some sum rules between correlation functions. This means that some thermodynamic quantities can have different values if one computes them through different routes. The amount of thermodynamic consistency can be used to judge the goodness of the approximation.

Empirically mixed Integral Equations

The observation that HNC solution and PY solution bracket the exact solution for simple liquids, as it emerges from simulations, gave rise to the Roger-Young mixed closure[70], that interpolates between the PY closure at short distances and the HNC one at long range. As a statement on the bridge functions, it can be expressed as

$$B_{\alpha\beta}(r) = \gamma_{\alpha\beta}(r) - \ln\left[1 + \frac{e^{f_{\alpha\beta}(r)\gamma_{\alpha\beta}(r)} - 1}{f_{\alpha\beta}(r)}\right] \qquad (3.19a)$$

that gives the closure relation

$$g_{\alpha\beta}(r) = e^{-\Phi_{\alpha\beta}(r)}\left[1 + \frac{e^{f_{\alpha\beta}(r)\gamma_{\alpha\beta}(r)} - 1}{f_{\alpha\beta}(r)}\right] \qquad (3.19b)$$

where f represents a mixing function of the form $f_{\alpha\beta}(r) = 1 - e^{-r/\xi_{\alpha\beta}}$ and $\xi_{\alpha\beta}$ are parameters that can be fixed by the requirement of Thermodynamic Consistency (TC) of the theory. In the same spirit another mixed closure have been proposed by Hansen and Zerah [71]; it interpolates between the HNC closure at long range, and the Soft-MSA approximation (a generalization of the MSA closure) at short range. It is expressed by

$$B_{\alpha\beta}(r) = \gamma_{\alpha\beta}(r) - \Phi^{(1)}_{\alpha\beta}(r) - \ln\left[1 + \frac{e^{f_{\alpha\beta}(r)(\gamma_{\alpha\beta}(r) - \Phi^{(2)}_{\alpha\beta}(r))} - 1}{f_{\alpha\beta}(r)}\right] \qquad (3.20a)$$

$$g_{\alpha\beta}(r) = e^{-\Phi^{(1)}_{\alpha\beta}(r)}\left[1 + \frac{e^{f_{\alpha\beta}(r)(\gamma_{\alpha\beta}(r) - \Phi^{(2)}_{\alpha\beta}(r))} - 1}{f_{\alpha\beta}(r)}\right] \qquad (3.20b)$$

where $\Phi^{(1)}_{\alpha\beta}(r)$ and $\Phi^{(2)}_{\alpha\beta}(r)$ are respectively the repulsive and the attractive parts of the potential, defined by

$$\Phi^{(1)}_{\alpha\beta}(r) = \begin{cases} \Phi_{\alpha\beta}(r) - \Phi_{\alpha\beta}(r_{min}) & if \;\; r < r_{min}; \\ 0 & otherwise. \end{cases}$$

$$\Phi^{(2)}_{\alpha\beta}(r) = \begin{cases} \Phi_{\alpha\beta}(r_{min}) & if \;\; r < r_{min}; \\ \Phi_{\alpha\beta}(r) & otherwise. \end{cases}$$

3.3 BRIDGE FUNCTIONS AND MODIFIED-HNC or IMPROVED-HNC EQUATIONS

RHNC and MHNC Equations

Rosenfeld and Ashcroft[72] and Lado [73] proposed to solve the closure relation (3.12) with the Bridge functions of a reference hard-sphere system with a packing ratio optimized to give Thermodynamic Consistency. This approach is based on the assumption that the bridge functions have a universal behaviour at short range, for any potential, so that they can adequately be represented by the bridge functions of a hard-sphere reference system of a suitable density, evaluated in the PY approximation. Two equivalent schemes were devised to enforce TC in the solution: one minimizes an expression for the free energy of the system (RHNC or Reference-HNC), and the other requires the equality of the compressibility computed from the equation of state (virial route) with that computed from the fluctuation route (Modified-HNC).

Improved-HNC Equations and Bridge Functions

It was realized by Ichimaru that non-universal features at medium range in the bridge functions could be important to describe the actual structure in some systems, i.e for the OCP at strong coupling. He obtained a formula[68] that relates the first term in the expansion (3.13) with the $h_{\alpha\beta}(r)$. Substituting in the expression (3.15) for $B^{(4)}$ the following approximation for the $c^{(3)}$

$$c^{(3)}(\mathbf{r_1},\mathbf{r_2},\mathbf{r_3}) = h(|\mathbf{r_1}-\mathbf{r_2}|)h(|\mathbf{r_2}-\mathbf{r_3}|)h(|\mathbf{r_1}-\mathbf{r_3}|) \tag{3.21}$$

one obtains

$$B^{(4)}(r) = -\frac{n^2}{2}\int h(r_1)h(r_2)h(|\mathbf{r_1}-\mathbf{r_2}|)h(|\mathbf{r_1}-\mathbf{r}|)h(|\mathbf{r_2}-\mathbf{r}|)\ \mathbf{dr_1}\ \mathbf{dr_2} \tag{3.22}$$

The corresponding expression for a two component system is

$$B^{(4)}_{\alpha\beta}(r) = -\frac{n^2}{2}\sum_{\gamma\delta} x_\gamma x_\delta \; E^{\gamma\delta}_{\alpha\beta}(r) \tag{3.23}$$

$$E^{\gamma\delta}_{\alpha\beta}(r) = \int h_{\alpha\gamma}(r_1)h_{\alpha\delta}(r_2)h_{\gamma\delta}(|\mathbf{r_1}-\mathbf{r_2}|)h_{\gamma\beta}(|\mathbf{r_1}-\mathbf{r}|)h_{\delta\beta}(|\mathbf{r_2}-\mathbf{r}|)\; \mathbf{dr_1 dr_2} \tag{3.23a}$$

The integral that we denoted with $E^{\gamma\delta}_{\alpha\beta}(r)$ can be represented graphically by the following "elementary" diagram.

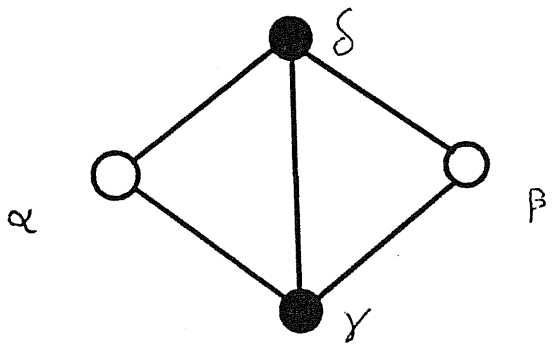

A line in this diagram gives the correlation between two particles as represented by the total pair correlation function $h_{\alpha\beta}(r)$, and black vertices represent variables to be integrated, namely $\mathbf{r_3}, \mathbf{r_4}$, while white vertices are the variables not integrated and $r = |\mathbf{r_2} - \mathbf{r_1}|$ is the distance r where the bridge function is evaluated. Ichimaru and Iyetomi[74] solved the closure relation using bridge functions determined through these relations, where the total correlation function h(r) from the HNC solution was used. They rescaled the computed function at low r in order to reproduce the 'universal' repulsive behaviour at short distances and obtained a certain degree of thermodynamic consistency. They named this approach improved-HNC, as it starts from the knowledge of the HNC solution to evaluate the approximate bridge function used to obtain the improved solution.

Crossover Approximation for the Bridge Functions

An approximation that is thermodynamic consistent and that retains both the universal behaviour of the bridge function at low r and the structural information present in the $B^{(4)}$, was employed by Pastore Ballone and Tosi in an extensive work on the structure and the thermodynamics of molten salts[75]. Its is based on the idea of interpolating between the short range behaviour of the HS bridge functions, and the values given by $B^{(4)}$ at intermediate distances. A similar idea has been used in a work by Ashcroft, Foiles and Reatto[76], who interpolated between the 'universal' behaviour at short range, and the expression given by the MSA at long range.

The crossover between the Hard-spheres bridge functions and $B^{(4)}_{\alpha\beta}$ employed by us has the following form

$$B_{\alpha\beta}(r) = [1 - f_{\alpha\beta}(r)]\, B^{(4)}_{\alpha\beta}(r) + f_{\alpha\beta}(r) B^{HS}_{\alpha\beta}(r) \tag{3.24}$$

where the $f_{\alpha\beta}(r)$ is the mixing function that specify the region in which one observes the crossing from the behaviour of one function to that of the other. We chose here for our work the same form chosen in ref.[75] that is

$$f_{\alpha\beta}(r) = \exp -(r/\xi_{\alpha\beta})^n \tag{3.25}$$

where $\xi_{\alpha\beta}$ are the parameters that determine the crossover region and have been fixed from the peaks' positions in the HNC result for $g_{\alpha\beta}(r)$. The exponent n has been fixed at a value 2, except when the elementary diagram $B^{(4)}_{AX}(r)$ presented a deep and narrow throat of negative value just above the distance σ_{AX}, where a value of 12 has been used in $f_{AX}(r)$ in order to make narrower the region of crossover. The thermodynamic consistency is to be enforced by the appropriate choice of the parameters of the reference HS-system. We used as HS bridge functions those determined by a numerical solution of the PY closure for a reference

system of hard spheres with the same ratio of diameters $d_{\alpha\alpha}/d_{12}$ as the ratio in the the peaks' positions of $g_{\alpha\beta}(r)$ in the HNC solution. In this way we have only one parameter d_{12} to vary to look for Thermodynamic Consistency. We didn't use as reference the analytical bridge functions of a one component system at a suitable density (as in ref.[75]) because the B_{AX} determined in such a way is very different from that obtained from the numerical solution of the PY equations for the full mixture.

The inverse isothermal compressibility $1/\rho k_B T \chi_T = \left(\frac{\partial \beta P}{\partial \rho}\right)_T$ was calculated from the fluctuation route as

$$\left(\frac{\partial \beta P}{\partial \rho}\right)_T = 1 - n \sum_\alpha \sum_\beta x_\alpha x_\beta \tilde{c}_{\alpha\beta}(k=0) \tag{3.26}$$

while the inverse compressibility from the virial route was determined by numerical differentiation of the virial equation of state $\frac{\beta P}{\rho}$, after repeating the calculation at a slightly higher value of density (we used $\rho_1/\rho_0 = 1.002$).

$$\left(\frac{\partial \beta P}{\partial \rho}\right) \approx \beta \frac{\Delta P}{\Delta \rho} \tag{3.27}$$

In finding the solution at higher density we also increased the density of the reference system used for the bridge functions, and also $B^{(4)}$ was scaled according to the density factor that appears in front of the integral (3.23).

The scheme we employed, that we call TC-IHNC (Thermodynamic Consistent Improved HNC), consist in solving the HNC approximation, calculating the bridge function $B^{(4)}_{\alpha\beta}$ from formula (3.23) and use in equation (3.12) the resulting crossover with the hard sphere part obtained from (3.24) to find a new solution.

We also explored the self consistency of the solution obtained in this scheme; that is after having obtained a solution and pair correlation function from the TC-IHNC scheme described above, we computed the next approximation for the

elementary diagrams $B^{(4)}_{\alpha\beta}$ and using them we iterate again the TC-IHNC scheme computing the next approximation for pair correlation functions and bridge functions. We found that one iteration is enough at low couplings, but around the freezing coupling strength two iteration are needed. In the supercooled region then more and more iteration are needed to reach the self-consistency. For the strongly supercooled region no convergence in this procedure is found.

3.4 NUMERICAL METHODS

Solution of the Integral Equations

The integral equations for the HNC and the TC-IHNC were solved using the algorithm of Gillan[77]. It consists of a mixed iterative Newton-Rapson Method that is rather stable and accurate, and doesn't require as many iterations as a pure iterative methods. It projects the unknown function onto a small basis, to represent its coarse shape, giving rise to a system of nonlinear coupled algebraic equations that can be solved by a Newton-Rapson method. The fine variation of the function is then determined iterating the coarse solution in the integral equations. The cycle is repeated until convergence in the solution is attained.

We used in the calculations 512 points for doing the fourier transforms involved in the algorithm, with a mesh in real space of $\Delta r = 0.02a$, and we employed 9 basis functions to project the $\gamma_{\alpha\beta}(r)$ for obtaining the coarse part. A particular care has to be taken in the treatment of the hard core discontinuity of $g_{\alpha\beta}(r)$, which is determined by both the value of the potential and the bridge function at contact.

Numerical Evaluation of the Bridge Functions

The integrals expressed by equation (3.23a) have been computed reducing them to double integrals by means of Legendre polinomial expansions[78,74]. Choosing $\mathbf{r}$ as the polar axis and denoting the angular coordinates of $\mathbf{r}_1$ and $\mathbf{r}_2$ by (θ_1, φ_1) and (θ_2, φ_2) one can expand

$$h_{\gamma\beta}(|\mathbf{r}_1 - \mathbf{r}|) = \sum_l H^l_{\gamma\beta}(r, r_1) P_l(cos\,\theta_1), \tag{3.28}$$

with

$$H^l_{\gamma\beta}(r, r_1) = (l + \tfrac{1}{2}) \int_{-1}^{1} h_{\gamma\beta}(|\mathbf{r}_1 - \mathbf{r}|) P_l(cos\,\theta_1)\, \mathrm{d}(\cos\theta_1). \tag{3.29}$$

A similar expression holds also for $h_{\delta\beta}(|\mathbf{r}_2 - \mathbf{r}|)$ and for

$$h_{\gamma\delta}(|\mathbf{r}_2 - \mathbf{r}_1|) = \sum_l H^l_{\gamma\delta}(r_1, r_2) P_l(cos\,\theta_{12}), \tag{3.30}$$

where θ_{12} denotes the angle between $\mathbf{r}_1$ and $\mathbf{r}_2$. Substitution of these expansions in the integrals (3.23a), expressed in polar coordinates $(r_1, \theta_1, \varphi_1)$ and $(r_2, \theta_2, \varphi_2)$, and use of the addition theorem of spherical harmonics and of the orthogonality relation to perform the angular integrations leads to the result

$$E^{\gamma\delta}_{\alpha\beta}(r) = \int_0^\infty r_1^2 \mathrm{d}r_1 \int_0^\infty r_2^2 \mathrm{d}r_2\; h_{\alpha\gamma}(r_1) h_{\alpha\delta}(r_2) \sum_l \left(\frac{4\pi}{2l+1}\right)^2 H^l_{\gamma\beta}(r, r_1) H^l_{\delta\beta}(r, r_2) H^l_{\gamma\delta}(r_1, r_2). \tag{3.31}$$

The integration required in formula (3.29) has been performed by a discrete transform, introduced by Attard[79,80], based on a Gauss-Legendre quadrature formula, which preserves the orthogonality of Legendre polynomials. Denoting with $f(|\mathbf{r}_1 - \mathbf{r}|)$ the function to expand, with x the cosine of the angle between $\mathbf{r}$ and $\mathbf{r}_1$, and with $F^l(r, r_1)$ the expansion coefficients, one has the N-point discrete transform corresponding to (3.28) and (3.29)

$$f(r, r_1, x_i) = \sum_{l=0}^{N-1} F^l(r, r_1) P_l(x_i) \tag{3.32}$$

$$F^l(r,r_1) = (l+\tfrac{1}{2}) \sum_{i=1}^{N} f(r,r_1,x_i) P_l(x_i)\, w_i \tag{3.33}$$

where the nodes x_i are the zeros of $P_N(x)$ and w_i are weights associated with the Gauss-Legendre quadrature[81]. Once N was fixed from the numerical accuracy required, we found that truncating the sum in (3.31) at $l_{max} = 18$ was sufficient for our purposes. As we are dealing with discontinuous functions discretized on a mesh, and we need to locate exactly the hard core discontinuity without having an indetermination of the order of the mesh size, we found necessary to transform by (3.29) (3.33) a continuous function, obtained from $h_{\alpha\beta}(r)$ by eliminating the discontinuity at contact, then subtracting analitically the transform of the added term to recover the transform of the original function. This procedure is also required because integration formulae give their best performances with continuous functions and the convergence with l in (3.31) is faster. We followed a procedure similar to that adopted by Attard[79,80]. We transformed

$$h^{ct}_{\alpha\beta}(r) = h_{\alpha\beta}(r) - g_{\alpha\beta}(\sigma_{\alpha\beta}) f_{\alpha\beta}(r), \tag{3.34}$$

Here f denotes the Mayer function

$$f_{\alpha\beta}(r) = \begin{cases} -1 & r \le \sigma_{\alpha\beta} \\ 0 & \text{otherwise} \end{cases}$$

whose discrete transform is, when $r = |\mathbf{r}_i - \mathbf{r}_j|$

$$F^l(r_i,r_j) = (l+\tfrac{1}{2}) \left[P_{l+1}(X_{ij}) - X_{ij} P_l(X_{ij}) \right]$$

for $l \ge 1$ and $F^0(r_i,r_j) = 0.5\ (X_{ij} - 1)$, where we denoted the cosine of the angle of contact with

$$X_{ij} = \begin{cases} \dfrac{r_i^2 + r_j^2 - \sigma_{\alpha\beta}^2}{2 r_i r_j} & |\mathbf{r}_i - \mathbf{r}_j| \le \sigma_{\alpha\beta} \\ 1 & |\mathbf{r}_i - \mathbf{r}_j| \ge \sigma_{\alpha\beta} \\ -1 & r_i + r_j \le \sigma_{\alpha\beta} \end{cases} .$$

From 40 to 80 points N has been used in performing the transform (3.33), together with a linear interpolation to evaluate the function $h_{\alpha\beta}(r)$ outside the tabulated points; the double integral in (3.31) was carried out by a trapezoidal rule using from 101 to 141 points, with a cutoff at half of the tabulation interval.

These numerical parameters were optimized in some test cases, contrasting the results for the computed elementary diagrams with Monte Carlo evaluation of the integrals (3.23a), expressed in polar coordinates, by means of the code **Vegas**[82]. Tests made using a trapezoidal integration to evaluate also the integrals in (3.29) showed that for the functions considered by us, for the same order l and number of points in the integrations, our method was definitively more accurate. The code to compute the elementary diagrams is easily vectorizable and parallelizable. A tipical computation of a set of elementary diagrams $B^{(4)}_{\alpha\beta}$ required 10 min. of Cpu time on a Cray Y-MP/4 using all four processors.

3.5 MONTE CARLO SIMULATION

The scope of our Monte Carlo simulation is to provide us with an " exact" result for the structural properties of the model (within the statistical error), in order to assess the accuracy of what is obtained from approximate integral equations theory. A preliminary set of simulations, reported by us in ref.[83], was repeated here to a greater accuracy; moreover we measured directly from the generated configurations to what extent the model shows the expected angular correlations. We made canonical ensemble Monte Carlo simulations of the LAM, employing the standard Metropolis algorithm[59], with 64 atoms and 128 bond particles inside a cubic simulation box of side 11.42635 Å, with periodic boundary conditions, and parameters of the model taken as in set 2 of table 2.1. We started with an

initial configuration corresponding to a diamond-type lattice for atoms, decorated with bond particles as shown in figure 2.3., and performed simulations at different values of the coupling parameter V^*, namely 0, 1, 3, 5, 6, obtaining a system in the liquid state. The system was equilibrated from the initial configuration for 10000 MCS (Monte Carlo steps, or attempted move per particles is the unit of " simulation time" in MC simulations). During the simulation the acceptance ratio was 1/3 and we monitored both the istantaneous values and the accumulated values (running averages) for the internal energy per particle, the virial pressure and modulus and phase of the order parameter $\rho_{\{G\}}$ for atoms and bond particles, choosing the reciprocal lattice vectors G that belong to the family of lattice planes $\{111\}$corresponding to the first Bragg reflection for atoms in a diamod-type lattice. Precisely the average value of the order parameter was measured according to

$$\rho_{\{G\}}^{(\alpha)} = \left\langle \frac{1}{N_\alpha m_G} \sum_{i=1}^{N_\alpha} \sum_{G \in \{G\}} e^{-i\ \mathbf{G}\cdot\mathbf{r}_i^\alpha} \right\rangle, \tag{3.34}$$

where $\mathbf{r}_i^\alpha$ is the position of the particle of kind α referred to the center of mass for the particles of the same kind in that configuration, m_G is the multiplicity of the star $\{G\}$. The value of this order parameter fluctuates around zero with a variance $1/N_\alpha$ in the liquid state, while for a solid it assumes a non zero real value. We also monitored the average position of particles during the simulation. As stated above, the system is in the liquid state up to a value of $V^* = 6$, as confirmed by the order parameter and from the observation that particles freely move in the simulation box. At $V^* = 7.5$ a sample equilibrated for a long time starting from the initial crystal remains in the crystalline state. From this observation we infer that, for the parameters chosen in the simulation, the melting coupling strenght is comprised between 6 and 7.5. In order to prepare the system in a disordered state, for couplings greater than 6, we quenched the system

to the desired value (7.5, 10 and 14) starting from a configuration obtained at $V^* = 5$ and annealed it for equilibration for about 40000 MCs, monitoring also the pair correlation functions every 10000 MCs, looking for systematic drifts in the structure. After the annealing we made longer runs to collect statistics; we refer to these samples as "amorphous", as we didn't observe crystallization in any sample, neither during the annealing, nor during data collection. The particles are seen to move around fixed equilibrium positions, as results from the measure of the Lindemann parameter, showing that we are sampling a restricted portion of configuration space that corresponds to a disordered solid. We measured also the correlation time between subsequent configurations, which is needed to determine precisely the statistical error in the simulation from the knowledge of the number of statistically independent configurations. The method proposed by Rahman and Jacucci[84] was applied to examine the istantaneous values of the internal energy at the first 100000 configurations (one for each MCS) after the equilibration or the annealing, and the values of τ_{corr} so obtained are listed in table 3.1.

TABLE 3.1 Correlation time τ_{corr}

V^*	τ_{corr} (MCS)
5	500
6	880
7.5	2700
10	4800
14	$\geq$5000

From the table we see that the statistics collected in the precedent preeliminary simulation $\approx$ 8000 MCS was insufficient at large couplings.

We performed simulations of about 500000 MCS at the values of V^* indicated in the table 3.1. Pair correlation functions of accuracy better than 1% were obtained. We checked the statistical errors in the pair correlation functions from their variance, computed considering the $g(r)$ accumulated from scratch every 10000 MCS. We did also simulations at $V^* = 22$, but now the system is sticky, and the Markov-chain sampling slow and with a long autocorrelation, thus the pair correlation function obtained have a much larger error.

A smarter sampling algorithm than the simple one employed here is required at high couplings, in order to sample efficently the phase space. A method that allows easily "bond forming and breaking" and changes the numbers of bonds efficently is needed. Some kind of umbrella sampling, with a large probability distribution might work.

Chapter 4

Results

4.1 LIQUID GERMANIUM

Localization of Bond Particles and Structural Trends

First we examine here the behaviour of the LAM model at constant density on varying the temperature, i.e. on increasing the coupling strength V^*, as it results from the analysis of structural trends in the partial pair correlation functions and structure factors. Our major aim in this presentation is to follow the process of localization of bond particles in bonds and to show that the degree of BP localization induce increasing directionality in the effective atom-atom interaction, leading to peculiar features in the structure. The calculations reported here were made solving the model in the liquid state by means of the HNC-integral equations, at a density and values of parameters, reported in table 2.1 as set 1, appropriate to liquid germanium.

On increasing the coupling strength, the atomic component A manifests a strong attraction to the BP component through the potential well present on its surface (see fig. 2.7), and one can gauge the degree of BP localization in this well from the values assumed by the main minimum of the pair correlation function $g_{AB}(\mathbf{R_{AB}})$ (see fig. 4.1). A main sharp minimum with value zero in this function, together with a first narrow and quite high peak signals the creation of a well

defined first coordination shell of BP around each A atom, and a slow exchange of particles from this shell with the rest of the fluid. In this sense we can say that these BP are temporary **localized** in the potential well at the surface of the A particle, the coordination number $N_{\alpha\beta}(R)$ being the number of BP trapped in it. They thus provide a preferred site of attraction to another A particle, that can form a bond by sharing the bond particle. This is what we mean saying that the model shows **association.** Directionality in the resultant A-A interaction is enforced when four BP are localized around that atom.

Figure 4.2 shows the partial pair distribution functions and the partial structure factors for coupling strength V^* equal to zero. These results can be compared with liquid structure in additive models for mixtures of hard spheres with very different diameters, for both neutral fluids[46] and charged fluids[85].

In both these cases, some degree of relative order of the two components is marked by a valley in $S_{AB}(k)$ in approximate correspondence with the main peak in $S_{AA}(k)$, while $S_{BB}(k)$(the structure factor of the small-sized component) is essentially featureless. As is evident from fig. 4.2, our choice of σ_{BB} by a tetrahedron rule (see formula 2.1) builds sharp structure in $S_{BB}(k)$and in $g_{BB}(r)$, while it preserves and somewhat strengthens the relative order of the two components. Localization of BP is nevertheless absent.

Figure 4.1 illustrate, starting from the A-B and A-A pair distribution function at $V^* = 0$, how localization of bond particles proceeds on increasing V^*, and shows the structural changes that it induces in the atomic component, down to strongly supercooled ($V^* > 7.5$) liquid states.

Bond particle localization starts to appear at ($V^* = 2$) and grows rapidly, with the exchange of bond particles between localized states and free states being rapidly suppressed and the atom-bond coordination number increasing towards 4. This is

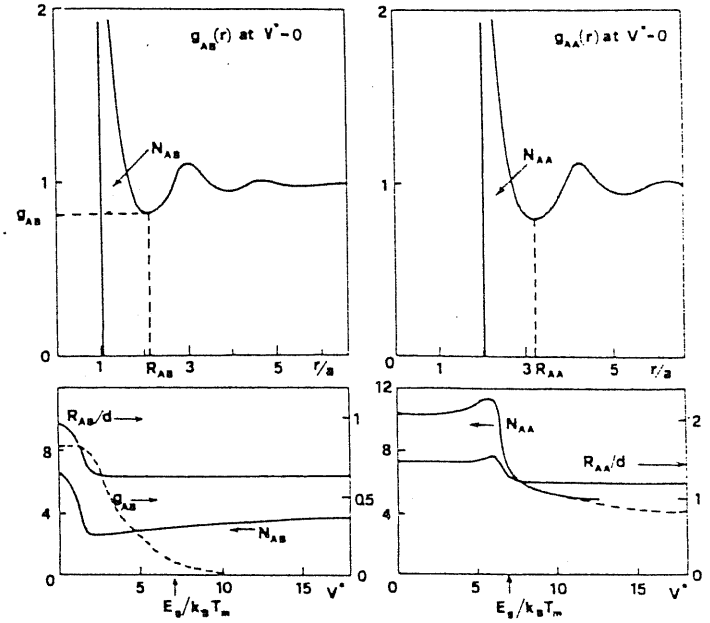

Fig. 4.1 – Schematic representation of bond particle localization and induced atomic structure changes with increasing coupling strenght V^* in the LAM. The top drawings show the atom-bond (left) and atom-atom (right) pair distribution functions at zero coupling strenght. The evolution of special features of these functions, as defined in the top drawings, is shown at constant liquid density in the bottom drawings. The dashed portion in the curve for N_{AA} shows the effect of reducing the density from that of freezing Germanium to that of compacted amorphous Germanium. The value $V^* = E_g/k_BT_m$ is marked on the bottom axes.

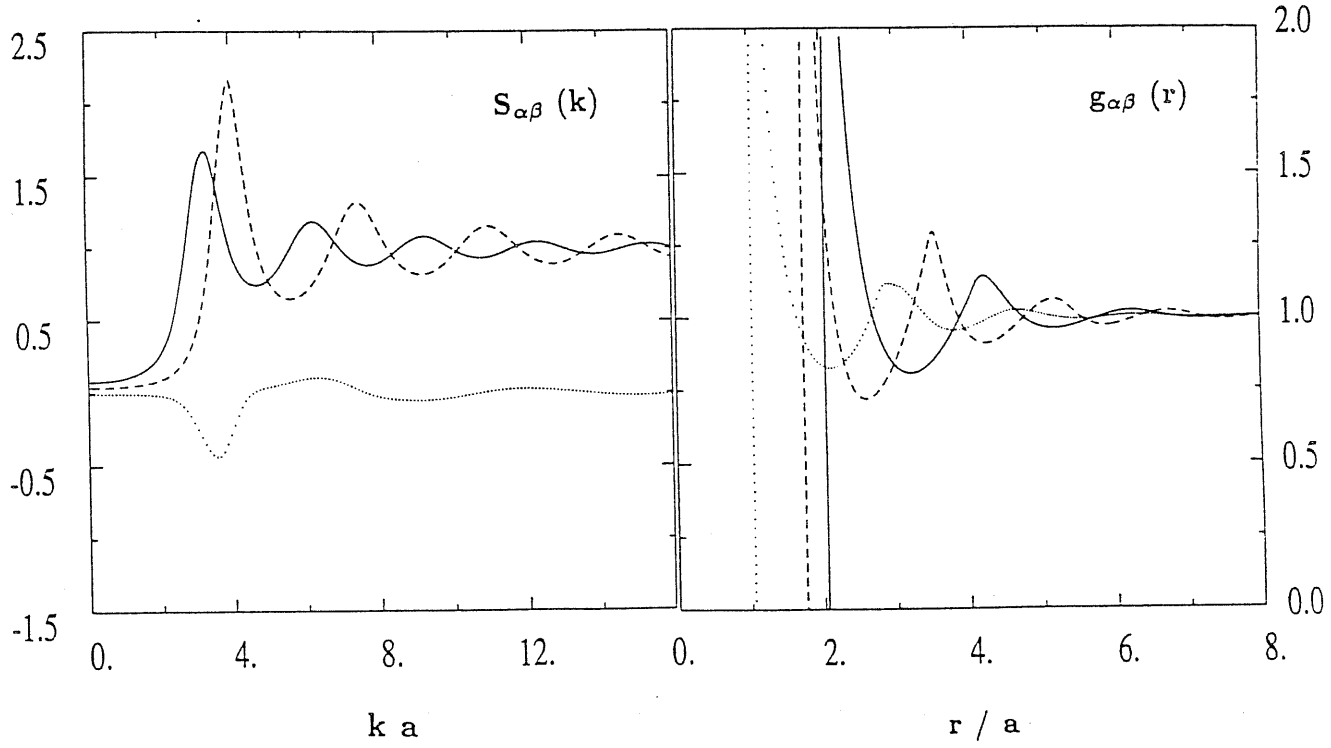

Fig. 4.2 – Partial structure factors $S_{\alpha\beta}(k)$ (left) and pair distribution functions $g_{\alpha\beta}(r)$ (right) for the LAM (set 1) at $V^* = 0$ in the HNC approximation. Full curves, A-A correlations; dotted curves, A-B correlations; broken curves, B-B correlations. Values of the peaks in $g_{\alpha\beta}(r)$ are: 3.65 (A-A); 3.04 (A-B); 6.02 (B-B).

signalled at ($V^* = 2$) by the rapid drop in R_{AB} and N_{AB}.

From $V^* = 2$ to $V^* \approx 5$ the potential well acts mainly as an ordering interaction between the components, as only g_{AB} is affected, showing the formation of well defined shells of BP around A atoms by a rapid drop in the value attained at its main minimum. Thus we can say, in a pictorial way, that in this range of couplings there is a certain amount of association of A atoms, although exchange of bond particles with the surrounding liquid is still consistent ($g_{AB} \approx 0.8 - 0.3$) and doesn't allow the formation of bonds with a lifetime longer than the characteristic time needed for diffusion.

The next rapid change in structural behaviour occurs for V^* in the range 6-7. Here the localization of BP becomes quite strong ($g_{AB} \approx 0.1$), as its also shown by the appearance in g_{AB} of a quite sharp and high first peak, with an height of ≈ 10 (to be compared with the value of 3 at $V^* = 0$) right at the position of the well minimum. This means that rather stable (with respect to the characteristic time of diffusion) bonds are forming between A atoms, the number of bonds being roughly proportional to $N_{\alpha\beta}(R)$, with an average of 3 bonds for each atom. The fact of having three BP localized **on average** means that there is a certain amount of atoms which have got four BP, and can form a number of bonds from 2 to 4. At this point a strong directionality in the Atom-Atom interaction is present for those atoms that are fourfold coordinated to BP. This is apparent in the changes occurring in g_{AA}, where the first coordination shells splits, with the appearance of a structure that grows on increasing coupling to constitute a second peak just in the place where the pair correlation function showed a minimum at $V^* = 0$. This is marked in fig. 4.1 by the sudden drop in the position of the main minimum R_{AA} at $V^* \approx 8$. The ratio between the position of this second growing peak, that develops in strongly supercooled states, and that of the main peak ranges from

1.5 and 1.6, and it compares well with the ratio between first and second neighbor atomic distance in a tetrahedrally bonded structure, that is the ratio between the edge of the tetrahedron and the length of the A-A bond (see fig 2.4) $\sqrt{\frac{8}{3}} = 1.63$. Upon further increase of V^* the coordination number N_{AB} slowly moves towards the value 4, while the localization of BP becomes essentially complete.

We can see from fig. 4.3 how the structural trends that we have followed from the pair correlation functions are reflected in the partial structure factors, on increasing coupling. Upon incipient localization of BP at $V^* \approx 2$, the valley in $S_{AB}(k)$ is shifted towards the position of the main peak in $S_{BB}(k)$, and a pre-peak grows in correspondence with the main peak in $S_{AA}(k)$. These features, together with the increasing depth of the valley, mark the increasing ordering between the components illustrated above.

More remarkable is the behaviour of the atom-atom structure factor $S_{AA}(k)$ that first becomes slightly asymmetric (V^* up to 5), then develops a shoulder at its right side for V^* in the range 6-7.5, where the splitting of the first A-A coordination shell occurs. On further increase this shoulder grows into a strong peak at essentially unshifted position, while the former main peak is reduced to a pre-peak at lower and lower wavenumbers.

We want to compare these trends with those observed experimentally in liquid germanium. A well known qualitative feature in the observed structure factor of liquid germanium near freezing is the presence of such a shoulder which is smoothed to an asymmetry in the peak shape at higher temperatures[48]. In figure 4.4 we show the structure factors for liquid germanium above freezing and amorphous germanium at room temperature from neutron diffraction experiments[12,50], plotted in units of the nearest-neighbour distance. The positions of the reciprocal lattice stars (Bragg reflections) of the diamond lattice are also displayed in the figure.

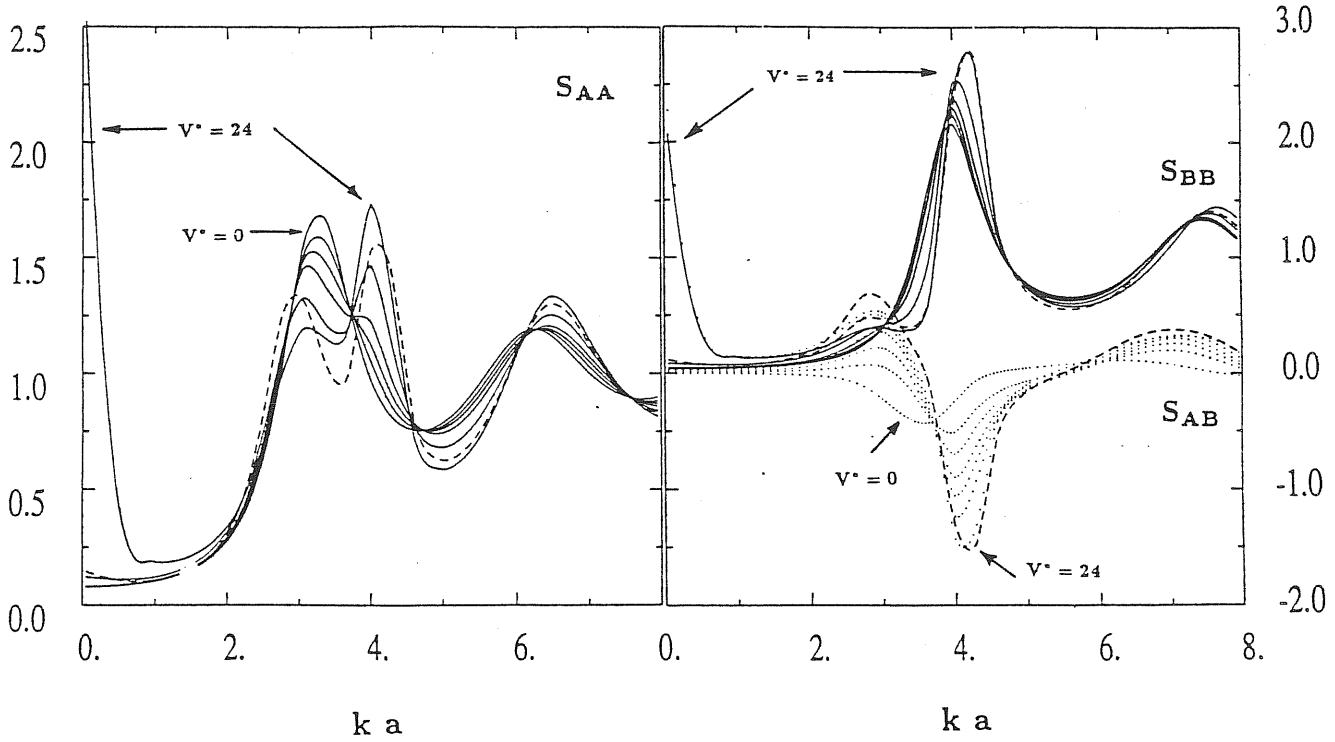

Fig. 4.3 – Partial structure factors $S_{AA}(k)$ (left), $S_{AB}(k)$ (right, dotted curves) and $S_{BB}(k)$ (right, full curves) for the LAM (set 1) in the HNC at a series of values of the coupling strenght V^* ($V^* = 0$, 3, 5, 7.5, 14, 24, the first and the last value being marked in the figures). The broken lines give the HMSA (with $b = 1$) results for $V^* = 24$.

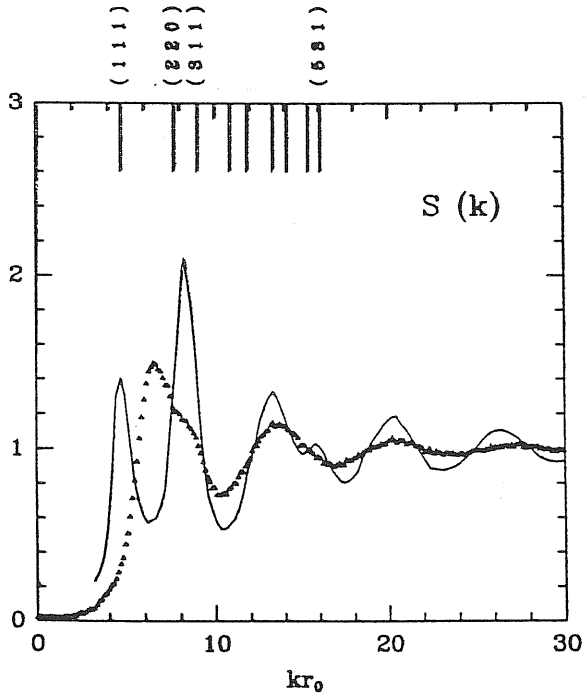

FIG. 4.4 Atomic structure factor of liquid Ge near freezing (triangles, from neutron scattering data of Salmon, ref.[12]) and of amorphous Ge at room temperature (solid line, from neutron scattering data of Etherington et al., ref.[50]). The vertical bars at the top show the location of the allowed Bragg reflections from the diamond structure, for each state of the material, the wave number k has been scaled with the appropriate value of the first-neighbour distance r_0.

The shoulder in the structure factor of the liquid is in approximate corrispondence with the (220) and (311) reflections, and in corrispondence the structure factor of the amorphous phase has its stronger peak. The position of the main peak in the liquid structure factor doesn't correspond to any Bragg reflection; it would approximately be near the (200) star of an f.c.c. lattice, which is a forbidden reflection in the diamond lattice. The amorphous phase shows its first peak just in corrispondence with the (111) Bragg reflection.

As one can see comparing figures 4.4 and 4.3 our model is able to reproduce the qualitative trends in the structure factors passing from the liquid to an amorphous phase that we represent on lowering the temperature as a supercooled liquid, but we are unable to describe in a qualitative manner with HNC theory the first peak in the structure factor of the amorphous phase. The same trend with temperature was also followed in the ab-initio Car-Parrinello simulation of Stich[15], with similar results.

As we can see in detail in the following sections we can make contact with the observed structure for the liquid near freezing and the result at ($V^* = 7.5$) while the structure of the supercooled liquid at $V^* \approx 20 - 24$ qualitatively resembles that observed in amorphous germanium.

Quantitative Comparison with Experiment

The partial structure factor of the model $S_{AA}(k)$ should be directly compared to the structure factor of Germanium as measured by neutron diffraction, as they are scattered only by the "atomic" component (scattering off nuclei), while X-ray are also sensitive to the electronic component. In a previous work [30] we made the comparison between the structure factor displayed by the model at $V^* = 7.5$ and the X-ray scattering data of Waseda[11], which were the only accurate data available to us in numerical form[13] at that time. Now accurate neutron scattering

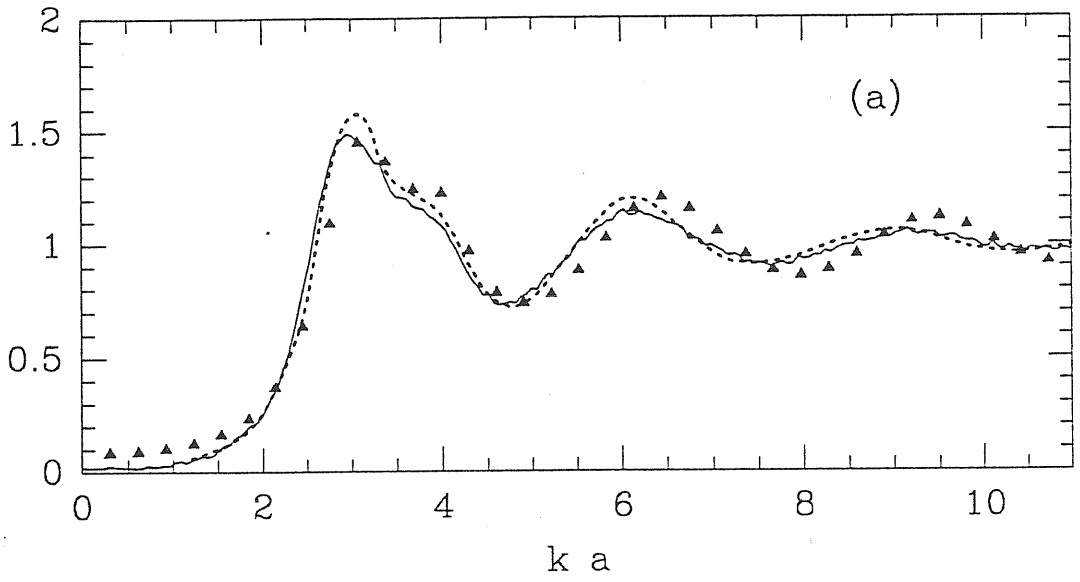

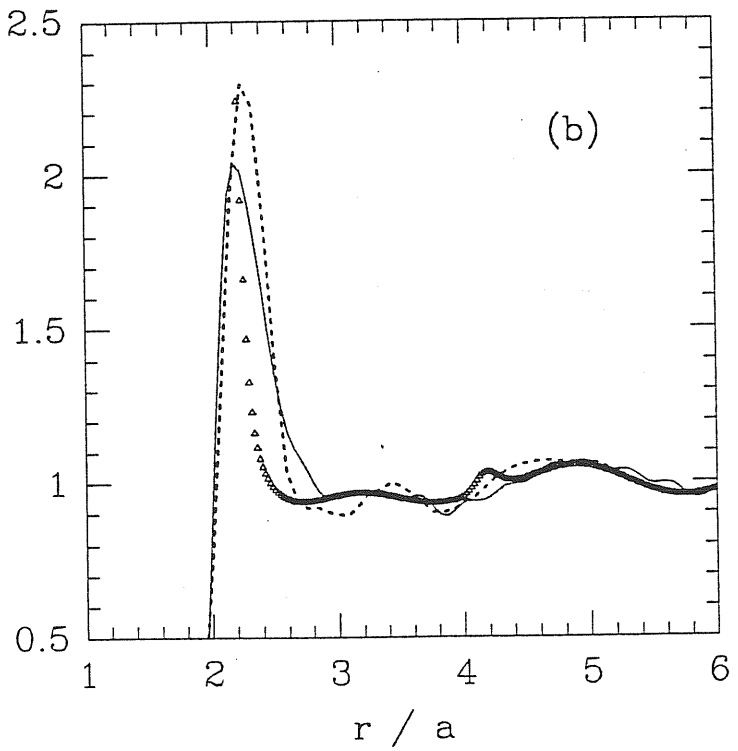

FIG. 4.5 **(a)** Partial structure factor $S_{AA}(k)$ and **(b)** pair correlation function $g_{AA}(r)$ of the LAM (set 1) at V^*=7.5 in the HNC (triangles) compared with experimental data for Germanium near freezing (solid line, neutron scattering work of Salmon, ref.[12]; dashed line, X-ray diffraction work of Waseda, refs.[11,13]. Lenghts are scaled with density, by a factor a=1.204 for the former and a=1.200 for the latter.).

data are available from the experiment of Salmon[12], thus we can compare our model directly with them. Figure 4.5 shows the data from both X-ray e neutron scattering experiments compared with our results.

From the figure it's apparent that there are slight differences between neutron and X-ray data, mainly in the height and the position of the first peak and its shoulder, and a little phase shift of the oscillations at high values of k. This difference can be only partially accounted for by the different data reduction algorithms employed in the two experiments, and should be attributed to the contribution of valence electron to the observed X-ray diffracted intensity[86].

From the figure we can see that there is a good qualitative agreement between our results and experiment, but we also notice that differences between the model's structure factor and the **neutron** scattering result amount to a scale factor. Then our result for $S_{AA}(k)$, contracted of a factor 1.037, were compared to the same neutron scattering data, and now the model fits quite well not only the first peak but also the overall shape of the observed results. Such a comparison is shown in fig. 4.6 for the partial structure factor $S_{AA}(k)$.

Thus in order to account for the experimental results in a quantitative way, we should repeat our calculation with values of the hard-sphere diameter A-A in reduced units $\sigma^*_{AA} = r_{AA}d/a$ (where r_{AA} is the value expressed in the first column of tab 2.1 and a is related to the density as explained in the previous section) enhanced by the factor 1.037. If we fix the bond length as $d = 2.68\mathring{A}$ from Salmon's experiment, discarding the previous value $d = 2.63\mathring{A}$ quoted in table 2.1, we need a density of $n_Ge = 0.0479\mathring{A}^{-3}$, that is 5% higher than the value of $0.0456\mathring{A}^{-3}$ found from experiment.

In conclusion the density required for the model to be in agreement with the diffraction data, once we have taken the bond length from the same experiment,

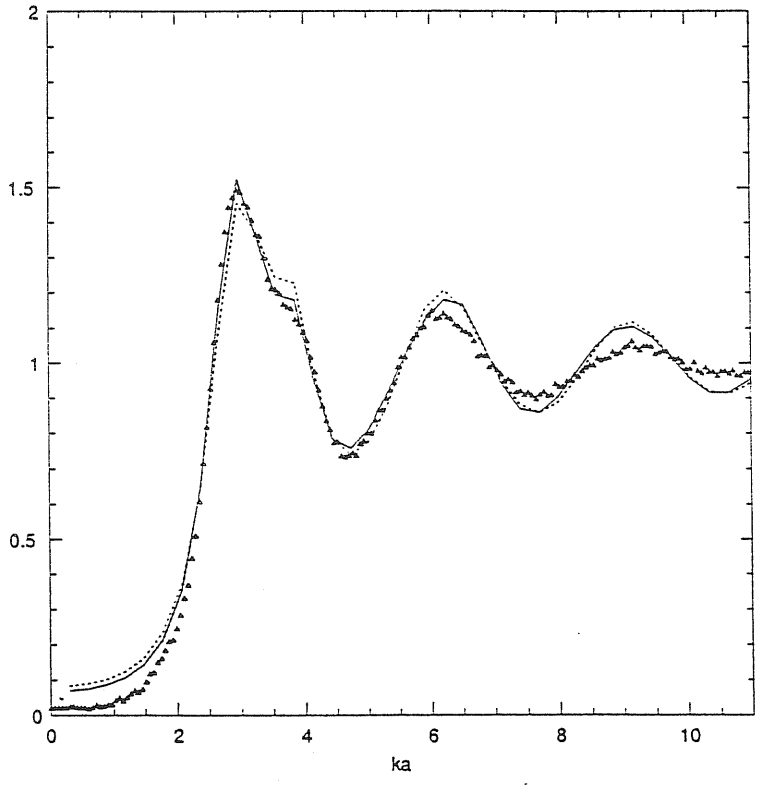

FIG. 4.6 Comparison of the experimental Structure factor of Germanium (triangles), from the neutron scattering work of Salmon, ref.[6], with Partial Structure Factor $S_{AA}(k)$ of the LAM in the HNC (dashed line) and in the TC-IHNC scheme at the second iteration for the self consistent determination of the elementary diagrams (solid line); the latter has been scaled by a factor 1.037, as explained in the text.

is higher than the experimental density of Ge. As the equilibrium density of a fluid at a given pressure is the result of a delicate balance between repulsive and attractive forces, it isn't strange at all that the rough schematization of repulsive interactions adopted in the model doesn't allow to predict the correct equilibrium density. It requires the adoption of more realistic repulsive potential to predict also the correct equilibrium density of Germanium.

We proceeded further on, asking whether the solution of the model by a more accurate approximation than the HNC closure could further improve the

agreement with experiment. We employed the scheme outlined in sec. 3.3, already used with success in previous work on molten salts[75],and we solved the integral equations derived from the closure relation (3.12). The bridge functions were determined as a crossover (see eq. 3.24, 3.25) between the bridge functions of an hard-spheres reference system (found in the PY approximation), and the first term in the expansion (3.13) $B^{(4)}_{\alpha\beta}(r)$ computed by the integral in formula (3.23) using as input the total correlation functions $h_{\alpha\beta}(r)$ of the HNC-solution. The mixing parameters $\xi_{\alpha\beta}$ where fixed at the main peak's position in the HNC solution. The ratio of diameters d_{11}/d_{12} and d_{11}/d_{12} for the hard-sphere reference system was fixed as well from the ratio in the peak's position. The only free parameter d_{12} was varied to enforce Thermodynamic Consistency (TC) between virial and fluctuation compressibility. From the solution obtained (I iteration) we computed again $B^{(4)}_{\alpha\beta}(r)$ and solved again the integral equations with it, to obtain a new TC solution (II iteration).

This solution is show in comparison with the HNC solution and neutron scattering data in fig. 4.6, and one can see that indeed a better agreement in S(k) is reached. We can make it even better by choosing a coupling of $V^* \approx 6.5 - 7$, in order to have less a marked shoulder.

We can conclude this section by stating that this model can fit the structure factor of liquid Germanium as well as the hard- sphere system is known to fit the structure factors of simple liquid metals and alloys[46]. We think that a better modelling of the real system can be achieved using A-A interactions more realistic than hard sphere repulsions.

4.2 Angular correlations

In the preceding discussion we inferred from the evolution of structural features shown in the pair correlation functions obtained with integral equation methods that effective many body-interactions among atoms set in due to the association of bond particles to Ge Atoms and consequently of atoms to atoms, caused by sharing a common bond particle. In particular from the observation that a second peak in $g_{AA}(r)$ appears and grows at a position correspondent to that of the second neighbours in a tetrahedral configuration, where the reference system (at $V^* = 0$) instead shows a minimum, we concluded that our model describes effective angular interactions among Atoms.

Additional informations on the short-range order can be obtained from higher correlation functions. In our case the triplet correlation function $g^{(3)}_{AAA}(\mathbf{r_{12}}, \mathbf{r_{13}}, \mathbf{r_{23}})$ is particularly important since we supposed that angular correlations arising from covalent bonding effects, which show angular dependence, are reproduced in our model. We gauged the amount of angular correlations by measuring the bond angle distribution function $g_3(\theta, r_c)$ from the configurations generated in our Monte Carlo simulation. Here θ is the angle between the two vectors that join a central particle with two neighbours at a distance less than a defined cutoff r_c. In figure 4.7 we see that the bond angle distribution function for the reference system which has no angular correlations, is rather broad, showing a peak around 60 degree, which is expected from a close packed sistemation of the atoms in the first coordination shell. At a value $V^* = 5$ where association is already important, as indicated by the high values of the peak in g_{AX} at the distance d, the peak at low angle decreases. A better understanding is obtained taking as cutoff the value of the bond length $2d$ in the model.

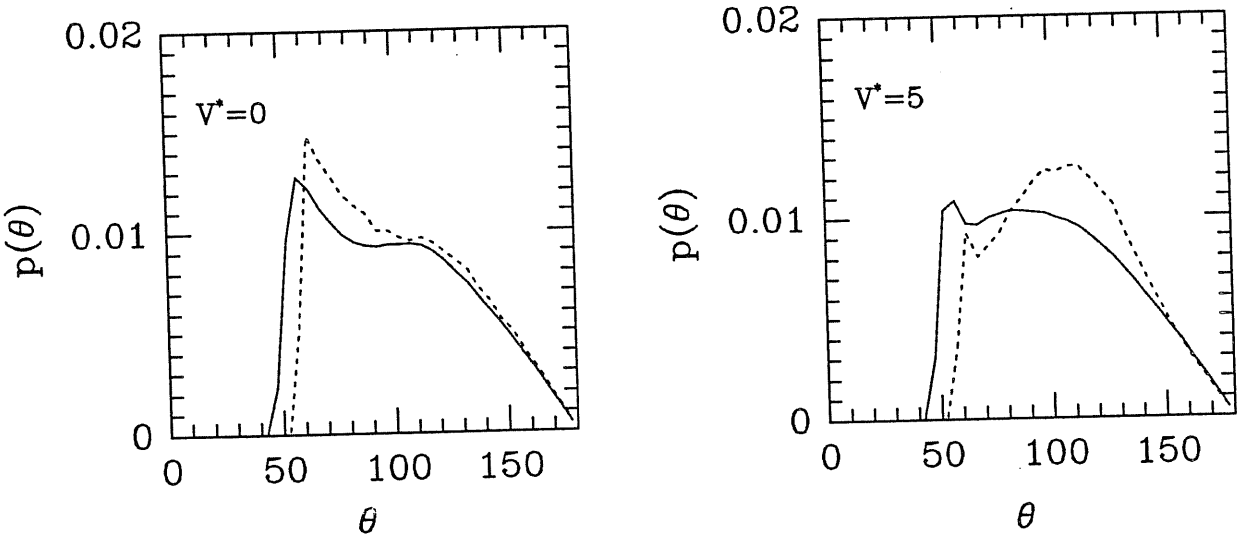

FIG. 4.7 Effect of the association in the angular distribution of Ge Atoms: the bond angle distribution function $g_3(\theta,r_c)$ is shown for a value of the cutoff at the minimum of the corresponding pair distribution function (solid line) and to the covalent cutoff (defined as $\approx 2d$). The left panel corresponds to the hard spheres reference system obtained when we set the coupling $V^*=0$, the right panel to a value where association of Germanium atoms through bond particles has already set in.

This is indicated in figure 4.8 by the dashed lines. As a consequence of an increasing probability of bonding two atoms by a shadow, triplets of atoms A-X-A-X-A are formed, with a preferred bond angle angle around the tetrahedral angle $\approx$ 109 degrees. We can follow the evolution of bond angles with lowering the temperature in figure 4.8. At progressively lower temperature the tetrahedral local disposition of atoms is preferred, ending in an amorphous solid with tetrahedral local coordination. The close packed fluctuations are signalled by the peak at 60 degrees, which is absent in models where explicit three body angular forces are included. In the same figure we show the temperature dependence of the angular correlations detected in the ab-initio simulation of Stich et al.[15] on Silicon. The observed trends in our model are the same as in the ab-initio simulation.

We notice that also pair potentials used in the treatment of liquid metals can give some preference to tetrahedral local coordination in the liquid, by adjusting

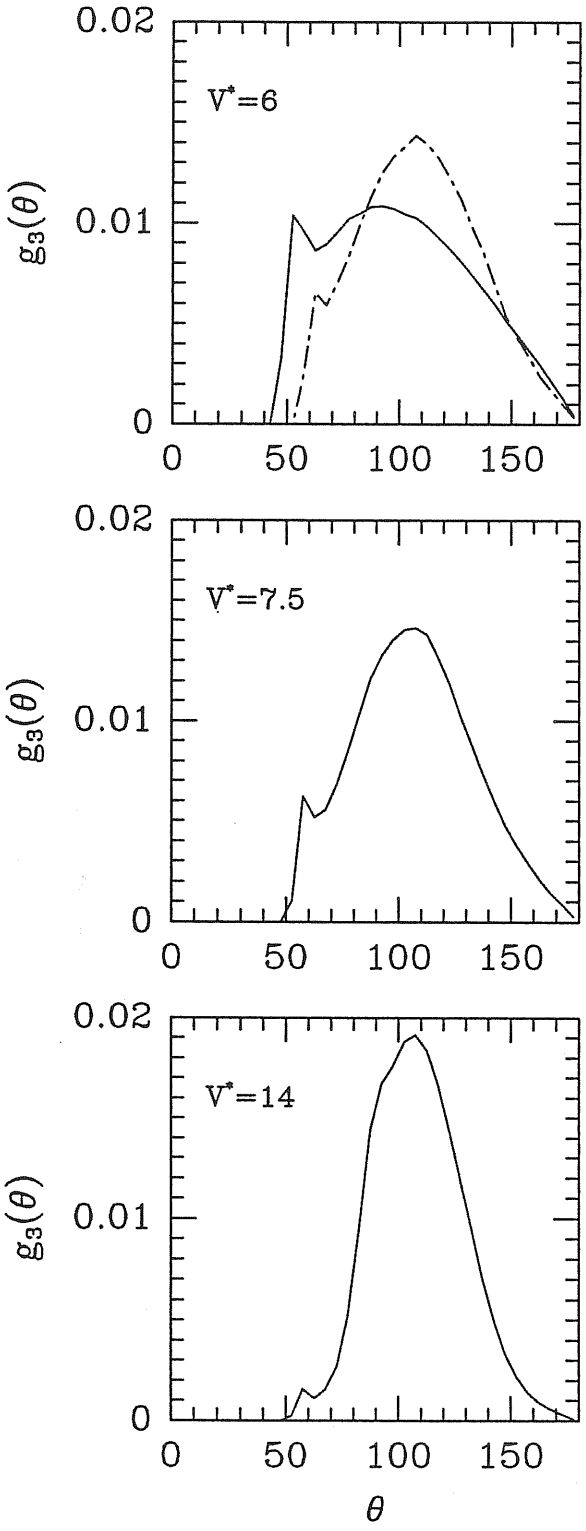

FIG. 4.8 Temperature dependence of the bond angle distribution function $g_3(\theta,r_c)$; **left panel:** results for the LAM (set 2) from Monte Carlo simulations at different values of V^* (V^*=6 corresponds approximatively at the freezing temperature for this set of parameters). **right panel:** results for liquid and amorphous silicon from the ab-initio simulation of Stich et al. ref.[15] **(l)** T~1800 K (above freezing), **(a)** T~1550 K (just below freezing), **(b)** T~1250 K and **(c)** T~950 K. The solid line corresponds to a cutoff radius r_c at the minimum of g_{AA}, the dashed-dotted line to the covalent cutoff, defined respectively as the bond length d in the model or the maximum bond length observed in the simulation of the liquid.

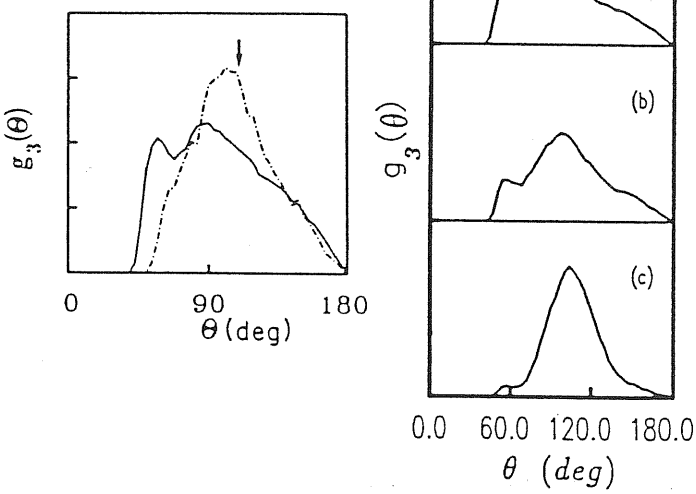

the position of the repulsive core and the attractive well minimum in a suitable way, and can reproduce angular correlation similar to the upper left panel in fig. 4.8 as in ref.[18], but they can't give rise to true angular correlations, and don't stabilize a tetrahedral structure on lowering temperature.

4.3 Accuracy of the Integral Equation Method

We shall discuss here the work done to test the quality of the structural predictions made by the liquid-structure theory in the LAM, for values of coupling corresponding to liquid states down to values in the supercooled- liquid region, and our attempts to improve the approximations involved by the use of empirically-mixed closures or the inclusion of bridge functions, in order to predict the structure with the best accuracy.

At this purpose, we made some Monte Carlo simulations in the canonical ensemble of the LAM at different values of coupling ($V^* = 1$, 5, 7.5, 10, 14, 22) choosing the parameters of the model as set 2 in table 2.1, where the tetrahedron rule has been somewhat relaxed, and the density was fixed to a lower value than in the liquid near freezing (it is precisely the density of the compacted amorphous phase). This choice for the density and for σ_{BB} is motivated by the need to accelerate the equilibration rate and to reduce the length of the sampling runs in the simulation. Further details on the simulation were given in chap. 3. The localization process of bond particles shows the same features as shown before at liquid density, but the splitting of the first coordination shell, that is the emergence of a new closer second coordination shell appears before, at $V^* = 6 - 6.5$ with respect to $V^* = 7 - 7.5$ for parameters at liquid density.

Figure 4.9 shows the HNC and Monte Carlo results for $g_{\alpha\beta}(r)$ at two different

values of the coupling strength, $V^* = 5$ in the liquid region that correspond to the onset of strong association, and $V^* = 10$ in the supercooled region. It is seen that the HNC solution is still in full quantitative agreement with the simulation up to the value $V^* = 5$, except that the value at contact in g_{BB} is slightly higher in the HNC. The TC solution found in the HMSA approximation is very similar to the HNC and to the data over this range of V^*.

On the other hand we found that from this value of V^* on, some quantitative discrepancies between HNC and simulation arise. Let's summarize with the help of the case $V^* = 10$, shown also in fig. 4.9, the other work done for greater couplings. We find in general that a good agreement between HNC and simulation persists up to large values of V^* for $g_{AB}(r)$, $g_{BB}(r)$, except for the height of the first peak (lower in HNC for A-B correlation, and higher for B-B correlations than in MC) slight asymmetries in the first peak of $g_{AB}(r)$ and in II peak of $g_{BB}(r)$ (that show also a lower value) for the HNC solutions. However there is a discrepancy, increasing with coupling, for $g_{AA}(r)$ in that the HNC seriously underestimates the structure of its second peak, that is gives too high a value of the main minimum, and too low a value of the II peak. Thus the HNC poorly predicts the progressive formation of the second shell of neighbours arising from the correlations of two atoms bonded to the same atom.

In parallel with the progressive underestimation of the A-A structure, another discrepancy is observed in the prediction of the A-B association as measured by the value of the first peak in the A-B pair correlation function. In table 4.1 we compare the values obtained from HNC with the results of the MC simulation. For couplings greater than 5, the amount of A-B association is underestimated in the HNC, and as a consequence also the amount of A-A bonding due to this association results lower, and A-A correlations are depressed. This fact clearly suggests that

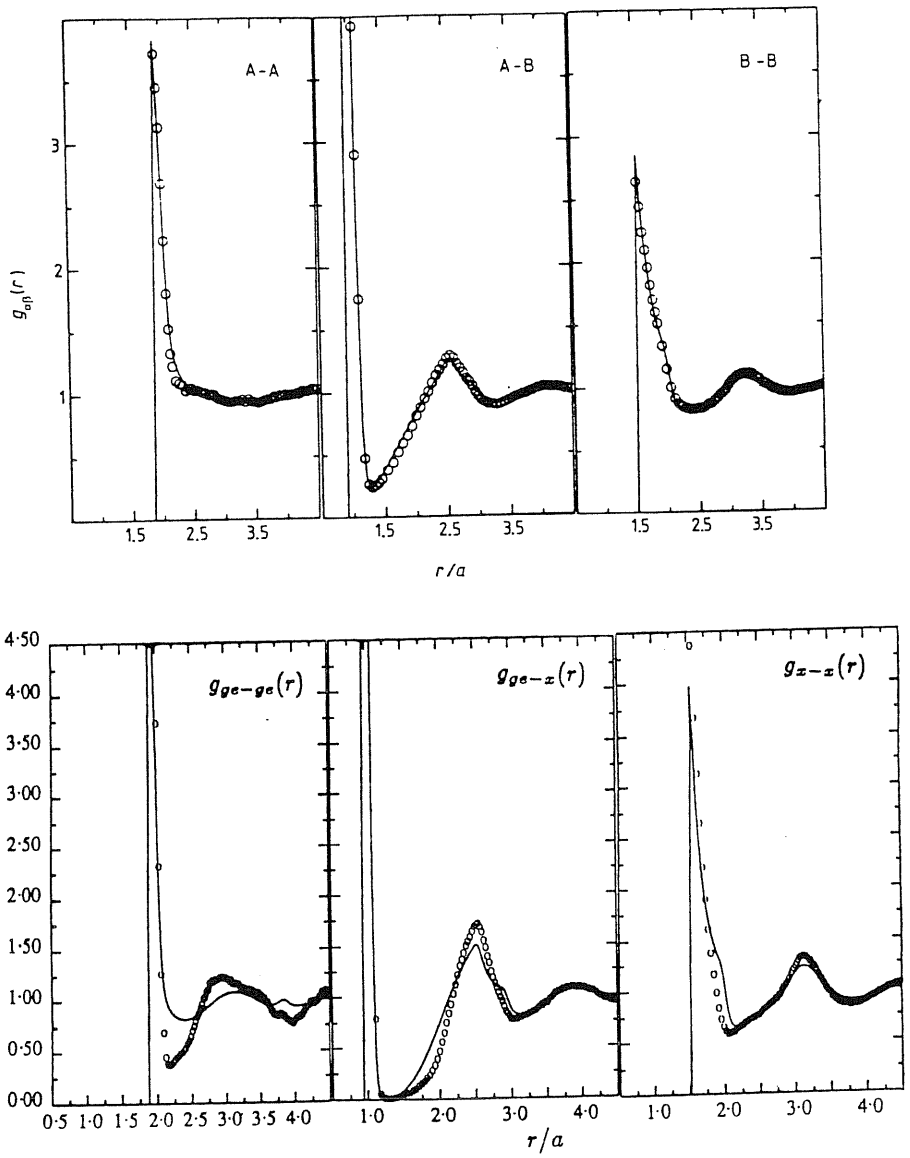

FIG. 4.9

Accuracy of the HNC approximation: Partial pair distribution functions $g_{\alpha\beta}(r)$ for the LAM (set 2) in the HNC (broken line) compared with Monte Carlo results (solid line). The HNC is still accurate in the medium range at $V^*=5$ (upper panel), while for values greater than 6 it is inaccurate, mainly for A-A correlations; The lower panel corresponds to $V^*=10$.

at variance with simple liquids some further attraction must be present at least in the Bridge function B_{AB}.

V^*	HNC	MC
5.	10.4	10.8
10	18.	20.9
14	23.	26.

Table 4.1
Value of the first peak in g_{AB} pair correlation function for different temperatures, as given by HNC theory and measured in MC simulations .

Defects of the HNC approximation are not remedied by the HMSA, that in the supercooled region performs worse that the HNC, predicting even higher values of the main minimum in g_{AA}; in addition it shows the disappointing feature of yielding a negative value for $g_{AB}(r)$ at its main minimum; PY approximation performs in a similar way.

A major drawback of the HNC approximation is shown in fig. 4.10 for the LAM at liquid density (set 1), in relation with the behaviour of the compressibility ξ_T evaluated from the fluctuation formula (3.26) and from the virial route, by numerical differentiation of the virial equation of state (see eq. 3.27). The increasing degree of thermodynamic inconsistency between the two routes showed by the HNC solution is evident from the fact that, while the virial compressibility increases only slowly up to $V^* \approx 20$, the fluctuation compressibility shows first a more rapid linear increase and then seems to diverge at values of $V^* \approx 22$ for the parameters quoted; the same behaviour is shown by the HNC solution at $V^* \approx 14$ for the parameters chosen in the Monte Carlo simulation (set 2).

It seems that the HNC somewhat misplaces the location of the spinodal line between the liquid and the solid phase in the (ρ, P) thermodynamic plane, that is the loci of points in which the the second derivatives of the free energy with respect to volume (or density) is zero, lines at which the compressibility diverges and that

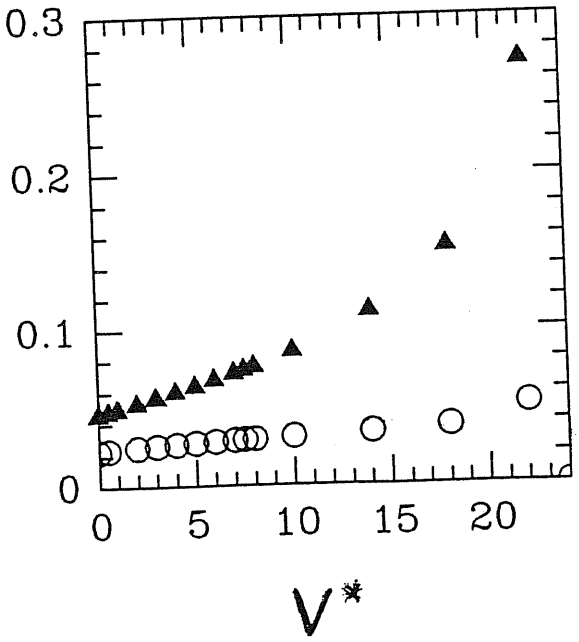

FIG. 4.10 Thermodynamic consistency in the HNC: inverse isothermal compressibility $(\partial\beta P/\partial\rho)_T$ of the HNC solution for LAM (set 1) from fluctuation formula (3.26),triangles, and from virial formula (3.27), circles, on increasing coupling V^*. The result is similar for set 2, but the sudden increase in $(\partial\beta P/\partial\rho)_T$ starts at $V^*\approx 13.5$.

marks the region of mechanical stability of the liquid state in the supercooled - metastable region. This prevents to obtain solutions in the HNC approximation for larger values of coupling in the supercooled region, due to the intrinsic sensibility

to the value of the fluctuation compressibility shown by the numerical algorithm of solution, that becomes unstable when this value is high enough. It can be largely remedied by the adoption of any TC empirical-mixed closure like the HMSA or by the inclusion in the closure relation of the bridge functions of hard spheres like in the thermodynamic consistent MHNC approach.

As we have assessed the importance of including the hard-sphere bridge function for the thermodynamic consistency, and in essence for the possibility of finding solutions for the LAM in the extreme supercooled region, we turn to the accuracy on the prediction of the structure.

For this analysis we solved the TC-IHNC equations, iterating the scheme to self consistence in the determination of Bridge functions, for the couplings $V^* = 6, 7.5, 10$. The iterative process was stopped when the difference between the old and new determined bridge functions was comparable to the numerical accuracy of our algorithm for computing them from the $h_{\alpha\beta}(r)$.

In the first case we found a good agreement with MC simulations both in the amount of A-B association and in the A-A structural features, and reached the consistency in two iterations, the first one being very close to the final result. In the second case the amount of association is again good, but four iteration are needed to get the self consistency in the elementary diagrams, and stopping at the first step of the procedure accounts only for half of the final result. The agreement in the predicted A-A structure is less satisfactory as the second coordination shell splits, and it has slightly less structured than in MC simulations. We shall comment these discrepancies, and the main features presented by the Bridge functions of this model presenting the results for the latter case examined, namely $V^* = 10$.

The resulting structure at convergence on $g_{\alpha\beta}(r)$ is shown in fig. 4.11a-c

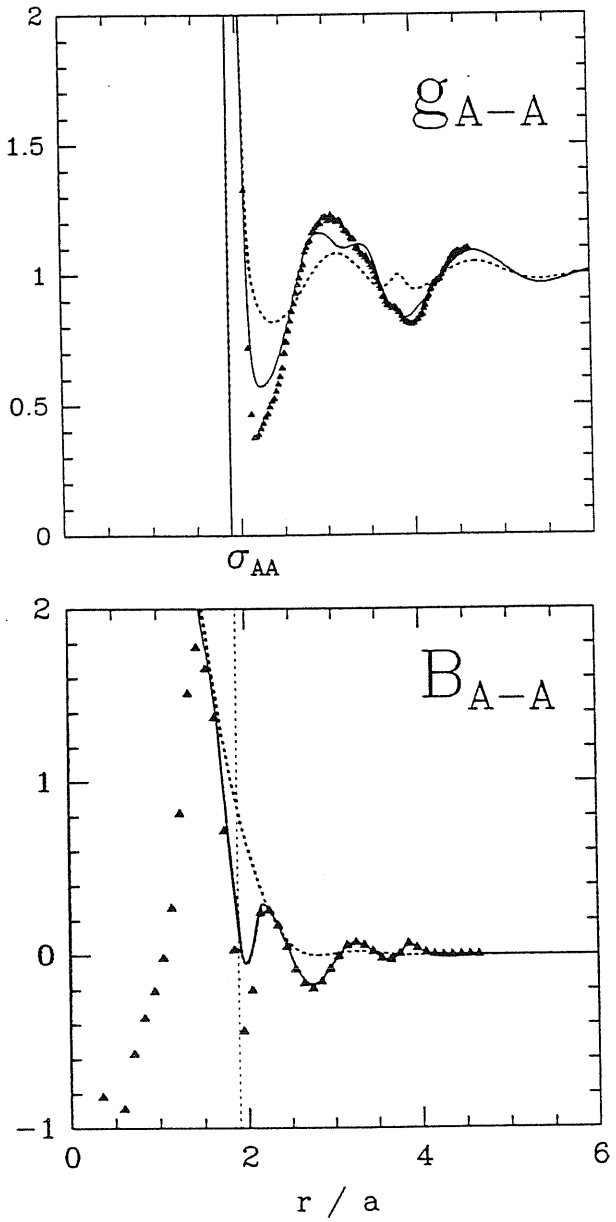

FIG. 4.11a Results for the TC-IHNC approximation at convergence on bridges (IV iteration) applied to the LAM (set 2): **upper panel:** Pair correlation function g_{AA}; the solid line is the TC-IHNC result, dashed line the HNC and triangles MC data. **lower panel:** $B^{(4)}(r)$ computed from eq. (3.23), triangles; PY bridge functions for the reference system, dashed line (the hard sphere diameter for the reference system is also displayed); crossover between them (eq. 3.24), solid line.

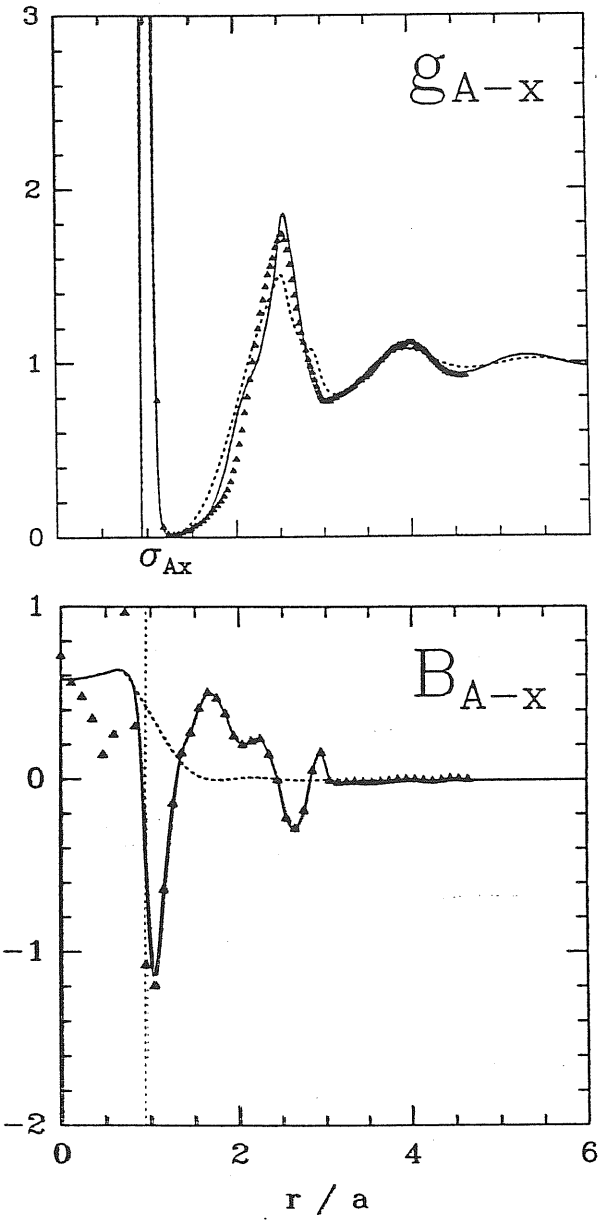

FIG. 4.11b The same as in the fig. 4.11a for: **upper panel:** Pair correlation function g_{AB}. **lower panel:** the corresponding Bridge functions.

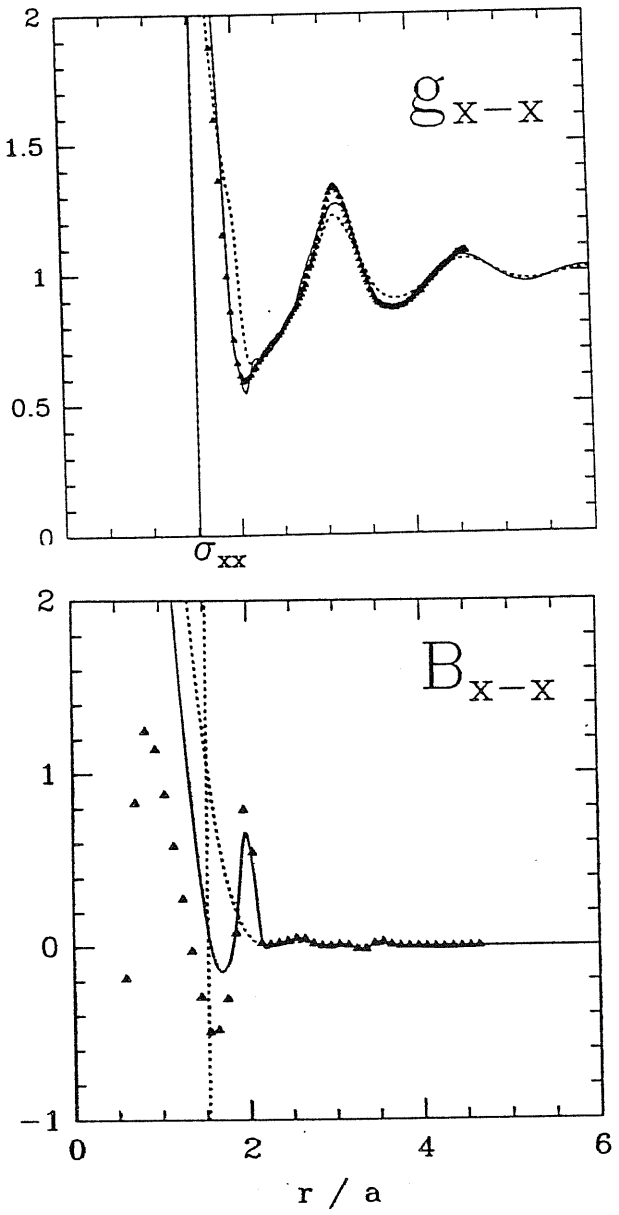

FIG. 4.11c The same as in the fig. 4.11a for: **upper panel:** Pair correlation function g_{BB}. **lower panel:** the corresponding Bridge functions.

together with the bridge functions, where also the crossover between the computed elementary diagrams $B^{(4)}$ and the short range "universal part is displayed. The three bridge functions are characterized by a strong structure at intermediate range, with an attractive part at the position of the first peak, which is particularly marked in $g_{\alpha\beta}(r)$, followed by a peak in the region of the main minimum, particularly evident in $g_{BB}(r)$.

Let's analyze the consequences of these features on the structure. The effect of the bridge functions on g_{AB} and g_{BB} is to eliminate the residual discrepancies with the simulation; the discrepancy remains in the value for the B-B peak that now is too low (3.51) in comparison with MC (5.28) and even worse than in HNC (4.19). The degree of association is not completely recovered since the peak in A-B is now 19.7, and this results also from the examination of the g_{AA}, where the structure is not fully recovered and in particular the second coordination shell is not well accounted for.

The TC-IHNC gives an overall improvement over the HNC, which could not be obtained with other integral equation schemes. It seems that the largest discrepancies of HNC can be also roughly accounted for if one simply rescales the A-B well depth, and one puts some repulsive hard-spheres like bridges in A-A and B-B only.

As the present determination of the bridge functions was quite accurate, and the discrepancies are outside the statistical error in our simulation, we should conclude that they are entirely due to terms neglected in the scheme that replaces $B_{\alpha\beta}(r)$ with $B^{(4)}_{\alpha\beta}$ as given by formula (3.23). To trace the origin of the remaining discrepancy, we should remind now that $B^{(4)}(r)$ is only the first term in the expansion (3.13) of $B(r)$, whose expression is given in formula (3.15), involving the $c^{(3)}(\mathbf{r_1}, \mathbf{r_2}, \mathbf{r_3})$ and that the relation used by us (eq. (3.22), (3.23)) can be derived

from it making the approximation (3.21). This simple factorization of $c^{(3)}$ might result inaccurate in our case. It is likely that higher order correlations are equally important, leading to some non negligible contributions of higher order terms in the expansion (3.13) at intermediate range. We shall give here an argument that strongly supports this conclusion.

The bridge functions $B^{(4)}_{\alpha\beta}$ take into account correlations between four particles, as one can see by the considerations of the diagram that correspond to the integral in the expression (3.23a). Now let's consider the kind of correlations present in a limiting case, that is in the solid phase. Rings of 6-atoms are present in the tetrahedral structure of the crystal, and it is evident that similar correlations are also strong in the amorphous phase. These correlations in the ring are described by terms in the bridge function's expansion (3.13) of order higher than 4.

It is very likely that to treat sticky interactions like our A-B potential it is better to take into account steric hinderance from the beginning in the derivation of the integral equations through an appropriate topological reduction, like it is done in Wertheim's scheme for associating objects[23].

4.3 STRUCTURE OF THE SUPERCOOLED STATES

We want to contrast here the results obtained in the LAM for high values of the coupling parameter V^*, to the experimental structure of amorphous Germanium. Usually amorphous Germanium is prepared by non-equilibrium techniques, like deposition from a gaseous phase onto a cold substrate. It's not possible to prepare it by fast cooling from the melt by usual fast-cooling-techniques[10], because it has a strong tendency to crystallize. Nevertheless one can think of obtaining it

by pulsed laser techniques as it was done for Silicon, by means of a short laser pulse that melts a portion of the solid, that is suddenly cooled very fast by the surrounding material. To this kind of experiment do correspond the simulation studies, made with various techniques and potentials, quoted in the introduction. It's likely that a well annealed sample prepared by deposition techniques tends towards the structure of a quenched 'glassy' material, that is essentially a system out of equilibrium because of long time-scale of its relaxation processes. Such a system is like a liquid with an arrested dynamics, and its average (spatial average) structure can be compared with the average structure of the ideal metastable-state of a supercooled liquid at the same temperature, as determined for example by the integral equations method. In this spirit, we make here such a comparison between a supercooled liquid and the actual structure of amorphous Germanium.

We saw in section 4.1 that the supercooled state of the LAM at liquid density reaches an high degree of localization of BP, being the number of bonded atoms slightly smaller (N_{AB} being 3.7), with a number of atoms in the first coordination shell (not yet sharply distinguished from the arising second coordination shell, as one can see from the value at the main minimum of g_{AA} not yet zero) of ≈ 5. In order to make contact with the observed coordination number, one as to take into account the reduced density of Amorphous Germanium, and we solved the integral equations at this reduced density (set 3) in the HNC down to last value of coupling at which the HNC has solutions ($V^* = 22$). The high degree of association present in the system due to bonding of atoms, is signalled by the sharp, high first peaks in g_{AA} and g_{AB}, of values 13 and 25 respectively, to be compared with the value 3 of the hard sphere liquid at zero coupling strength. The coordination number atom-atom N_{AA} now tends towards the value 4, while the bond-bond N_{BB} reaches the value 7, not too far from the value corresponding

to a tetrahedral structure (N_{BB} =6).

In Fig. 4.12 we show the structure predicted by the HNC for $S_{AA}(k)$ and $g_{AA}(r)$ in comparison with the S(k) and g(r) from the neutron scattering data of Etherington[50]. The HNC result represent only qualitatively the features in g(r), with peaks in the correct positions but too low structure, and in S(K), the main discrepancy being the height of the first diffraction peak, and the position of the pre-peak. It's also evident the effect of the thermodynamic inconsistency, in the low k part, that can be remedied by the adoption of any TC closure, like in the case shown in fig. 4.3 for liquid densities, where the HMSA solution is illustrated, showing a better behaviour at low k, and a more marked separation between peaks than the HNC solution.

The next step was to use a bridge function obtained from the crossover between a reference hard-sphere bridge function at low r and the $B^{(4)}_{\alpha\beta}$, determined from the HNC solution. The comparison with experiment for S(k) (see fig. 4.12) shows that the structure of the pre-peak is better resolved, but the solution doesn't achieve yet quantitative accuracy. This is connected to the fact that the g(r) in the solutions determined until now with the integral equation method doesn't show a second peak clearly resolved from the first one. The pre-peak and the main peak in the structure factor essentially arise from the presence of the main peak and the second peak, that is from correlations connected to the short range tetrahedral order, as can be shown by back transforming the g(r) truncated after the second minimum[50]. Thus the failure of integral equation method in providing an accurate descriptions of the second peak in g(r) explains its failure in providing an accurate description of the pre-peak position in S(k).

At the present state of our investigations it seems that only resorting to Monte Carlo simulations an accurate quantitative comparison with experiment can be

attempted. TC-IHNC provide at the first iteration too deep a valley in A-B elementary diagram that doesn't allow us to solve the integral equations.

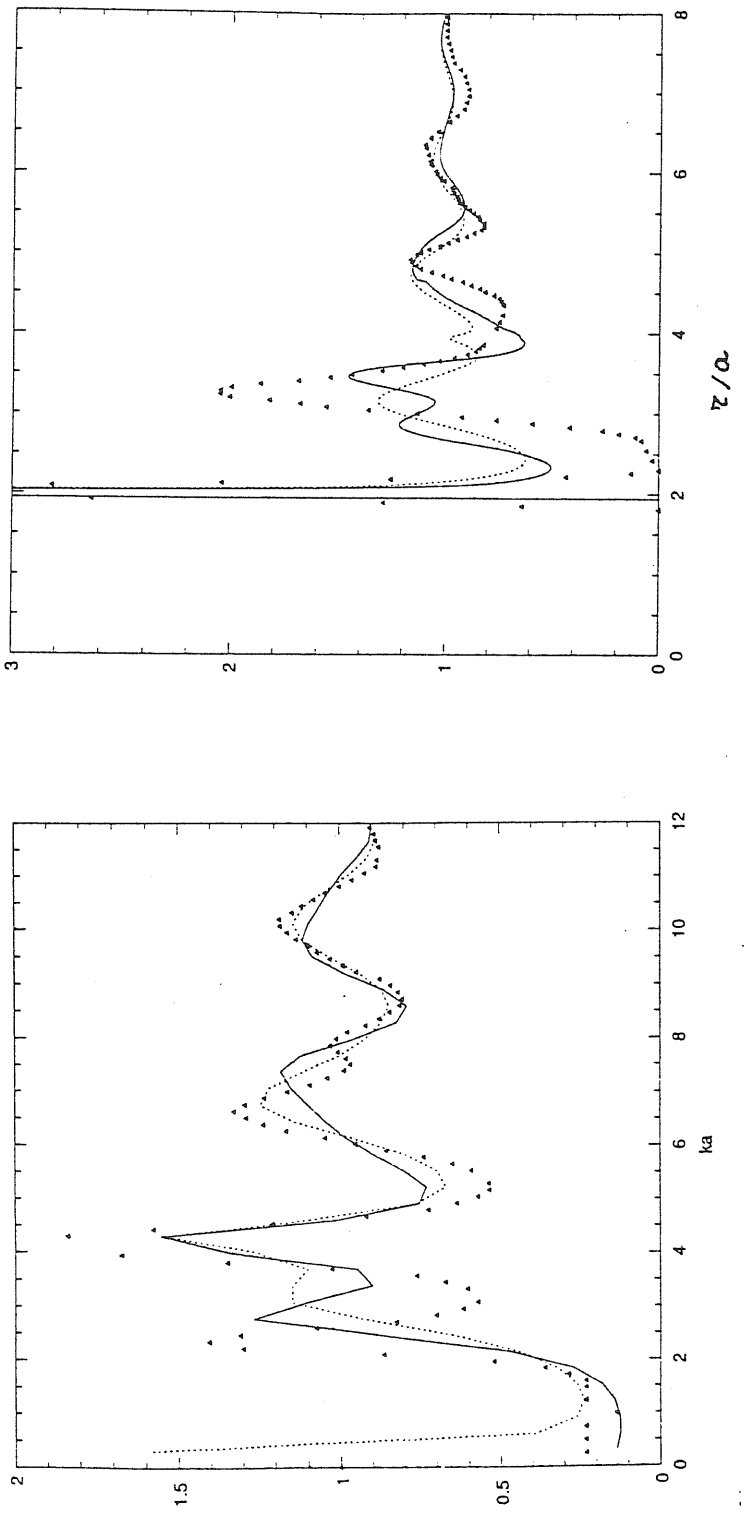

Fig. 4.12 – Structure factor $S_{AA}(k)$ (left) and pair correlation function $g_{AA}(r)$ (right) of the LAM (set 3) at $V^* = 22$ and the experimental structure factor S(k) for amorphous Germanium (triangles), in reduced units. Solid line, TC solution (see text); dashed line, HNC solution. Data are from the neutron scattering work of Etherington, ref.[50]. The scaling factor a is 1.229.

Chapter 5

Conclusions

In this thesis we presented an elementary, primitive statistical mechanical model showing in the liquid phase both association and directionality in the interactions in a variable degree on varying the temperature, which is meant to represent in a semiclassical way the structural consequences of the incipient electronic localization process that occurs near freezing in the melts of IV group and III- IV semiconductors.

This aim was achieved introducing, in analogy with BCM used in the solid state, a Bond Particle component in addition to the atomic one, subjected to localization between two different atoms with the constraint that the maximum coordination number possible is of 4 BP around an atom, an 2 atoms around a BP. In particular we explored a representation of the model, the Localized Attraction Model, consisting essentially of a mixture non-additive hard spheres where the atomic component shows on his surface adhesion to the BP component, in the form on a narrow, spherically symmetric well. This permits to represent the characteristic fluctuations towards local tetrahedral configurations present in the liquid near freezing, due to the process of forming and breaking of covalent bonds, that was shown to be present by the recent first principle molecular dynamics simulation of Stich and Car on liquid Silicon[15]

The inclusion of the BP component permits to treat an effective directional, many body interaction between atoms by the introduction of only pair interactions between components, and allowed us to employ the formalism of standard liquid

state theory (integral equation method) to explore the structural features of the model.

We showed that this model shows quantitative agreement in describing the structure of liquid Germanium near freezing, as results from the form of the neutron scattering structure factor. A picture of a restructuring network of bonds in the liquid emerges from the model, that is similar to ideas arose in the past in the study of water. The peculiar features of the structure factor arise from correlations between atoms belonging to tetrahedral units temporary forming in the liquid. The model offers the possibility to follow the build up of a disordered network by the connection of these units on cooling, towards the formation of a disordered solid-like fourfold coordinated network structure.

The importance of the effective angular correlation in the melt an their variation with temperature have been studied by Monte Carlo simulations. A point of interest for further work on the model is connected to a better modelling of germanium that could be obtained substituting the hard-sphere atom-atom interaction with more realistic repulsions. The development of Monte Carlo methods to sample in an efficient way the configuration space of the primitive version of the model constitutes another point that deserves further investigations.

From the statistical mechanical point of view, we explored the accuracy of the structural prevision made by the HNC closure, and we can conclude that it is able to give semi-quantitative agreement in the liquid state up to freezing when compared with the results of a restricted set of Monte Carlo runs (made mainly in the liquid region and partially in the supercooled region). The agreement can be made quantitative in the liquid state, until the association is low, by the inclusion of appropriate bridge functions in the closure relation. This method, even if represent a valuable tool in the exploration of the accuracy of the model, demands

an higher computational effort than common algorithms for solving integral equations. Other commonly used closure relations were found to be inadequate. Thus it should be interesting to explore the possibility of obtaining quantitative results for structure and thermodynamics by means of integral equations for associating liquids like in Wertheim's scheme.

The accurate numerical evaluation of elementary bridge diagram for the system of interest, that involves a five-dimensional integration over functions with one very high and narrow peak, was a delicate point that required a considerable effort. It was shown that in case of medium and strong association the elementary diagrams departs consistently from the simple "universal" behaviour at short range, and for high association higher order diagrams became also important.

It was explored, for the first time to our knowledge, the achievement of self-consistency in the determination of the elementary diagrams, by means of subsequent iterations in the solution of the integral equations, and the approximation of the first iteration commonly employed was found not to be very accurate for our model, but for very low association.

Moreover we showed that, connected to the increasing directionality built in in the model, the integral equation method based on the closure relation, supplemented by the elementary diagrams $B^{(4)}$ is not adequate to describe with accuracy the structural features connected to the second atomic coordination shell, in the supercooled state, and we strongly suggest that this is due to the neglect of higher order terms in the expansion of the bridge functions, due to the increasing importance of many-body correlations in the supercooled states. This indicate that future investigation of the supercooled region should rely on computer simulation methods, performed with appropriate sampling algorithms.

The model found also an application in the calculation of the possibility of

freezing from the melt in a tetrahedral open structure, with consequent increasing in volume. Calculation by Badhirkan *et al.*[31] based on the density functional theory of freezing, showed that indeed it seems possible to achieve the freezing in such an open structure.

The Bibliography

[1] J.A.E. Desa, A.C. Wright, J. Wong, R.N. Sinclair: *J. Non-Cryst. Sol.* **51**, 57 (1982).

[2] S.C. Moss, D.L. Price: in *Physics of disordered Materials* , edited by D. Adler, H. Fritsche, S.R. Ovshinsky, (Plenum, N.Y. 1985), pag. 77.

[3] W. Andreoni: *Helv. Phys. Acta* **58**, 226 (1985).

[4] U. Walter, D.L. Price, S. Susman, K.J. Volin: *Phys. Rev. B* **37**, 4232 (1988).

[5] See, for istance, S. Sugai: *Phys. Rev B* **35**, 1345 (1987) and references therein.

[6] I.T Penfold, P.S. Salmon: *Phys. Rev. Lett.* **67**, 97 (1991).

[7] P.S. Salmon: *Proc. R. Soc. London A* **437**, 591 (1992).

[8] S. Biggin, J.W. Enderby: *J. Phys. C* **14**, 3129 (1981).

[9] O. Uemura, Y. Sagara, D. Muno, T. Satow: *J. Non-Cryst. Sol.* **30**, 155 (1978).

[10] S.R. Elliot: *Physics of Amorphous Materials*, (Longman, London 1983).

[11] Y. Waseda, K. Suzuky: *Z. Physik B* **20**, 339 (1975).

[12] P.S. Salmon: *J. Phys. F: Met. Phys.* **18**, 2345 (1988).

[13] Y. Waseda: *The Structure of non crystalline Materials: Liquids and amorphous Solids* (McGraw Hill, New York 1980).

[14] C. Bergman, C. Bichara, P. Chieux, J.P. Gaspard: *J. de Phys. (Paris)* **12**, C8-97 (1985).

[15] I. Stich, R.Car, M. Parrinello: *Phys. Rev. Lett.* **63**, 2240 (1989); *Phys. Rev. B* 44, 4262 (1991); 44, 11092 (1991).

[16] Q. Zhang: *Phys. Rev. B* **42**, 5071 (1990).

[17] G. Galli, R. M. Martin, R. Car, M. Parrinello: *Phys. Rev. B* bf 42, 7470 (1990).

[18] see, A. Arnold, N. Mauser, J. Hafner: *J. Phys.: Cond. Matt.* **1**, 965 (1989) and references therein.

[19] N.W. Ashcroft: *Nuovo Cimento D* **12**, 597 (1990).

[20] W. D. Luedtke, U. Landman: *Phys. Rev B* **37**, 4656 (1988); M.D. Kluge, J.R. Ray, A. Rahman: *Phys. Rev B* **36**, 4234 (1987).

[21] P. Vashishta, R.K. Kalia, G.A. Antonio, I. Ebbsjo: *Phys. Rev. Lett.* **62**, 1651 (1989); P. Vashishta, R.K. Kalia, J.P. Rino: *Phys. Rev B* **41**, 12197 (1990).

[22] see, J. Tersoff: *Phys. Rev B* **39**, 5566 (1989) and references therein.

[23] M. S. Wertheim: *J. Chem. Phys.* **88**, 1145 (1988) and references therein.

[24] C.G. Joslin, C.G. Gray, W.G. Chapman, K.E. Gubbins: *Mol. Phys.* **62**, 843 (1987); G.J. Jackson, W.G. Chapman, K.E. Gubbins: *Mol. Phys.* **65**, 1 (1988); *Mol. Phys.* **65**, 1057 (1988).

[25] W.R. Smith, I. Nezbeda: *J. Chem. Phys.* **81**, 3694 (1984); J. Kolafa, I. Nezbeda: *Mol. Phys.* **61**, 161 (1987); J. Kolafa, I. Nezbeda, Y.V. Kalyuzhnyi: *Mol. Phys.* **68**, 1 (1989); I. Nezbeda, G.A. Iglesias-Silva: *Mol. Phys.* **69**, 767 (1990); J. Kolafa, I. Nezbeda: *Mol. Phys.* **72**, 777 (1991).

[26] J.C. Phillips: *Covalent Bonding in Crystals and Molecules* (University of Chicago Press, Chicago Ill. 1969); *Bonds and Bands in Semiconductors* (Academic Press, New York 1973) and references therein.

[27] R.M. Martin: *Phys. Rev.* **186**, 871 (1969).

[28] W. Weber: *Phys. Rev. Lett.* **33**, 371 (1974); *Phys. Rev. B* **15**, 4789 (1977).

[29] K.C. Rustagi, W. Weber: *Sol. State Comm.* **18**, 673 (1976).

[30] A. Ferrante, M.P. Tosi: *J. Phys.: Cond. Matter* **1**, 1679 (1989).

[31] Z. Badirkhan, A. Ferrante, M. Rovere, M.P. Tosi: *Nuovo Cimento D* **12**, 619 (1990); Z. Badirkhan, M. Rovere, M.P. Tosi: *Phil. Mag. B* **65**, 921 (1992).

[32] R. G. Parr, W. Yang: *Density-Functional Theories of Atoms and Molecules* (Oxford University Press, Oxford 1989), pag. 229

[33] J.P. Walter, M.L. Cohen: *Phys. Rev. B* **4**, 1877 (1971).

[34] O.H. Nielson, R.M. Martin: *Phys. Rev. B* **32**, 3792 (1985); for experimental determination by electron scattering see: J.M. Zuo, J.C.H. Spence, M. O'Kneefe: *Phys. Rev. Lett.* **61**, 353 (1988).

[35] U.Pietsch, V.G. Tsirelson, R.P. Ozerov: *Phys. Stat. Sol. B* **137**, 441 (1986).

[36] C.M. Bertoni, V. Bartolani, C. Calandra, F. Nizzoli: *J. Phys. C* **6**, 3612 (1973).

[37] B.G. Dick Jr., A.W. Overhauser: *Phys. Rev.* **112**, 90 (1958);
for references about its application to the lattice dynamics of ionic systems by Cochran see Peter Brüesch: *Phonons: Theory and Experiments*, Vol.I, ch.4 (Springer, Berlin, 1982).

[38] A. Fleszar, R. Resta: *Phys. Rev B* **34**, 7140 (1986); see also the same comparison for *GaAs* in
– L. Miglio, L. Colombo: *Physica Scripta* **40**, 238 (1989).

[39] R.P. Messmer, W.X. Tang, H.X. Wang: *Phys. Rev. B* **42**, 9241 (1990).

[40] G.J. Ackland: *Phys. Rev. B* **44**, 3900 (1991); **40**, 10351 (1989).

[41] F. Wooten, K. Winer, D. Weaire: *Phys. Rev. Lett.* **54**, 1392 (1985); K. Winer: *Phys. Rev. B* **35**, 2366 (1987).

[42] L. Miglio, L. Colombo: *Surf. Sci.* **221**, 486 (1989); L. Miglio, L. Colombo: to appear in *Surf. Sci.* (1990).

[43] A. Goldberg, M. Batanouny, F. Wooten: *Phys. Rev B* **26**, 6661 (1982); K. Winer, F. Wooten: *Phys. Stat. Sol. (b)* **136**, 519 (1986).

[44] L. Miglio, P. Santini, P. Ruggerone, G. Benedek: *Phys. Rev. Lett.* **62**, 3070 (1989); U. Harten, J.P. Toennies, Ch. Wöll, L. Miglio, P. Ruggerone, L. Colombo, G. Benedek: *Phys. Rev B* **38**, 3305 (1988).

[45] V.M. Glazov, S.N. Chizhevskaya, N.N. Glagoleva: *Liquid Semiconductors* (Plenum, New York, 1969).

[46] N.W. Ashcroft, D.C. Langreth: *Phys. Rev.* **156**, 685 (1967).

[47] J.E. Enderby, D. North: *Phys. Chem. Liquids* **1**, 1 (1968).

[48] J.P. Gabathuler, S. Steeb: *Z. Naturf. a* **34**, 1314 (1979).

[49] P. Viscor: *J. Non-Cryst. Sol.* **101**, 170 (1988).

[50] G. Etherington, A.C. Wright, J.T. Wentzel, J.C. Dore, J.H. Clark, R.N. Sinclair: *J. Non-Cryst. Sol.* **48**, 265 (1982).

[51] D. Gazzillo, G. Pastore, R. Frattini: *J. Phys.: Cond. Matter* **2**, 8463 (1990).

[52] D.Gazzillo, G. Pastore, S. Enzo: *J. Phys.: Cond. Matter* **1**, 3469 (1989).

[53] P. Ballone, G. Pastore, J.S. Thakur, M.P. Tosi: *Physica B* **142**, 294 (1986).

[54] Landolt-Börnstein: *Numerical Data; Group IV and III-V Semiconductors*, vol. 17a (Springer, New York, 1982).

[55] L.R. Godefroy, P. Aigrain: *Proc. Int. Conf. Physics of Semiconductors (Exeter)*, pag. 234, (1962).

[56] M. Aniya: *J. Chem. Phys.* **96**, 2054 (1992).

[57] W.A. Harrison: *Electronic Structure and the properties of Solids* (Freeman, San Francisco 1980); *Phys. Rev. B* **24**, 5835 (1981); **41**, 6008 (1990).

[58] J.P. Hansen, I.R. McDonald: *Theory of Simple Liquids* (2nd Ed., Academic Press, London 1986).

[59] M.P. Allen, D.J. Tildesley: *Computer Simulation of liquids* (Oxford University Press, Oxford 1987).

[60] D. Chandler, Y. Singh, D.M. Richardson: *J. Chem. Phys.* **81**, 1975 (1984);

K.S. Schweitzer, J.G. Curro: *Phys. Rev. Lett.* **58**, 246 (1987).

[61] J.M. Caillol: *Chem. Phys. Lett.* **156**, 357 (1989).

[62] P. Attard: *J. Chem. Phys.* **95**, 4471 (1991).

[63] J.L. Barrat, J.P. Hansen, G. Pastore: *Mol. Phys.* **63**, 747 (1988).

[64] J.M.J. van Leeuwen, J. Groeneveld, J. DeBoer: *Physica* **25**, 792 (1959) for a systematic and detailed exposition of the diagrammatic techniques see also the article by Stell in the following ref.

[65] G. Stell, article in: *The equilibrium Theory of classical Fluids*, edited by H. L. Frisch, J.L. Lebowitz, p.II-171 (Benjamin, New York 1964).

[66] J.K. Percus, article in: *The equilibrium Theory of classical Fluids*, edited by H. L. Frisch, J. L. Lebowitz, (Benjamin, New York 1964).

[67] G. Stell, article in: *Phase Transitions and Critical Phenomena*, Vol 5b, edited by C.Domb, M.S. Green, p.205 (Academic, London 1976).

[68] S.Ichimaru, H.Iyetomi, S.Tanaka: *Phys. Rep.*, **149** , 91 (1987)

[69] H.IYetomi: *Progr. on Theor. Phys.* **71**, 427 (1984); L.Blum, C.Gruber, J.L. Lebowitz, P. Martin: *Phys. Rev. Lett.* **26**, 1769 (1982).

[70] J.R.Forrest, D.A. Young: *Phys. Rev. A* **30**, 999 (1984).

[71] J.P.Hansen, G. Zerah: *J. Chem. Phys.* **84**, 2336 (1986).

[72] Y. Rosenfeld, N.W. Ashcroft: *Phys. Rev. A* **20**, 1208 (1979).

[73] F. Lado: *Phys. Rev. A* **8** 2548 (1973).

[74] S.Ichimaru, H.Iyetomi: *Phys. Rev. A* **25**, 2434 (1982); *Phys. Rev. A* **27**, 3241 (1983).

[75] P. Ballone, G. Pastore, M.P. Tosi: *J. Chem. Phys.* **81**, 3174 (1984).

[76] S.M. Foiles, N.W. Ashcroft, L. Reatto: *J. Chem. Phys.* **80**, 4441 (1984).

[77] M. J. Gillan: *Mol. Phys.* **38**, 1781 (1979); *Mol. Phys.* **39**, 839 (1980).

[78] J.A. Barker, J.J. Monagham: *J. Chem. Phys.* **36** 2564 (1962); A.D. Haymet,

S.A. Rice, W.G. Madden: *J. Chem. Phys.* **74**, 3033 (1981).

[79] P. Attard: *J. Chem. Phys.* **91**, 3072 (1989).

[80] P. Attard, G.N. Patey: *J. Chem. Phys.* **92**, 4970 (1990).

[81] W.H. Press, B.P. Flannery, S.A Teukolsky, W.T. Vetterling: *Numerical Recipes* (Cambridge Univers. Press, 1989), chap. 4.

[82] G.P. Lepage: *J. Comp. Phys.* **27**, 192 (1978).

[83] A. Ferrante, Wang Li, M. P. Tosi: *Phil. Mag. A* **58**, 13 (1988).

[84] G. Jacucci, A. Rahman: *Nuovo Cimento D* **4**, 341 (1984).

[85] M.Gillan, B. Larsen, M.P. Tosi, N.H. March: *J. Phys. C: Sol. St. Phys.* **9**, 889 (1976).

[86] J. Chirara: *J. Phys. F: Met. Phys.* **17**, 295 (1987).

PART TWO

On Shadow Wave Functions

for Helium 4.

Chapter 6

Introduction and overview

The physics of ^{3}He and ^{4}He has always been a subject of great interest in quantum statistical mechanics and many-body theory[1,2]; quantum effects are essential here as they are responsible for these systems to be in the liquid state, at standard pressure, even at temperatures very close to 0 K. A transition to the crystalline state can only occur at higher pressure. At low temperature both systems undergo a phase transition to a superfluid phase, of different origin. ^{4}He, a Bose system, undergoes a Bose-Einstein condensation in the liquid phase at the λ temperature (2.17 K at standard pressure), while the transition occurs in ^{3}He, a Fermi liquid, at a much lower temperature (some mK) due to a mechanism of pairing that can be described by BCS theory; the phase diagram of this system is richer and more complicated than that of ^{4}He and will not be considered here.

Realistic pair potentials have been extracted from experiments and simulation data to represent the interaction between helium atoms in the condensed system, from the Lennard-Jones potential adopted in early studies to the class of pseudopotentials developed and refined by Aziz and coworkers[3,4,5]. Ground state properties of ^{4}He homogeneous phases have been well described by Green Functions Monte Carlo (GFMC) simulations of the liquid and the solid phase[6,7,8] that with modern potentials well reproduce experimental data. Also at finite temperature a satisfactory description has been given by exact Path Integral Monte Carlo (PIMC) simulations[9], even at low temperature where the statistics and exchanges play an important role. From PIMC simulations the λ-transition[10],

the momentum distribution and the condensate fraction have been studied with precision[11,12].

Freezing properties[13,14] and response function of the ground state[15] have also been extracted from Diffusion Monte Carlo simulations. At higher temperature the melting line on pressure as also been subject of PIMC studies[16], but there exist still some controversy and discrepancy with experiment regarding the behaviour at higher pressures and the importance of statistics for the melting temperature[17].

For ^{3}He the situation is less satisfactory as Quantum Monte Carlo results are not as accurate as for ^{4}He ; GFMC simulations for the unpolarized system have been performed in the fixed node approximation[18] (employing nodes from accurate variational wave functions), which gives an upper bound to the exact energies, and very recently a PIMC method to treat Fermi systems has been developed by Ceperley[19], who employs a fixed node approximation for the high temperature density matrix, and has been used to study ^{3}He down to 0.5 K taking into account also the statistics.

Current interest is focussed, both from the experimental and the theoretical point of view, on ground state and finite temperature properties of inhomogeneous systems like droplets and clusters of different sizes[20] (see ref.[21] and references therein), low dimensional systems adsorbed on a substrate, free surfaces and interfaces between liquid and solid phases.

Variational methods have been employed from the beginning (for a review see refs[1,2]), first in HNC calculations[22,23,24], then in Variational Monte Carlo simulations[25,26], and wave function of increasing sophistication have been developed. Today VMC studies are also the first necessary step in performing QMC simulations. The simplest wave function is represented as a product of pair correla-

tions and takes into account correlations due to the excluded volume effect caused by the short range repulsion between helium atoms. Triplet correlations[22,25] and backflow correlations[27,22,25] have also shown to play an important role. The crucial part of a variational method lies in parameters or functional form optimization for the correlations employed in the wave function. Both HNC methods (Euler Equations)[28] and VMC optimization methods[29,26] have been developed to this scope. The existing optimal variational wave functions for ^{4}He give a ground state energy that is still somewhat higher than that obtained by "exact" QMC methods, i.e. at the equilibrium density $\rho = 0.365\sigma$ the best variational result obtained in VMC with a Jastrow plus Triplets trial wave function[26] gives an energy of -6.86 (1) K versus -7.12 (2) K of the GFMC study in ref.[6]).

The solid phase has been usually described with variational wave functions that assume particle localization around lattice sites by means of a one- body term which associate one particle to a gaussian orbital centered at each lattice site, and breaks both the translational and the Bose symmetry of the wave function. Recently a new class of wave functions, the shadow wave functions have been introduced by Kalos and Vitiello[30] to study the ground state of ^{4}He , and have been subsequently investigated by Reatto *et. al.* [31,32] with respect to the presence of a condensate in both the liquid and the solid phase and employed by Kalos and Reatto[33,34] to describe also excitations (rotons and vortices) by means of a Feynman-like[27] ansatz. The original motivation was to define a wave function able to describe both the liquid and the solid phase within the same functional form, and without breaking explicitly the symmetries of the wave function with one- body terms. Moreover these functions were able to recover a great part of the energy obtained with the best variational wave functions, without introducing triplet terms explicitly.

Our aim in this work has been twofold: from one hand to study some properties of SWF, like the effective-three body correlations built in it by the use of the auxiliary shadow particles, and on the other hand to investigate some generalization of it with the final objective to find a good variational wave function for the ground state of inhomogeneous systems. As a first step, tests of reliability for these new wave functions were made on the homogeneous phases by means of Variational Monte Carlo simulations. Part of our effort has been dedicated to extend the shadow form originally suggested by Kalos and Vitiello, allowing each shadow to interact with each particle (Extended SWF)[35] or including triplet correlations among the shadow particles. Some work has also been done to develop integral equations for both SWF and ESWF. Finally, a new parametrization of the SWF that could be employed to describe solid-liquid interfaces have been tested in the homogeneous case.

Although SWF can reproduce both phases, the problem is that they actually do it by means of different parameters for each phase. The key parameter, in the original formulation of ref.[30], is the effective diameter of shadow particles, which controls the crystallization of the shadow particles and thus induces localization of particles and the effective breaking of translational symmetry. An interface between solid and liquid phase at the freezing density could only be described by changing continuously the value of these parameters from the liquid to the solid phase, a way that would correspond in usual wave functions to the introduction of a self-consistent one-body term for the surface profile. The parametrization here explored follows a suggestion by Reatto[36], of evaluating the shadow parameters according to the local density around each particle.

Chapter 7

Variational Studies on liquid and solid He

Variational methods in quantum mechanics are based on the variational principle for the Schrödinger equation that can be considered the Euler equation of a suitable functional[37]. The exact ground state solution of this equation for fixed boundary conditions minimize the functional $< \Psi \mid \mathbf{H} \mid \Psi > / < \Psi \mid \Psi >$. Thus for any wave function (continuous with first continuous derivative) that satisfies the given boundary conditions the following inequality holds

$$\frac{< \Psi_t \mid \mathbf{H} \mid \Psi_t >}{< \Psi_t \mid \Psi_t >} \geq E_0, \tag{7.1}$$

where E_0 is the exact ground state energy. One can obtain an approximation to the ground state energy (upper bound) by minimizing the parameters of a chosen class of trial wave functions. A similar principle holds also for the excited states, provided that one can project out exactly from the trial wave function (i.e by symmetry considerations) the ground state and other eigenfunctions with lower eigenvector than that considered.

Another variational principle holds for the variance of the energy (see ref.[38] and references therein). Consider the residue vector $\mid \mathbf{r}_{\Psi_t} >= (\mathbf{H} - E_{\Psi_t}) \mid \Psi_t >$, where $\mid \Psi_t >$ is a trial wave function and E_{Ψ_t} its energy expectation value; the norm of the residue vector equals the variance of the energy. Expanding $\mid \Psi_t >$ in an orthonormal set gives

$$\sigma_E^2 =< \mathbf{r}_{\Psi_t} \mid \mathbf{r}_{\Psi_t} >=< \Psi_t \mid (\mathbf{H} - E_{\Psi_t})^2 \mid \Psi_t >= \sum_i |\alpha_i|^2 (E_i - E_{\Psi_t})^2. \tag{7.2}$$

For instance if $E_{\Psi_t} \approx E_0$, $\sigma_E^2 / < \Psi_t \mid \Psi_t >$ expresses in a quantitative manner the projection of Ψ_t on the subspace orthogonal to Ψ_0; it is exactly zero for the exact ground state wave function. Minimizing the variance of the energy one increases the overlap of the trial wave function with the chosen eigenfunction.

It should be noticed that a trial wave function which gives a good variational energy is not guaranteed to be a good wave function for describing other properties of the system than the energy, although this is certainly true if the ground state wave function is contained in the space spanned by the trial wave functions, or at least it has a substantial overlap with it. In this respect the minimization of the energy variance gives a better way to gauge the best wave function, measuring directly its overlap with the ground state. Techniques to minimize the variance of the energy in VMC simulations will be described later in this chapter.

Apart from simple cases the evaluation of the integrals in (7.1) is impossible from direct numerical integration, and one has to resort HNC equations or to Monte Carlo methods. In the following sections we review the VMC method and applications to ^{4}He. For a broad review of VMC studies in many-body systems see the review articles of Kalos and Ceperley[2] and Lewart and Pandharipande[39].

The hamiltonian which describes a system of N particles of He is

$$\mathbf{H} = \mathbf{T} + V = -\frac{\hbar^2}{2m} \sum_{i=1}^{N} \Delta_{\mathbf{r_i}} + \sum_{i<j} V(r_{ij}). \tag{7.3}$$

In recent work, and also in the calculation presented here, the potential HFDHE2 developed by Aziz[3] was employed. The recent paper of Ceperley and Schmidt[1] provide an updated review of QMC simulations on ^{4}He and ^{3}He.

7.1 Variational Monte Carlo

It is convenient to reformulate the integral in (7.1) introducing $|\Psi_t(\mathbf{R})|^2$

$$E_{\Psi_t} = \frac{\int |\Psi_t(\mathbf{R})|^2 \, E_{loc}(\mathbf{R}) \, d\mathbf{R}}{\int |\Psi_t(\mathbf{R})|^2 \, d\mathbf{R}}, \tag{7.4}$$

where $\mathbf{R}$ represents a set of positions $(\mathbf{r}_1, ..., \mathbf{r}_N)$ and

$$E_{loc}(\mathbf{R}) = \frac{\mathbf{H}\,\Psi_t(\mathbf{R})}{\Psi_t(\mathbf{R})} = \frac{\mathbf{T}\,\Psi_t(\mathbf{R})}{\Psi_t(\mathbf{R})} + V(\mathbf{R}), \tag{7.5}$$

defines the local energy. Now one can evaluate the integral (7.4) (and the expectation value of any operator expressed as a function of the coordinates) by a Monte Carlo method, that is by sampling configurations according to the normalized probability density defined by

$$p(\mathbf{R}) = \frac{|\Psi_t(\mathbf{R})|^2}{\int |\Psi_t(\mathbf{R})|^2 \, d\mathbf{R}}, \tag{7.6a}$$

This is equivalent to simulate a classical system in the canonical ensemble, whose probability density is

$$p(\mathbf{R}) = \frac{e^{-V(\mathbf{R})}}{\int e^{-V(\mathbf{R})} \, d\mathbf{R}}, \tag{7.6b}$$

The sampling is usually done by means of the standard Metropolis algorithm (for details on it see ref.[40]). Its simplest implementation consists in generating a new configuration in the Markov-chain by moving one particle at random in a box of size Δ (choosing Δ according to a fixed acceptance ratio). Then one evaluates the quantity

$$w_i = \frac{|\Psi_t(\mathbf{R}_{new})|^2}{|\Psi_t(\mathbf{R}_{old})|^2}, \tag{7.7}$$

and accepts the attempted move according to the transition probability $min(1, w_i)$. The "time" for the generated Markov-chain of configurations is represented by the number M of attempted moves per particle (MCS). The required average is given, according to the central limit theorem of statistics,

$$< A(\mathbf{R}) > \simeq \frac{1}{M} \sum_{i=1}^{M} A(\mathbf{R}_i). \tag{7.8}$$

To obtain the energy per particle one averages $A(\mathbf{R}) = E_{loc}(\mathbf{R})/N$. Since the generated configurations are correlated, instead of averaging over the whole chain of configurations one can sum in (7.8) the configurations only every τ-steps,where τ represents the correlation time for the quantity considered.

Generalizations to improve the sampling have been used in VMC studies of atoms[41] based on biased sampling[40], that is one generates the attempted move according to some biased distribution, then the transition probability is corrected to take this bias into account. It is also possible to sample configurations according to a distribution broader than $|\Psi_t(\mathbf{R})|^2$, doing the same as "umbrella sampling" in classical simulations[42]. A similar idea has been employed by Coldwell[43]in variational studies of atoms and molecules.

The scheme outlined above is valid also for simulating Fermi system, once an antisymmetric wave function is employed; a convenient algorithm for fermionic simulations is described in ref.[44].

As the result of the simulation is exact apart from statistical errors and systematic biases, one should be very careful in equilibrating correctly the system and evaluating the statistical errors. Technical details are similar to that employed for classical simulations[40]. We shall emphasize here only those peculiar of quantum simulations.

Periodic boundary conditions are employed to represent an infinite system

by means of few particles, and the continuity of the logarithmic derivative of the wave function must be imposed in order to have a meaningful variational estimate. To this purpose if only short range correlations are present in the wave function, they should be cut off with continuity at a distance equal to half the simulation box side, and the minimum image convention has to be used in computing the interactions; if long range correlations are taken into account, Ewald sums must be used. The value of the potential energy must be corrected by a tail correction, evaluated as the integral

$$2\pi\rho \int_{L/2}^{\infty} r^2 V(r) \mathrm{d}r.$$

Different estimators can be employed to define the local energy, as different form of the kinetic energy operator are possible. The simplest form, called the Pandharipande-Bethe form, is obtained from the direct evaluation of $\Delta_{\mathbf{r_i}}$ on Ψ_t, namely

$$t_{PB} = \frac{\mathbf{T}_{PB}\,\Psi_t}{\Psi_t} = -\frac{\hbar^2}{2m}\sum_{i=1}^{N}\frac{\Delta_{\mathbf{r_i}}\,\Psi_t}{\Psi_t} = -\frac{\hbar^2}{2m}\sum_{i=1}^{N}\left[\,\Delta_{\mathbf{r_i}}\,\ln\Psi_t + (\nabla_{\mathbf{r_i}}\,\ln\Psi_t)^2\right] \quad (7.9)$$

Another form can be obtained by means of Green's integral theorems

$$-\int \Psi_t^*\,\Delta\,\Psi_t\;\mathrm{d}\mathbf{R} = \int \nabla\,\Psi_t\cdot\nabla\,\Psi_t\;\mathrm{d}\mathbf{R} = \int |\Psi_t|^2\,(\nabla\,\ln\Psi_t)^2\;\mathrm{d}\mathbf{R}. \quad (7.10)$$

The kinetic energy estimator obtained through the application of this formula to the average $< t_{PB} >$ is called the Jackson-Feenberg form

$$t_{JF} = \frac{T_{JF}\Psi_t}{\Psi_t} = -\frac{\hbar^2}{4m}\sum_{i=1}^{N}\Delta_{\mathbf{r_i}}\,\ln\Psi_t, \quad (7.11)$$

and was extensively used in early simulations (i.e by the Orsay group), because of its simplicity. However the best estimator for the total energy, in terms of lower variance for a fixed number of MCS, is obtained using the PB kinetic energy. For ^{4}He it is true that the JF kinetic energy t_{JF} has a lower variance that

the corresponding PB form, but it turns out that there is a negative covariance $cov(t_{PB}, V)$that lowers quite a lot the variance of the sum $t_{PB} + V$. In the Fermi case even t_{JF} itself can have a variance greater than the corresponding PB form, as the transformed form is unbound near the nodes. Nevertheless it's useful to monitor both values during the simulation, as they should converge to the same value if the sampling is correct.

As in the classical case it's easy to obtain from the simulation radial distribution function, the pressure (the virial theorem is valid for the wave function that minimizes the energy, see ref.[44,2]); the momentum distribution can be also measured (see refs.[11,12]).

7.2 Trial wave functions

Jastrow Wave Functions

The simplest wave function for the Helium system can be written as a product of pair correlations as

$$\Psi(\mathbf{R}) = \prod_{i<j} f(r_{ij})\ \Phi_{1B}, \tag{7.12}$$

where Φ_{1B} is a one-body term which is 1 for liquid ^{4}He, a Slater Determinant of plane waves for liquid ^{3}He and is related to the one-body density in inhomogeneous systems, like in crystal, as we shall see later. This form was first considered by Bijl[45] and then reinvented by Dingle[46], Jastrow[47] and Mott[48] and first used in a Variational calculation by McMillan[49]. The correlation f is often expressed, along the classical analogy, by means of a pseudopotential $u(r)$ as

$$f(r_{ij}) = e^{-u(r_{ij})/2}. \tag{7.13}$$

The long-range part of the correlation f is analytically known, as its asymptotic

behaviour at infinity is connected to the long wavelenght limit of the Structure Factor, which at $T = 0\,K$ must go to zero[27] as

$$\lim_{k\to 0} \frac{S(k)}{k} = \frac{\hbar}{2mc} \tag{7.14}$$

(where c is the sound velocity). Reatto and Chester have shown[50] that asymptotically $u(r) \sim mc/\rho\pi^2\hbar\ r^2$. However it has been shown that neglecting the correct long range behaviour has little influence on the ground state energy, and almost all VMC calculations use a short range form, thus avoiding Ewald sums, while there is no difficulty in retaining such term in HNC calculations. The pseudopotential must be parametrized and its parameters optimized. A simple parameterization is the McMillan form $u(r) = (b/r)^5$, arising from the exact short range behaviour of the wave function for a Lennard-Jones potential. Optimal form for the correlation can be obtained with the methods described in sect. 7.3. The physical meaning of the Jastrow wave function is that, due to the sharp repulsive part of the interaction potential $V(r)$ in the hamiltonian, He atoms prefer to avoid each other.

In order to simplify the presentation of the local energy expression, its useful to introduce[44], exploiting the classical analogy, the classical potential energy of one particle in the field of the others, and the classical Pseudoforce on particle i

$$U(i) = \sum_{\substack{j=1 \\ j\neq i}} u(r_{ij}), \qquad\qquad F(i) = -\nabla_{\mathbf{r_i}} U(i).$$

The kinetic energy in the PB form is

$$t_{PB}^{(jas)} = \frac{\hbar^2}{4m} \sum_{i=1}^{N} (\Delta_i U(i) - \tfrac{1}{2} F(i) \cdot F(i)) \tag{7.15a}$$

and in the JF form

$$t_{JF}^{(jas)} = \frac{\hbar^2}{8m} \sum_{i=1}^{N} \Delta_i U(i) \tag{7.15b}$$

Triplet Correlations

The simple Jastrow form is insufficient to describe accurately the correlations present in the exact wave function, as one can see in table 6.1 from the comparison of variational energies obtained from this wave function and the "exact" GFMC results. A better trial wave function that includes also the effects of triplet correlations in the ground state of Helium was employed both in VMC[25] and HNC studies[22,51] (with LJ potential; corresponding work with Aziz potential: VMC[26], HNC[23,24]). It is obtained multiplying the Jastrow form (7.12) by a triplet term of the form

$$\Psi_3 = e^{-T_3} = \prod_{i<j<k} f_3(\mathbf{r}_{ij}, \mathbf{r}_{ik}) = \prod_{i<j<k} e^{-\frac{1}{2}\sum_{cyc} \xi(r_{ij})\xi(r_{ik})\ \mathbf{r}_{ij}\cdot\mathbf{r}_{ik}}. \qquad (7.16)$$

The exponent in the right part of eq. (7.16) can be as

$$\frac{1}{2}\sum_{cyc} \xi(r_{ij})\xi(r_{ik})\ \mathbf{r}_{ij}\cdot\mathbf{r}_{ik} = \frac{1}{4}\sum_{i=1}^{N} \mathbf{G}(i)\cdot\mathbf{G}(i) - \frac{1}{2}\sum_{i<j} \xi(r_{ij})^2\, r_{ij}^2, \qquad (7.17)$$

where

$$\mathbf{G}(i) = \sum_{\substack{j=1 \\ j\neq i}}^{N} r_{ij}\ \xi(r_{ij}). \qquad (7.18)$$

This expression is more convenient for the computation because the first term in the l.h.s of eq. (7.17) is a true three body term, but involves only updating the pair form $\mathbf{G}(i)$, while the second term is simply a pair correlation which modifies the Jastrow pseudopotential. There are two parametrized forms for the functions $\xi(r_{ij})$ used in VMC simulations. One parameterization is that employed in refs.[25]

$$\xi(r_{ij}) = \sqrt{\lambda}\ e^{-\left(\frac{r-R_0}{\omega}\right)^2}\ \left(\frac{r-r_c}{r_c}\right)^3, \qquad (7.19)$$

in which a cutoff term has been used to ensure the continuity of the logarithmic derivative of the wave function. The other form, quoted in ref.[52], can be expressed as a sum of reflected correlations

$$\xi_r(r_{ij}) = \xi(r) + \xi(2L - r) - 2\xi(L) \tag{7.20}$$

and was employed by us in some calculation reported later. Here L is the simulation box side an we have used for ξ the same functional form as before

$$\xi(r_{ij}) = \sqrt{\lambda}\, e^{-\left(\frac{r - R_0}{\omega}\right)^2} \tag{7.21}$$

The two forms represent two different way of implementing in a VMC the expression (7.21) used in HNC simulation, and differ in the way they are smoothed to zero at some cutoff distance r_c; actually they represent two different parameterizations as in eq. (7.21) the cutoff term also renormalizes the other parameters, which are very sensible to the value of r_c. There are three parameters in the triplet correlation, namely the strength λ, the position and the width of the gaussian. The cutoff value r_c should be chosen equal to $L/3$ in order to avoid counting different images of the same triplet in eq (7.17), but as the correlation (7.21) is very short range and already is almost zero at $L/3$, even values larger than that, as those reported in literature, can be used without troubles. The figure 7.1 illustrates the form of the correlation ξ adopted for the VMC study of ^{4}He (eq. 7.19);

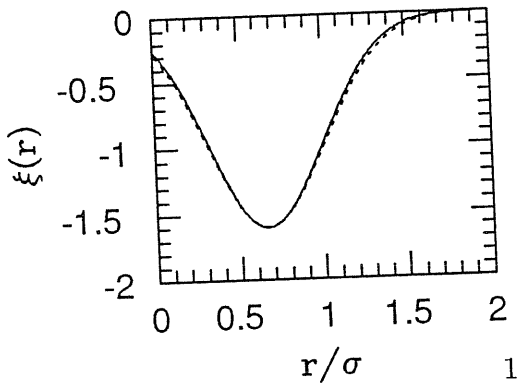

Figure 7.1
The same correlation $\xi(r)$ represented by the parametrized form (7.19), solid line and by the parameterization (7.20), dashed line. Parameters values are given in table 7.1.

the same correlation can be fitted with the second form (eq. 7.20), with parameters reported in the table 7.1.

$\lambda\sigma^2$	R_0/σ	ω/σ	R_c/σ
-14.0	0.82	0.5	3.0
-2.56	0.66	0.49	2.0

Table 7.1
Optimal Triplet parameters for the parameterization (7.19) from ref.[26] and values corresponding to the same correlation $\xi(r)$ but with the parameterization (7.20).

The expression of the local energy is the same as for the Jastrow form, plus a term due to triplet correlations, but is too complicated to be reported here and can be found in ref.[25]. The triplet wave function was proposed by Pandharipande[22] from studies of a ^{3}He impurity in ^{4}He[53] in which state dependent (k-dependent) correlations where employed to take into account the backflow of ^{4}He atoms around the impurity (which is responsible of its effective mass being different from the bare mass)[27]. In the long wavelenght limit one obtains a wave function that takes into account backflow correlations as

$$\Psi = \left(S \prod_{i<j} \mathbf{F_{ij}} \right) \Phi, \tag{7.22}$$

which is of the Jastrow form, with pair correlations $f_J(r_{ij})$ substituted by Correlation Operators

$$\mathbf{F_{ij}} = f_J(r_{ij}) + \eta(r_{ij})\, \mathbf{r_{ij}} \cdot \nabla_{\mathbf{ij}}. \tag{7.23}$$

When one adopts this kind of wave function for ^{4}He the operator $\nabla_{\mathbf{ij}}$ acts only on the correlations $f_J(r)$, and truncating the expression (7.22) to the terms of order η, one gets triplet terms[22] of the form (7.16,7.17) taking $\xi(r) = \sqrt{(\lambda)}\eta(r)/f_J(r)$

and approximating $\nabla_{ij} \ln f_J$ with $r\,\xi(r)$. The physical interpretation given by Pandharipande[22] to this wave function for ^{4}He was that the three-body correlations primarily takes into account the Feynmann-Cohen backflows produced by two particle recoiling from each other in the liquid.

A different justification for the triplet term can be given in the following way. If one applies powers of the hamiltonian to a trial wave function, one can partially project it on the ground state; thus looking at the terms arising in the expression of the local energy for a Jastrow trial wave function, one can guess a better variational form. Relaying on the minimum variance principle stated at the beginning, one notices that the term $(\nabla_{\mathbf{r_i}} \ln \Psi_t)^2$ contains three body contributions of the kind $\nabla_{\mathbf{r_i}} \ln(f_{ij}) \cdot \nabla_{\mathbf{r_i}} \ln(f_{ik})$. Since its fluctuation cannot be cancelled by any pair term one introduces triplet correlations of the form (7.16,7.17) and, once again approximating $\nabla_{ij} \ln f_J$ with $r\,\xi(r)$, one obtains the requested cancellation with an appropriate choice of $\xi(r)$ that minimizes the variance of the local energy. A reasonable parametrized choice is simply the gaussian form (7.21) since the short range behaviour of ξ is cutoff by the repulsive two-body potential and the long range behaviour can also be cutoff since it should decay like r^{-4} in 3D because the long range part of the Jastrow correlation decays as r^{-2} due to zero point phonon excitations.

A remarkable property of the triplet term is that the optimal values of its parameters, apart from λ, have a weak dependence on the density ρ.

A more general form of f_3 has been employed in the HNC study in ref.[23]. There f_3 has been expanded in Legendre polynomial $P_l(\mathbf{r}_{ij} \cdot \mathbf{r}_{ik})$, with the result that the term with $l = 1$, i.e that of (7.17), gives the leading contribution to the energy.

Wave Functions for Solids

The simple Jastrow form is not able to describe a quantum crystal. Let's take for instance the McMillan pseudopotential; when a suitable value of b is chosen, the corresponding classical system of particle freezes but the quantum total energy corresponding to this situation is very high, always higher then the liquid phase[54]. A trial wave function to describe properly a quantum crystal has been proposed by Nosanow[55] and Saunders[56] and first employed in VMC simulations by McMillan[49] and Hansen and Levesque[57]. It consists of a product of a correlation term, which can be either Jastrow or Jastrow plus Triplets, and a one body term Φ_{1B} which explicitly breaks the translational invariance of the wave function; in the classical analogy $\Phi_{1B}^2 = e^{-V_{ext}}$ corresponds to an external periodic potentials imposed to the system, which in turn induces a periodically modulated one-body density. The localized Nosanow form is given by

$$\Phi_{1B} = \prod_{i=1}^{N} \varphi(\mathbf{r}_i - \mathbf{R}_i),, \tag{7.24}$$

where $\mathbf{R}_i$ are the lattice sites and $\varphi(\mathbf{r}_i - \mathbf{R}_i)$ are single-particle orbital localized around lattice sites, usually taken to be a Gaussian function

$$\varphi(\mathbf{r}_i - \mathbf{R}_i) = e^{-\frac{\alpha}{2}(\mathbf{r}_i - \mathbf{R}_i)^2}. \tag{7.25}$$

This form of the wave function breaks also the Bose symmetry. A symmetrized form that maintains this symmetry

$$\Phi_{1B} = \sum_{P} \prod_{i=1}^{N} \varphi(\mathbf{r}_i - \mathbf{R}_{P(i)}), \tag{7.26}$$

has been studied for bosons interacting with Yukawa potentials[58] and for ^{4}He with the Aziz potential[59], and in both cases the energy didn't change very much (actually resulted to be slightly higher). As the frequency of exchanges in the

solid is very low[60,1] due to the sharp repulsion at short distances, even a non symmetric wave function can safely be used in a variational calculation.

Writing the PB estimator for the local kinetic energy as $t_{PB} = t_{PB}^{(jas} + t_{PB}^{(nos)}$, the contribution from the one-body Nosanow term is

$$t_{PB}^{(nos)} = \frac{\hbar^2}{4m} \sum_{i=1}^{N} \left[\Delta_i V(r_i) + \frac{1}{2} F(i) \cdot \Delta_i V(r_i) - \frac{1}{2} (\nabla_i V(r_i))^2 \right], \qquad (7.27a)$$

Where $V(r_i) = -2 \ln \varphi(r_i)$ is the part of the "external potential" due to the localized orbital in site R_i. For a gaussian orbital it takes the form

$$t_{PB}^{(nos)} = 3\alpha N \frac{\hbar^2}{2m} + \frac{\hbar^2}{4m} \sum_{i=1}^{N} \left[\alpha F(i) \cdot (\mathbf{r}_i - \mathbf{R}_i) - 2\alpha^2 (\mathbf{r}_i - \mathbf{R}_i)^2 \right] \qquad (7.27b)$$

7.3 Wave function optimization

A crucial point in each variational method is to actually find the best trial wave function of a given class. One approximate method relies on the solution of the Euler equation obtained in the HNC approximation[28] the other uses VMC[29,26].

Optimization in VMC

Once a parametrized functional form is given for the pseudopotential, the "direct" approach often followed[39] consist in repeating many simulations at different values of the parameters and then one fits the energy to a quadratic form of the parameters in order to locate the minimum of the energy. This is a long and painful procedure, and becomes impracticable when the number of parameters is too large; moreover the statistical error in the energy values makes difficult to locate precisely the minimum.

A more efficient way, the correlated sampling and reweighting techniques[29], makes maximal use of the information contained in a single simulation corresponding to a given set of parameters $\{\lambda\}$, to obtain the behaviour of the energy (or the variance) in the neighbourhood of $\{\lambda\}$. This method, together with the principle of minimum variance is currently used in the optimization of many-parameters (30-100) in the variational wave functions employed for the electronic structures studies on atoms and molecules[29]. Recently, Schmidt and Vitiello[26] used these techniques together an appropriate choice of the basis function to span the space of Jastrow correlations in the optimization of a Jastrow +Triplets wave function for ^{4}He.

Correlated sampling techniques give a practical way of computing differences between the mean value of some operator O on a trial wave function $\Psi(\lambda)$ at different values of λ, from a simulation made at one value only[1,29]. It is also an accurate way of determining the derivative of the mean value with respect to λ. Denoting for convenience with $\Psi_{old} = \Psi(\lambda_0)$ the wave function used to generate the Markov-chain in the simulation done at the value λ_0 of the parameter and with $\Psi_{new} = \Psi(\lambda_0 + \Delta)$ the wave function at a different value, it follows from the definition of averages that one can obtain averages at a different value $\lambda_0 + \Delta$ as

$$< \Psi_{new} | O | \Psi_{new} >= \frac{\int \left(\frac{O \Psi_{new}(\mathbf{R})}{\Psi_{new}(\mathbf{R})} \right) w(\mathbf{R}) p(\mathbf{R}) \, \mathrm{d}\mathbf{R}}{\int w(\mathbf{R}) p(\mathbf{R}) \, \mathrm{d}\mathbf{R}}. \qquad (7.28)$$

where the probability used in the sampling is that of the function at λ_0

$$p(\mathbf{R}) = \frac{|\Psi_{old}(\mathbf{R})|^2}{\int |\Psi_{old}(\mathbf{R})|^2 \, \mathrm{d}\mathbf{R}}. \qquad (7.28a)$$

and the weights are

$$w(\mathbf{R}) = \frac{|\Psi_{new}(\mathbf{R})|^2}{|\Psi_{old}(\mathbf{R})|^2}. \qquad (7.28b)$$

This techniques can be exploited to minimize the variance of the energy as follows: one writes on tape some hundreds of independent configurations sampled from $|\Psi_{old}(\mathbf{R})|^2$ and uses them later to minimize the variance. The values obtained for the parameters are used to perform another simulation and so on; usually a few iteration are sufficient. When only linear parameters in the pseudopotential are varied, the method greatly simplifies as there is no need to store configuration to perform the reweighting, and the minimization can be done in a single simulation as in ref.[61]. When the starting point is not close to the optimal or there is the need to span a larger portion of the parameter space, the reweighting gets into trouble as the weights w_i becomes too large or too small, then minimizing the unreweighted variance is more appropriate. Schmidt and Vitiello[26] used correlated sampling with variance minimization to optimize Jastrow+Triplets and Jastrow+Nosanow+Triplets wave functions for liquid and solid ^{4}He, employing the following form for the pair Jastrow correlation

$$f(r) = \sum_{i=1}^{n} a_i f_i(r) \tag{7.29}$$

where a_i are variational parameters and $f_n(r)$ are the eigenfunctions of the 2-body Schrödinger equation[62]

$$-\frac{1}{m}\,\Delta f_n(r) + v(r) f_n(r) = \lambda_n\, f_n(r), \tag{7.30}$$

with boundary condition such that the solutions goes smoothly to 1 at some resonable healing distance d. The advantage of the correlation given by (7.29) is that it automatically satisfies the correct short range behaviour for f; This is very difficult to achieve with a general free parameterization, as the long range tail contributes little to the energy, and short distances are poorly sampled when using $|\Psi|^2$ as importance function.

Chapter 8

Shadow wave functions

A new class of wave functions, the Shadow wave functions, have been recently proposed by Vitiello and Kalos[30] to represent the physical correlations in the ground state of ^{4}He, and have been subsequently investigated by Reatto, Vitiello *et al.*[31,32]. SWF have been employed also to describe the excited states[33,34] by means of a Feynman-ansatz. A variational density matrix of the Shadow form has been recently proposed by Reatto *et al.*[63] to describe properties of ^{4}He at finite temperature. An attempt to use SWF as guiding functions in GFMC calculation has also been reported[64]. In this chapter we present this wave function and review the work done on it. We also report some original work done by us.

8.1 Shadow Wave Functions

The shadow wave function can be expressed as a product of two parts

$$\Psi_{SWF}(\mathbf{R}) = \varphi_{pp}(\mathbf{R})\Phi_S(\mathbf{R}), \tag{8.1}$$

where the first part is written as a product of pair correlations among Helium atoms, like in the Jastrow wave function (7.12)

$$\varphi_{pp}(\mathbf{R}) = \prod_{i<j}^{N} e^{-\frac{1}{2}u_{pp}(r_{ij})}, \tag{8.2}$$

and the second part assumes the following convolution form

$$\Phi_S(\mathbf{R}) = \int \varphi_{ss}(\mathbf{S})\,\Phi(\mathbf{R},\mathbf{S})\,\mathrm{d}\mathbf{S}, \tag{8.3}$$

where $\mathbf{S}$ represents the integration variables $(\mathbf{s}_1, ..., \mathbf{s}_N)$. The convolution kernel Φ associates each Helium atom to one integration coordinate by means of a gaussian correlation[30]

$$\Phi(\mathbf{R}, \mathbf{S}) = \prod_{i=1}^{N} e^{-C\,|\mathbf{r}_i - \mathbf{s}_i|^2}, \tag{8.4}$$

where C is a variational parameter. The integration coordinates represent a set of auxiliary degrees of freedom denoted as Shadow particles[30]; the correlations among shadow particles are taken into account by the Jastrow term present inside the integral

$$\varphi_{ss}(\mathbf{S}) = \prod_{i<j}^{N} e^{-\,u_{ss}(s_{ij})}, \tag{8.5}$$

where u_{ss} is a suitable pseudopotential. Due to the integration made on the subsidiary variables, one has to take into account two kind of shadow particles in writing averages, as it is easily seen by writing, for instance, the normalization integral

$$\langle\, \Psi \,|\, \Psi \,\rangle = \int \varphi_{pp}(\mathbf{R})^2\, \Phi(\mathbf{R}, \mathbf{S}^R)\, \Phi(\mathbf{R}, \mathbf{S}^L)\, \varphi_{ss}(\mathbf{S}^R)\, \varphi_{ss}(\mathbf{S}^L)\; \mathrm{d}\mathbf{R}\, \mathrm{d}\mathbf{S}^R \mathrm{d}\mathbf{S}^L. \tag{8.6}$$

In the classical analogy, eq .(8.6) is equivalent to the partition function for a system of N flexible molecules[31], composed of three kind of atoms, let's say P (central Helium Atom) and R (right), L (left) shadows, with harmonic intramolecular interactions PR, PL , and intermolecular interactions given by u_{pp} between Helium atoms and u_{ss} respectively between shadows RR and LL; notice that no interaction is present between one shadow R and one L. Operators that depend on particles coordinates $A(\mathbf{R})$ are averaged as in

$$< A(\mathbf{R}) >= \frac{\int \Psi_t^*(\mathbf{R})\, A(\mathbf{R})\, \Psi_t(\mathbf{R})\; \mathrm{d}\mathbf{R}}{< \Psi_t \,|\, \Psi_t >} = \int A(\mathbf{R})\, p(\mathbf{R}, \mathbf{S}^R, \mathbf{S}^L)\; \mathrm{d}\mathbf{R}\, \mathrm{d}\mathbf{S}^R \mathrm{d}\mathbf{S}^L, \tag{8.7}$$

integrating over the probability density

$$p(\mathbf{R}, \mathbf{S}^R, \mathbf{S}^L) = \frac{\varphi_{pp}(\mathbf{R})^2\, \Phi(\mathbf{R}, \mathbf{S}^R)\, \Phi(\mathbf{R}, \mathbf{S}^L)\, \varphi_{ss}(\mathbf{S}^R)\, \varphi_{ss}(\mathbf{S}^L)}{\langle\, \Psi_t \,|\, \Psi_t \,\rangle}. \tag{8.8}$$

The total energy is obtained by averaging the "local energy" expression

$$E_{loc}(\mathbf{R},\mathbf{S}^R,\mathbf{S}^L) = \frac{1}{2}\left(\frac{\mathbf{H}(\mathbf{R})\,\varphi_{pp}(\mathbf{R})\,\Phi(\mathbf{R},\mathbf{S}^R)}{\varphi_{pp}(\mathbf{R})\,\Phi(\mathbf{R},\mathbf{S}^R)} + \frac{\mathbf{H}(\mathbf{R})\,\varphi_{pp}(\mathbf{R})\,\Phi(\mathbf{R},\mathbf{S}^L)}{\varphi_{pp}(\mathbf{R})\,\Phi(\mathbf{R},\mathbf{S}^L)} \right)$$
$$= t_{PB} + V(\mathbf{R}). \tag{8.9}$$

The simmetrization of this expression with respect to shadow R and L is convenient for the computations since in VMC simulations the estimator (8.9) has a lower variance than the unsymmetrized form. The kinetic energy part of this operator, in the PB form, is given by the expression $t_{PB} = t_{PB}^{(jas)} + t_{PB}^{(shad)}$, where

$$t_{PB}^{(shad)} = -\frac{\hbar^2}{4m}\sum_i \tfrac{1}{2}\,F_{pp}(i)\cdot[F_{pR}(i)+F_{pL}(i)] + [F_{pR}^2(i)+F_{pL}^2(i)]. \tag{8.10}$$

Here we adopted the same pseudoclassical notation as in chap.7, and $F_{pp}(i)$ is the (pseudo)force acting on the particle i, due to the other particles while $F_{pL}(i) = 2C(\mathbf{r}_i - \mathbf{s}_i^L)$ is the (pseudo)force acting on it due to shadow Left; substituting in (8.10) this expression and the corresponding one for shadow Right one obtains

$$t_{PB}^{(shad)} = \frac{3NC\,\hbar^2}{m} + \frac{\hbar^2}{4m}\sum_i \{\, C\,F_{pp}(i)\cdot[(\mathbf{r}_i - \mathbf{s}_i^L) + (\mathbf{r}_i - \mathbf{s}_i^R)]$$
$$-4C^2\,[(\mathbf{r}_i - \mathbf{s}_i^L)^2 + (\mathbf{r}_i - \mathbf{s}_i^R)^2]\}\,. \tag{8.10b}$$

Two motivations have been given[30,31] for the introduction of shadow particles and for the functional form expressed by equations (8.1) (8.2), in terms of analogies based upon specific features of PIMC and GFMC methods.

One motivation[30,31,32] adopts a similarity to PIMC methods employed in the study of quantum systems at finite temperatures (see refs.[1,9] for a review of PIMC techniques). The equilibrium properties of a quantum system of particle at temperature T are specified by its density matrix

$$\rho(\mathbf{R},\mathbf{R}';\beta) = \langle\, \mathbf{R}\,|\,e^{-\beta\,\mathbf{H}}\,|\,\mathbf{R}'\,\rangle = \sum_n \Psi_n^*(\mathbf{R})\;\Psi_n^*(\mathbf{R}')\;e^{-\beta\,E_n} \tag{8.11}.$$

Here $\{\Psi_n\}$ is the set of exact eigenstates for the Hamiltonian $\mathbf{H}$. The density matrix satisfies the following convolution identity

$$\begin{aligned}\rho(\mathbf{R},\mathbf{R}';\beta) &= \int \rho(\mathbf{R},\mathbf{R}_1;\tau)\,\rho(\mathbf{R}_1,\mathbf{R}_2;\tau)....\rho(\mathbf{R}_M,\mathbf{R}';\tau)\;\mathrm{d}\mathbf{R}_1....\mathrm{d}\mathbf{R}_M \\ &= \int e^{-S(\mathbf{R}_1...\mathbf{R}_M)}\;\mathrm{d}\mathbf{R}_1....\mathrm{d}\mathbf{R}_M\end{aligned} \quad , \tag{8.12}$$

where S is the Action and $\tau = \frac{\beta}{(M+1)}$ corresponds to an higher temperature.

The simplest algorithm to make a simulation of a Feynman path-integral, for the case of Boltzmann particles, exploits the mapping to a classical system[65], corresponding to the following choice for the Action

$$S(\mathbf{R}_1...\mathbf{R}_M) = \sum_{i=1}^{M} \frac{(\mathbf{R}_i - \mathbf{R}_{i-1})^2}{4\lambda\tau} + \tau\, V(\mathbf{R}_i), \tag{8.13}$$

(with $\lambda = \hbar^2/2m$) where a system of quantum particle is represented by interacting ring polymers, necklaces of N beads connected by springs. The distribution of beads describes the delocalization of the quantum particle around its "classical" position represented by the center of mass of each chain. As a result of the hard core repulsion among particles and of the rather large density in liquid and solid Helium, the probability of exchange is low, and only a few percent of the chains are cross-linked (see refs.[1,60]), and the major part of paths are rather compact. The idea is that, as an approximation, each chain can be represented by means of its center of mass position and of the distribution of beads around it. The extension of this picture to the ground state leads to the SWF form (8.1,8.2) where the chains centers of mass in PIMC are represented by the shadow particles, which are in essence pseudoclassical variables which represent the combined effect of quantum delocalization and of the excluded volume due to hard core repulsions. Shadow particles play the role of a "quantum correlation hole" that particles carry around them.

The other motivation[30] makes reference to the Diffusion Monte Carlo (DMC) method (see the article by Schmidt and Kalos in ref.[66], chap. 4). We shall show here, following ref.[1], that the Green's function Projector technique can be employed to give a more precise justification of the SWF form, opening the way to improvements and generalizations. When one writes the time-dependent Schrödinger equation in imaginary time $\tau = it$, one can propagate the wave function from one "time" τ to a subsequent interval $\tau' = \tau + \Delta\tau$ by means of

$$\Phi(\mathbf{R}, \tau + \Delta\tau) = \int G(\mathbf{R}, \mathbf{S}, \Delta\tau)\, \Phi(\mathbf{S}, \tau)\, \mathrm{d}\mathbf{S} = \sum_n a_n\, \Psi_n(\mathbf{R}) e^{-(E_n - E_0)\,\tau'}, \quad (8.14)$$

where

$$G(\mathbf{R}, \mathbf{S}, \Delta\tau) = \left\langle \mathbf{R} \,|\, e^{-\Delta\tau\, \mathbf{H}} \,|\, \mathbf{S} \right\rangle = \left\langle \mathbf{R} \,|\, e^{-\Delta\tau\, [\mathbf{T} + \mathrm{V}(\mathbf{S})]} \,|\, \mathbf{S} \right\rangle, \quad (8.15)$$

is the short time approximation to the Green's function (or propagator). In the DMC technique one iterates many times the relation (8.14), starting from an initial wave function $\Phi(\mathbf{R}, 0)$, and projects it until, after a time long enough, one ends up with the ground state.

The idea now is to use as a variational ansatz the wave function Φ which is obtained just after the propagation over one time slice in eq. (8.14); one can safely approximate the propagator (8.15) inserting some variational parameters, ending up with a variational wave function that has a greater overlap with the ground state than the initial one. Starting from the simple Jastrow form

$$\Psi_0 = \Phi(\mathbf{R}, 0) = \prod_{i<j} f_0(r_{ij}),$$

as initial choice and performing just one iteration by means of eq. (8.14), one obtains a wave function of the shadow form (8.1, 8.2), when one takes for the Green's function (8.15) the following approximation

$$G(\mathbf{R}, \mathbf{S}) = \varphi(\mathbf{R}) \prod_i e^{-C\,|\mathbf{r}_i - \mathbf{s}_i|^2}\, \varphi(\mathbf{S}), \quad (8.16)$$

(where now C is a variational parameter) obtained by "dressing" with Jastrow terms $\varphi = \prod_{i<j} f_1(ij)$ the Green's function $G_0(\mathbf{R},\mathbf{S}) = < \mathbf{R} \mid e^{-\Delta\tau \mathrm{T}} \mid \mathbf{S} >$ of the non-interacting system. Comparing the expression (8.1) to (8.14) after these substitutions one has

$$\varphi_{pp}(\mathbf{R}) = \varphi(\mathbf{R}) \qquad \text{and} \qquad \varphi_{ss}(\mathbf{S}) = \varphi(\mathbf{S})\,\Psi_0(\mathbf{S}),$$

that employing a McMillan pseudopotential $(b/r)^5$ in all the Jastrow terms amounts to rescale the parameter b_s. In the original work of Kalos and Vitiello[30] only McMillan pseudopotential were employed for both u_{pp} and u_{ss}. It was suggested by Reatto [31] on the basis of the PIMC analogy that the bead-bead interaction τV could induce an effective potential of the same kind, with an attractive part, among centers of mass of the different polimers, that is to say the pseudopotential u_{ss} for shadows must have also an attractive part. One possible parametrization is the simple rescaling of the Aziz potential present in the hamiltonian, like in

$$u_{ss}(s_{ij}) = \frac{V(d\,s_{ij})}{A}, \tag{8.17}$$

where d and A are variational parameters. This was tested by MacFarland, Vitiello and Reatto[32] and the wave function with the attractive pseudopotential of eq. (8.17) was shown to be superior to the simple McMillan form. We summarize in table 8.1 some results for the SWF with both the parametrizations at various densities, from the liquid density at standard pressure ($\rho\sigma^3 = 0.365$), to the equilibrium freezing density ($\rho\sigma^3 = 0.438$) and the equilibrium melting density($\rho\sigma^3 = 0.491$) (as indicated by GFMC work[6]) and one value of density corresponding to the high pressure solid ($\rho\sigma^3 = 0.55$). In the same table we also show some results obtained by us as a test of our code. For comparison we show in table 8.2 values of the total energies and potential energies at each density as

obtained from GFMC work[6,12].

$\rho\sigma^3$	b_p	C	par. of u_{ss}	$< E/N >$	ref.
0.365	1.13	4.0	(a) 1.20, 9	-6.24 (3)	[30]
"	"	"	" " "	-6.20 (2)	present work
"	"	"	" 1.40, 5	-6.06 (3)	[30]
"	"	"	" " "	-6.03 (2)	present work
0.365	1.13	5.5	(b) 10.5,0.94	-6.52 (2)	present work
"	1.12	"	" " "	-6.62 (2)	[32]
"	?	?	(b) ?	-6.53 (2)	[63]
"	OPT	5.5	(b) 10.5,0.94	-6.69	[36]
0.438	1.12	4	(a) 1.55, 5	-5.36 (3)	[30]
"	"	"	" " "	-5.34 (2)	present work
0.491	1.10	4.8	(a) 1.70, 5	-5.00 (6)	[30]
"	"	"	" " "	-4.97 (2)	present work
0.55	1.10	5.7	(a) 1.35, 9	-3.53 (3)	[30]
"	"	"	" " "	-3.58 (2)	present work

Table 8.1
Optimal parameters and variational energies for SWF at various densities. For ss pseudopotential (a) is the McMillan parametrization with b_s, (b) is the attractive pseudopotential (8.17). OPT indicates an optimized form of the correlation. Energies in Kelvin and length in σ=2.556Å.

$\rho\sigma^3$	$< E/N >$	$< T/N >$	$< V/N >$
0.365	-7.12 (3)*	14.47 (9)**	-21.59 (9)**
0.438	-6.56 (6)*	20.1 (2)**	-26.7 (1)**
0.491	-5.61 (3)*	25.70 (7)**	-31.31 (7)**
0.55	-4.23	-	-
0.559	-3.87 (3)*	31.8**	-35.7 (1)**

Table 8.2
GFMC results for ^{4}He at various densities: equilibrium density, freezing density, melting density and two values of the crystal density. The fourth row is a result interpolated from the energy curve fit of GFMC results given in ref.[6]. Energies are in Kelvin. Results marked * are from ref.[6]; * from ref.[12].

We want to point out here that the need for a pseudopotential u_{ss} with an attractive part, of the form indicated in eq. (8.17) can be also derived from the DMC argument, by making a better approximation for the propagator (8.15) than the free particle one. A step further is given by the approximation

$$\left\langle \mathbf{R} \left| e^{-\Delta\tau(\mathrm{T}+\mathrm{V})} \right| \mathbf{S} \right\rangle \approx \left\langle \mathbf{R} \left| e^{-\Delta\tau \mathrm{T}}\, e^{-\Delta\tau \mathrm{V}} \right| \mathbf{S} \right\rangle = G_0(\mathbf{R},\mathbf{S})\, e^{-V(\mathbf{S})/A}, \quad (8.18)$$

where the approximation consists in neglecting the commutator $[T,V]$ (see eq. 4.29 in the article by Kalos and Schmidt in ref.[66]); in fact this is the same approximation used in deriving the simple primitive action of eq. (8.13). Now one dresses as before this approximate propagator with Jastrow correlations and applies it to the initial Jastrow wave function. One ends with a Shadow correlation of the following form

$$\Phi_{ss} = e^{-u_{ss}} = e^{-V(\mathbf{S})/A}\, \varphi(\mathbf{S})\, \Phi(\mathbf{S},0). \quad (8.19)$$

The resulting pseudopotential is the sum of the Aziz potential with two repulsive terms of the McMillan form, and has an attractive part. One can approximate this pseudopotential writing down the simple parametrization (8.17), where another variational parameter d has been introduced to take into account the shift of the minimum in u_{ss} caused by the addition of repulsive terms. As a matter of fact it turns out from VMC that the optimal d is lower than one, meaning that the minimum occurs at larger distances.

As we shall comment in depth later, the presence of an attractive part in u_{ss} is very useful in inhomogeneous systems, where it allows for the description of self-bounded systems without the need of introducing a confining external one-body term.

8.2 SWF and the solid phase

One important feature of the SWF is that they allow for the description of both liquid and solid phases within the same functional form. We want to make here some remark about this property.

As it was already stated in sect. 7.2 one can break the translational invariance and obtain a crystal phase even with a simple Jastrow wave function, but this procedure will give too high an energy and a crystal of the classical type, with very localized particles, that doesn't correspond to the quantum crystal. In SWF the crystal phase is obtained at a suitable value of the parameter b_s that makes the shadow particles crystallize. The spontaneous crystallization of the shadow component in turn induces the crystallization of the Helium atoms into a quantum crystal; particles move around fixed positions provided by the localized shadows, but have a greater mean square displacement due to the gaussian coupling. This is confirmed indeed by the measurement of the order parameter (defined as the first fourier component of the one body-density, or first Bragg reflection, and measured by means of formula (3.34)) of both the components and from the values of the corresponding Lindemann parameters

$$\gamma = \frac{1}{a}\sqrt{\left\langle \frac{1}{N}\sum_{i=1}^{N}(\mathbf{r}_i - \mathbf{R}_i)^2 \right\rangle}, \tag{8.20}$$

where $\mathbf{R}_i$ are the lattice sites and a is the nearest-neighbour distance. The crystallization is still due to excluded volumes effect like in the classical case, but in the quantum crystal it is not the true hard core diameter of the potential responsible for that but the much higher effective excluded volume represented by the shadow particle.

One can verify that freezing is indeed driven by shadows crystallization, by comparing the values for the optimal choice of b_s and that obtained from the freezing (and melting) parameter of a classical system of particles interacting with

	$\rho\sigma^3 = 0.365$	$\rho\sigma^3 = 0.438$	$\rho\sigma^3 = 0.491$	$\rho\sigma^3 = 0.550$
n=6	1.811, 1.822	1.707, 1.714	1.643, 1.650	1.582, 1.589
n=9	1.540, 1.555	1.449, 1.464	1.395, 1.458	1.343, 1.357
n=12	1.466, 1.507	1.379, 1.397	1.328, 1.366	1.279, 1.295

Table 8.3
Values of the freezing and melting parameters b_{freez}, b_{melt} (in scaled units b/σ) at various densities, for the potential $(b/r)^n$. They have been calculated from the freezing parameters for soft sphere potentials published by Hoover et. al., ref.[67].

$(b/r)^n$ potential. This comparison is shown in table 8.3 for various densities. We also verified in some exploration of parameters that the value of b_s at which the system stays in a crystalline state in VMC simulations is very close to the value expected for the classical freezing of shadows. One can always obtain both phases at any density, but whether the system remains solid or becomes a liquid depends on the value of the optimal parameter b_s^{opt} (for which we have the minimum of the energy), being higher or lower of the critical value for shadow crystallization.

The value b_s^{opt} depends on the density, as it will be shown in detail in sect. 9.1. As a consequence, the main disadvantage of this SWF parametrization is that, because the densities of the solid at melting and the liquid at freezing are different, one needs different values of the parameter b_s for each phase. This poses problems if one wants to describe an interface between the liquid and the solid phases at coexistence in that one must use different values of the parameters, namely different wave functions, in regions of different density. Similar problems arise in the treatment of clusters or free surfaces. A way out of this problem will be described in sect (9.1).

We want to make here a remark about an observation made by Ceperley and Schmidt in ref.[1], stating that SWF in the solid phase (the realization made in a VMC simulation) are equivalent to a Nosanow wave function. Comparing the expressions (7.27b) and (8.10b) for the local energies due to the one-body term (set $\alpha = 2C$) we see that this is indeed true provided that we localize both shadows R and L strictly on a lattice site; this limit is reached only when $b_s \to \infty$, that's usually not the case. It is true only in the sense that they both break translational symmetry one by construction and the other spontaneously.

To be more precise, once the shadow have crystallized, they provide a rigid reference frame and $\Phi(\mathbf{R})$ of eq. (8.2) describes the one body density of a crystal, in that $|\Phi(\mathbf{R})|^2 = e^{-V_{ext}}$ is not translational invariant any more if measured in this special reference frame (which is not the reference frame of the simulation box, in which for small enough systems the crystal center of mass can freely move) and corresponds to an external periodic field V_{ext}.

The difference between the SWF description of a solid and the Nosanow one lies in that the lattice sites are fixed (with respect to the simulation box) in the latter and coincide with "equilibrium position" for Helium particles while in SWF Shadows also move around some lattice sites (apart for trivial translations of the crystal center of mass with respect to the simulation box) and the baricenter of R and L position provides the positions around which particle move. Physically this means that the "quantum correlation hole" represented by shadows fluctuates around the lattice sites in the solid phase. This behaviour represents true correlations in the system, as it has been shown in GFMC simulations on quantum solids, where the walkers representative of the wave function show a similar behaviour[8]. The average of the center of vibration for particles coincides with the lattice sites showing a motion around them.

In principle one can also observe exchange in SWF due to the preserved Bose symmetry, but actually it's hopeless to observe exchange in VMC simulations with the usual sampling driven by $|\Psi|^2$, even if exchange moves are explicitly coded, and particular sampling techniques are needed to this scope, similar to that employed in classical simulations for sampling rare events[40]. This feature might explain why in the simulations reported in ref.[30] no condensate was observed in the solid phase, although theoretically it was expected that SWF give a finite non zero value even in the solid phase[31].

8.3 Angular correlations in SWF

Let us discuss in this section the angular correlations embodied in the following trial wave functions:

a) simple Jastrow-McMillan form

b) the same plus triplet correlations

c) SWF with McMillan u_{pp} and Aziz rescaled as (8.17) for u_{ss}.

The energy upperbounds provided by the above trial wave functions are -5.69 (2) K for (a), -6.68 (1) K for (b), -6.52 (2) K for (c), where the number in parentheses indicates the error in the last digit (details of the simulations are given below in this section). It follows that the SWF form has built in some effective three body correlations among the particles; this is not unexpected, as integrating over the shadow particles must give rise in principle to many-body correlations among particles although their importance depends from the detailed form of the pseudopotentials involved. Due to the one to one correspondence between shadow and particles it's not easy to see which diagrams in the cluster expansion contributes

to three body terms; the simplest of these diagrams is the one in which three particles interact through their shadows.

In order to study the angular correlations built in SWF, we measured the following angular distribution functions, $P(\theta, r_{01} < R, r_{02} < R)$ obtained sitting on a particle 0 and measuring the probability distribution of the angle between the position vectors of two other particles, say 1 and 2 that lies inside a sphere of radius r centered in 0, and the probability distribution of the angle between the position vectors of other two particles comprised in a spherical shell $R_1 < r < R_2$ $P(\theta, R_1 < r_{01} < R_2; R_1 < r_{02} < R_2)$. They are related to integrals of the three body distribution function $g^{(3)}(\mathbf{r}_{01}, \mathbf{r}_{02})$. We analyzed the configurations generated in VMC and dumped on tape for the three cases a) b) and c). In a) we used the parameter $b = 1.21\sigma$ to perform a simulation of 30.000 MCS, saving 6000 configurations; in b) the same McMillan correlation was supplemented by a triplet term of the form (7.16); the parametrization (7.20) was employed together with the triplet parameters values shown in tab. (7.1) dumping 5000 configurations out of 20.000 generated. The SWF with the parametrization (8.17) and parameters $d = 0.94$ and $A = 10.5K$ for the shadow-shadow correlations and $b_p = 1.13\sigma$, $C = 5.5$ for the other were used in a simulation of 120.000 MCS saving 3000 configurations. The simulations were planned to achieve roughly the same statistical error in the energy; the difference between the number of steps used for J+T and SWF is due to the larger variance and autocorrelation in the latter case. We show in fig.8.1the overall shapes of the angular distribution $P(\theta, R_1 < r_{01} < R_2; R_1 < r_{02} < R_2)$ for five selected shells inside the first peak in the g_{PP} for the three cases considered; in fig. 8.2we compare the three angular distributions obtained in a) b) c) for shells lying below the maximum in g_{PP}, on the maximum and between the maximum and the first minimum.

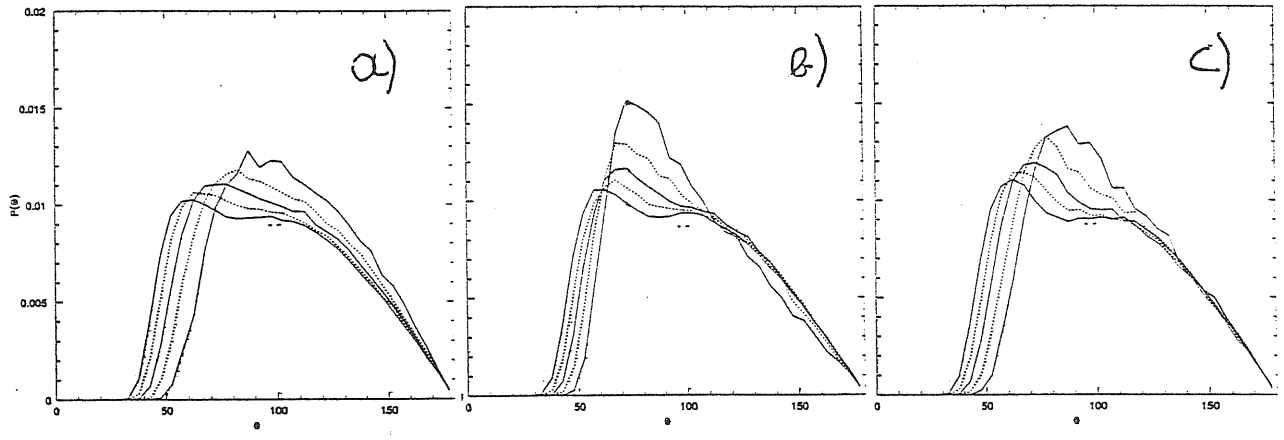

Figure 8.1
The angular distribution function $P(\theta)$ (see text) for five selected shells ($r_1<r<r_2$) inside the first coordination shell for a) McMillan trial wave function b) McMillan plus Triplets c) SWF with attractive shadow-shadow pseudopotential. The selected shells are (0,1.1), (1.1,1.2) (1.2,1.3), (1.3,1.4),(1.4,1.5)

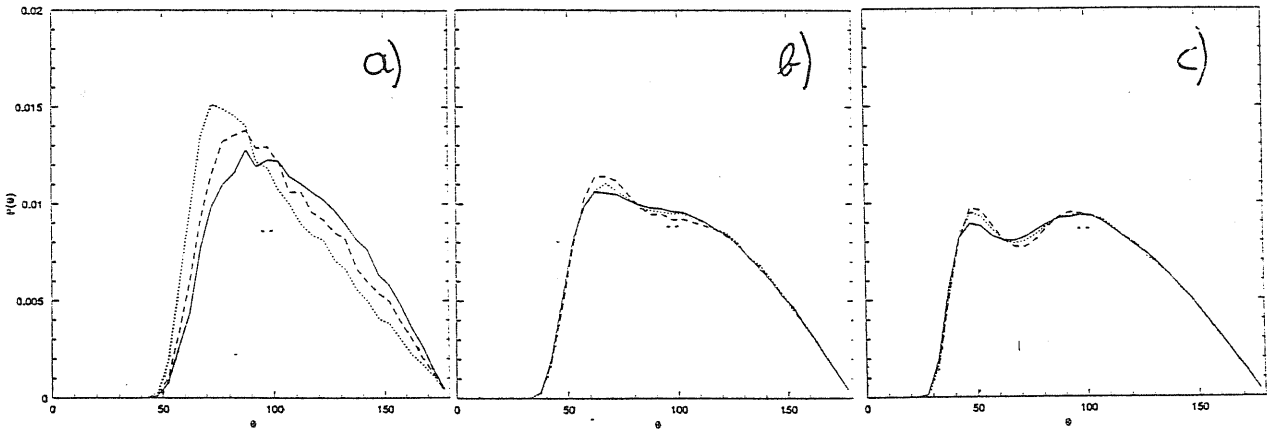

Figure 8.2
Comparison of the angular distribution functions $P(\theta)$ for the three wave functions: McMillan, solid line, McMillan plus Triplets, dotted line and SWF with attractive shadow-shadow pseudopotential, dashed line. They are displayed for three different shells: a) (0,1.1) before the first peak in g(r); b) (1.3,1.4) in the region of the peak; c) (1.7,1.8) between the peak and the first minimum.

We see that the main difference between a) J and b)J+T is for shells before the main peak in g(r) with a peak around 100 degrees for a) and 70 degrees for b) that signals triplet formation at low r; the SWF form recovers most of the correlation in this region; At larger distances there is a small difference in the height of the peak at 50 degrees that the shadow form c) overshoots. Results for SWF with the McMillan correlation is u_{ss} are intermediate between those presented here c) and the jastrow case a).

8.4 Notes on SWF optimization

It has been stated by Ceperley and Schmidt[1] that the minimum variance principle for the local energy is not valid for SWF. We want to show here some considerations related to the optimization of this kind of wave functions in VMC simulations.

The argument in ref.[1] is that even when the true ground state is used as initial guess in the variational procedure derived by (8.14), the noise due to the integration over shadow variables causes always a finite value for the variance of the local energy. Fist of all one has to distinguish between the local energy previously defined in eq. (8.9) and the true local energy

$$E_{loc}(\mathbf{R}) = \int E_{loc}(\mathbf{R}, \mathbf{S}^R, \mathbf{S}^L)\ \mathrm{d}\mathbf{S}^R \mathrm{d}\mathbf{S}^L, \tag{8.21}$$

which is expressed as an integral over shadow configurations compatible with a fixed particle configurations, and clearly is not measured in actual VMC simulations. The minimum variance principle strictly holds for this local energy, provided one takes enough MC steps in performing the average (8.21) for an ensemble of particle configurations, in order to reduce the noise due to shadow fluctuations.

What one can actually measure in VMC simulations is the variance of the local energy (8.9) that contains also the effect of shadow fluctuations, and nothing

is known for this case. We shall show in the following that also the variance of this estimator is minimum for the optimal wave function, but only with respect to some parameters in the wave function, namely those explicitly contained in the local energy (8.9). We performed some parameters explorations around the optimal solution at the solid density ($\rho\sigma^3 = 0.55$), using the McMillan form for the u_{ss} pseudopotential. We varied b_p, b_s and C around the optimal parameters, measuring the energy $< E/N >$ and the variance of the local energy $Var(Eloc)$ given by eq.(8.9). a well defined minimum is found in both of them, centered around the optimal parameter, when b_p is varied and also when C is varied (see fig. 8.3), on the contrary no minimum at all was detected in $Var_(Eloc)$ with respect to variations of b_s, even if energy has one (see fig. 8.4). Our conclusion is that one can resort to correlated sampling methods, described in chap. 7, to optimize the wave function only with respect of variational parameters b_p and C.

We found that the method without reweighting is particularly convenient in case of C, due to the presence of the gaussian correlation that make the weights (7.28b) to vary widely. One alternative choice is to perform a simulation with a Markov chain guided not by $|\Psi|^2$ but by a wider function, like in classical umbrella sampling methods[42,43]. In particular as $(b_p)^{n_p}$ and C are linear parameters in the pseudopotential a simple efficient optimization procedure like that used in ref.[61] could be employed to optimize those parameters in one single simulation, at fixed b_s. Correlated sampling is of no use in optimizing b_s as the variance has no minimum, and the reweighting method applied to the energy fails; the unreweighted energies are always constant as u_{ss} doesn't enter in the expression of the local energy (8.9).

At the present stage it seems that the only way to optimize the wave function with respect to b_s is to actually perform a different simulation for each value of

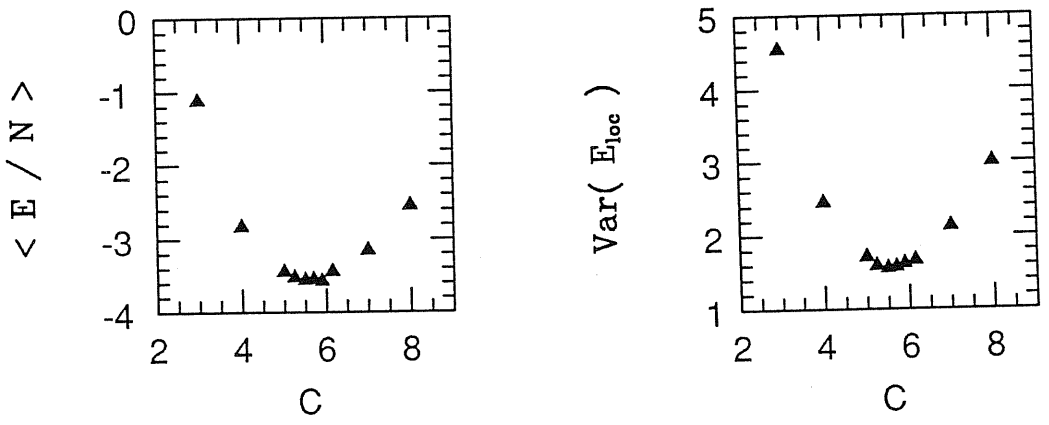

Figure 8.3
We show how (a) the variational energy (per particle) for SWF and (b) the variance of the local energy (per particle) changes on varying the parameter C in the wave function. The sizes of the symbols are of the order of the statistical error.

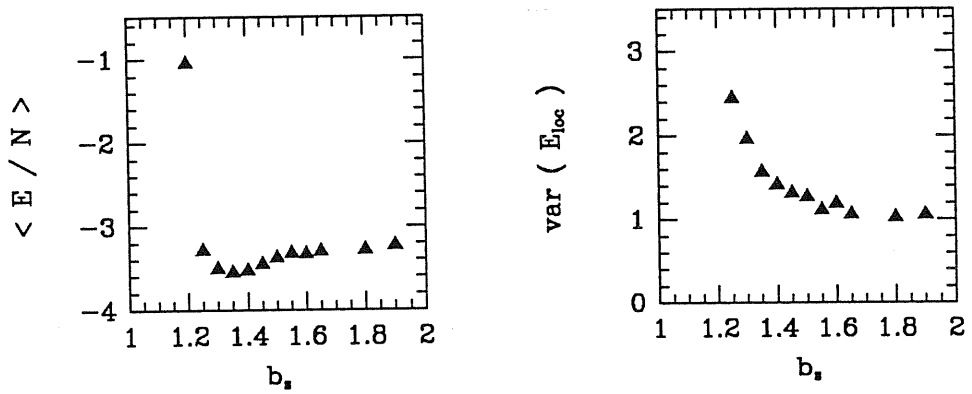

Figure 8.4
We show how (a) the variational energy (per particle) for SWF and (b) the variance of the local energy (per particle) changes on varying the parameter C in the wave function. The sizes of the symbols are of the order of the statistical error..

the parameter b_s. One possibility, still unexplored, is to measure of measuring the overlap of $|\Psi_t>$ with the ground state $|GS>$ by means of

$$\frac{<\Psi_t|GS>}{<\Psi_t|\Psi_t>} = 1 - \frac{\sigma_E^2}{<\Psi_t|\Psi_t>}, \qquad (8.22),$$

taking into account also the variation of the normalization with the parameter varied, and to see if this estimator is minimum for optimal wave functions. The difficulty is that one needs to estimate $<\Psi_t|\Psi_t>$ which is analogous to the partition function in classical simulations, and can't be sampled with the usual Boltzmann transition probability. Techniques similar to those employed in free energy estimation would be needed.

8.5 Integral Equations for SWF

Exploiting the mapping to a classical system of flexible molecules, Reatto and Masserini[31] derived integral equations based on Chandler's RISM equations for molecular fluids[68].

We derived a different set of integral equations[35] by writing each pair correlation function $g_{\alpha\beta}$ as a sum of different terms, defined in terms of diagrams contributing to their cluster expansion with an appropriate definition of points and lines, and resumming some diagrams with topological reduction techniques to obtain integral equations. In the following we adopt a different notation from our work in ref.[35] in order to use the same standard notation as in Part I, chap. 3.

In particular we draw the reader's attention to the fact that in this section the symbol $f_{\alpha\beta}$ doesn't indicate a correlation $e^{-u_{\alpha\beta}}$ (Mayer e-bond) but denotes the Mayer f-bond $f_{\alpha\beta} = e^{-u_{\alpha\beta}} - 1$ following a convention widely used in statistical

mechanics. Θ-bonds are defined as the correlation Particle-Shadow

$$\Theta(|\mathbf{r}_i - \mathbf{s}_i|) = e^{-C(\mathbf{r}_i - \mathbf{s}_i)^2}.$$

We examined both the case of SWF for a Bose homogeneous system given by equations (8.1) (8.2) than the case for a Fermi system defined simply by multiplying equation (8.1) by a Slater determinant Φ_{FG} of plane waves.

The cluster expansions of the distribution functions for the SWF are based on the reference state Ψ_{MF} which is 1 for Bose systems and $\Psi_{MF} = \Phi_{FG}$ for Fermi systems. The cluster expansion of a particular distribution function is obtained by expanding it in power of $f_{pp}(x) = e^{-u_{pp}}(x) - 1$ and $f_{ss}(x) = e^{-u_{ss}}(x) - 1$. Each term of the cluster expansion is called cluster term and is more conveniently represented by a diagram made up of bonds and points. The limitation due to the one to one correspondence between shadow and real particles in eq. (8.2) leads to a variety of topologically different points in the cluster diagrams and, consequently, to a quite involved HNC scheme which, however, can be handled numerically.

Bose case

In the Bose case one must distinguish five types of bonds in correspondence to the five functions $f_{pp}(x)$, $f^R_{ss}(x)$, $f^L_{ss}(x)$, $\Theta^R(x)$ and $\Theta^L(x)$, where f^R_{ss} and Θ^R come from Ψ_t while f^L_{ss} and $\Theta^L(x)$ from Ψ^*_t. Although $f^R_{ss} = f^L_{ss}$ and $\Theta^R = \Theta^L$, diagrammatically they need to be distinguished. Correspondingly, there are eight different types of points:

(i) four types of particle-points, denoted as p_i $(i = 0, 3)$; p_0 is reached by f_{pp}-bonds only (p-points of diagrams (1a) and (1d)), p_1 is also reached by Θ^R (p-points of diagrams (1b), (1e) and (1f)), p_2 by Θ^L and p_3 by both Θ^R and Θ^L (p-points of diagram (1c));

(ii) two types of right (left) shadow-points, denoted as $s^{R(L)}$ $(i = 0, 1)$; $s^{R,L}_0$ is

reached by $f_{ss}^{R(L)}$ only (s-point of diagram (1b)), and $s_1^{R(L)}$ is also reached by $\Theta^{R(L)}$ (s-points of diagrams (1c), (1e) and (1f)).

The following diagrammatical rules result from the properties of the cluster expansion:

(a) a point p can be reached by an unlimited number of f_{pp}-bonds;

(b) a point $s^{R(L)}$ can be reached by an unlimited number of $f_{ss}^{R(L)}$-bonds. An f_{ss}-bonds can never join s^R with s^R points;

(c) f_{pp}-bonds are never connected to s-points as well as f_{ss}-bonds are never connected to p-points;

(d) $\Theta^{R(L)}$ connects a p-point with its associate $s^{R(L)}$-point; there may be at most one $\Theta^{R(L)}$ reaching $s^{R(L)}$ and at most one Θ^R and one Θ^L connected to a point p.

Few examples of cluster diagrams of the nodal (diagrams (1a), (1b) and (1e)), composite (diagram (1c)) and bridge (diagrams (1d) and (1f)) type are displayed in Fig.8.5. One can see from diagrams (1e) and (1f) that triplet correlations are induced by pair correlations with shadow particles.

The diagrammatical rules listed above lead to the following HNC equations: we have the nodal equations corresponding to the usual Ornstein-Zernicke equations

$$\gamma_{\alpha_i\beta_j}(x_{12}) = \sum_{\epsilon_k\delta_l} A_{\epsilon_k\delta_l} \int \left(g_{\delta_e\beta_j}(x_{32}) - \gamma_{\delta_e\beta_j}(x_{32}) - \delta_{l0}\delta_{j0}\right) \left(g_{\alpha_i\epsilon_k}(x_{13}) - \delta_{i0}\delta_{k0}\right) \mathrm{dx}_3, \tag{8.23}$$

where the indices $\alpha_i, \beta j, \ldots$ denote the particular type of external point of the nodal (γ) or distribution (g) functions. The greek letters $\alpha, \beta, \ldots$ are here used to indicate p, s^R or s^L, whereas the latin letters are used for the subindices and run from 0 to 3 for p and from 0 to 1 for both s^R and s^L. The matrix A embodies the

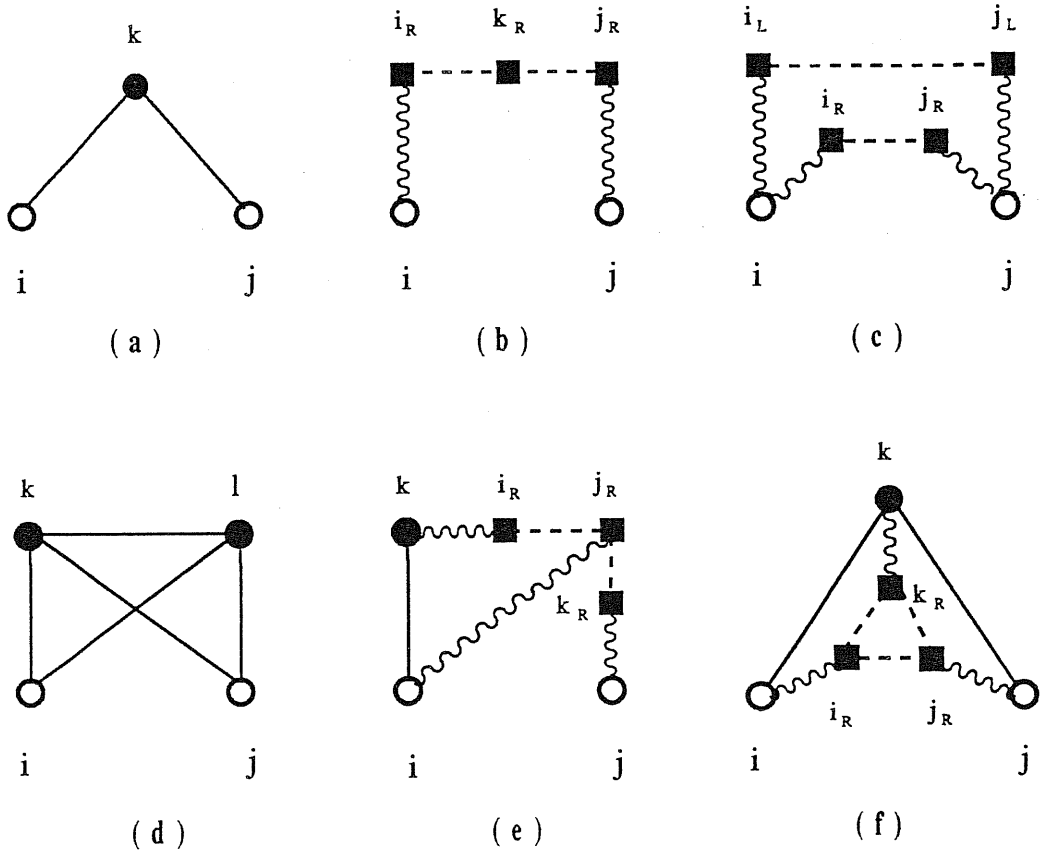

Fig.8.5-*Cluster diagrams contributing to $g_{pp}(r_{ij})$ for SWF. The solid, dashed and wavy lines represent f_{pp}, f_{ss} and Θ bonds respectively. The particle variables are represented by circles and the shadow by squares.*

diagrammatical rules. It is given by

$$A_{p_i p_j} \equiv T_{ij} \equiv \begin{pmatrix} \rho & \rho & \rho & \rho \\ \rho & o & o & o \\ \rho & o & \rho & o \\ \rho & \rho & o & o \end{pmatrix}, \tag{8.24}$$

$$A_{s_i^L s_j^L} = A_{s_i^R s_j^R} \equiv S_{ij} \equiv \begin{pmatrix} \rho & 1 \\ 1 & 0 \end{pmatrix}, \tag{8.25}$$

and it vanishes elsewhere. Here ρ denotes the number density. The 64 distribution functions $g_{\alpha_i\beta_i}(x)$ may be written in the following highly compact form (closure relations):

$$g_{\alpha_0\beta_0}(x) = (1 + \delta_{\alpha\beta} f_{\alpha\alpha}(x))\, e^{S_{\alpha_0\beta_0}(x)}, \tag{8.26}$$

$$g_{\alpha_i\beta_j}(x) = g_{\alpha_0\beta_0}(x) \sum_{<ij>} \prod_n S_{\alpha_{i(n)}\beta_{j(n)}}(x), \tag{8.27}$$

with the functions $S_{\alpha_i\beta_j}(x)$ given by

$$S_{\alpha_i\beta_j}(x) = \left(\delta_{\alpha_i p_1}\delta_{\beta_j s_1} + \delta_{\alpha_i s_1}\delta_{\beta_j p_1}\right) \Theta(x) + \gamma_{\alpha_i\beta_j}(x) + E_{\alpha_i\beta_j}(x), \tag{8.28}$$

where the functions $E_{\alpha_i\beta_j}(x)$ denotes the bridge (or elementary) diagrams. In eq.(8.27) the summation $\sum_{<ij>}$ is extended over all the possible products of S-functions, with the exclusion of $S_{\alpha_0\beta_0}(x)$, under the conditions $\sum i(n) = i$ and $\sum j(n) = j$, where each set $\{i(n)\}$, $\{i(n)\}$ may contain the values 1 and 2 at most once. For instance, $i(n) \equiv \{0,0,3\}$ or $\{0,1,2\}$ are allowed combinations, whereas $\{0,1,1\}$ is not. Such an algebraic rule ensures that the superposition of subdiagrams $S_{\alpha_i\beta_j}$ satisfies the diagrammatical rules $(a) - (b)$.

Considering the symmetry $\gamma_{\alpha\beta} = \gamma_{\beta\alpha}$ and that $f_{ss}^R = f_{ss}^L$ and $\Theta^R = \Theta^L$, one ends up with only 21 different distribution functions. Therefore, the HNC scheme requires the solution of 21 coupled integral equations, which is a completely feasible numerical problem. In fact the main difficulty with this method is on the

approximation of the bridge diagrams, which are expected to be not negligible. However, it should be noted that, already at the level of HNC/0 approximation ($E_{\alpha\beta} = 0$), the effect of the induced triplet and higher order correlations is taken into account (see diagram (1e)).

Following ref.[23] a reasonable approximation for the bridge functions may consist on taking $E_{p_0p_0} \approx sE^{(4)}_{p_0p_0}$, $E_{s_0s_0} \approx tE^{(4)}_{s_0s_0}$ and $E_{\alpha_i\beta_j} \approx E^{(4)}_{\alpha_i\beta_j}$ for $(\alpha_i\beta_j) \neq (p_0p_0),(s_0s_0)$ where the elementary diagrams $E^{(4)}_{\alpha\beta}$ are calculated using the $g-1$ bonds. The scaling factors s and t are calculated by equating the Jackson-Feenberg (JF), the Pandharipande-Bethe (PB) and the Clark-Westhaus (CW) kinetic energy expectation values among themselves.

The full particle-particle distribution function $g_{pp}(x)$ is obtained by summing up all the distribution functions of the *pp*-type:

$$g_{pp}(x) = \sum_{i,j=0,3} g_{p_ip_j}(x). \tag{8.29}$$

Fermi case

In addition to the bosonic links, previously discussed, one has to include also the fermionic exchange link $\frac{1}{2}l(k_Fx)$, where k_F is the Fermi momentum and $l(x) = \frac{3}{x}j_1(x)$ is the Slater function. This link connects only the points p_i among themselves. As in standard FHNC theory[69,70] the points p_i reached by exchange lines (at most two) need to be distinguished from those connected to bosonic bonds only.

We denote such points with e_i or c_i whether the related exchange loop is closed or not. Obviously, the exchange loops in any cluster diagrams are always closed. However, as it is well known, FHNC theory introduces subdiagrams which may have open exchange loops and that is where the point c_i come in. The subindex i

in both e_i and c_i runs from 0 to 3 as in p_i. The extra-diagrammatical rules due to the exchange bonds trivially follows from FHNC theory.

The nodal equations have the same structure as in eq. (2.1). The indices $\alpha_i, \beta_j, ...$ run here over a larger class of points, namely p_i $(i = 0,3)$; e_i $(i = 0,3)$; c_i $(i = 0,3)$, s_i^R $(i = 0,1)$, s_i^L $(i = 0,1)$ so that A is a 16x16 matrix, given by

$$A_{\alpha\beta} \equiv \begin{pmatrix} T & T & 0 & 0 & 0 \\ T & 0 & 0 & 0 & 0 \\ 0 & 0 & T & 0 & 0 \\ 0 & 0 & 0 & S & 0 \\ 0 & 0 & 0 & 0 & S \end{pmatrix}, \tag{8.30}$$

where the 4x4 matrix T and the 2x2 matrix S are given in eqns. (8.24) and (8.25) respectively.

The distribution functions $g_{\alpha_i\beta_j}(x)$ have the same structure as in eqns. (8.26) and (8.27). In addition to the 21 distribution functions g_{pp}, g_{ss}, g_{ps} of the Bose case, there are here 38 new functions having e or c as indices, namely g_{pe}, g_{ee}, g_{ce} and g_{es}. The explicit expressions of these distribution functions can be trivially obtained by generalizing eq. (8.26) to the Fermi case by using standard FHNC theory[70] and will not be reported here for the sake of brevity.

The above FHNC scheme for SWF, although feasible, is quite involved numerically.

Chapter 9

Generalizations of SWF

9.1 SWF for inhomogeneous systems

The optimal values of the variational parameters b_s, C, and b_p vary with the density of the system. As we can see in figure 9.1 where the optimal parameters determined in ref.[30] are shown, the dependence of b_s on the density is roughly linear and can be represented by

$$b_s = b_s^{(0)} + b_s^{(1)}\rho, \tag{9.1}$$

with $b_s^{(0)}$ different from zero, and similar relations hold for the other parameters.

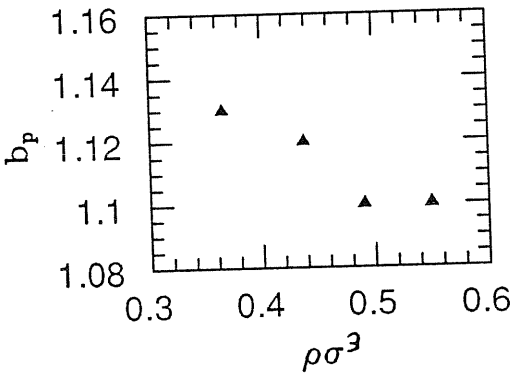

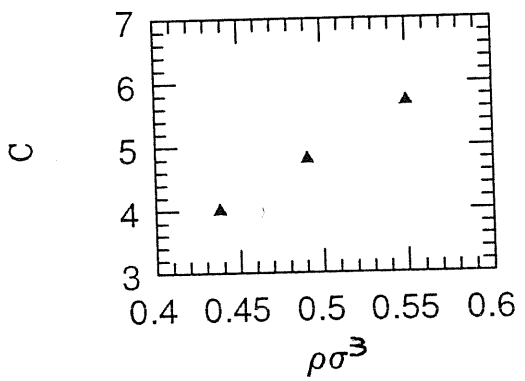

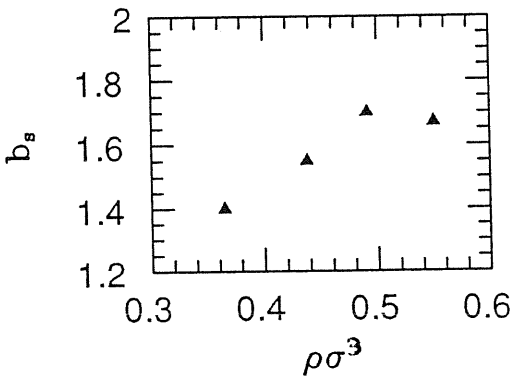

Figure 9.1
Variation with density of the optimal parameters b_p, C and b_s for standard SWF; data from ref.[30].

In the case of Jastrow wave functions it is known that b in the McMillan parametrization varies as $1/\rho^3$ for a Lennard-Jones potential[57] and also for the Aziz potential this scaling property is approximatively valid[2]. The scaling of α in the Nosanow wave function is known[57] to be $\alpha \sim \rho^{(2/3)}$. Thus the linear scaling of figure 9.1 is somewhat surprising.

We have already illustrated in sect. 8.2 the difficulties that arise from the change of variational parameters with density if one wants to describe a solid-liquid interface. Similar difficulties are met if one studies the free surface of the crystal and also when one studies small clusters there are big variations of the density profile, and the usage of SWF with values of the variational parameters taken optimizing the homogeneous phases, at a suitable average density, as it was done in refs.[71,72] is questionable.

An inhomogeneous system is characterized by a one-body density which is not constant in space, and could be considered as composed by many small homogeneous regions of density given according to the density profile. In describing such a system one has two problems: the optimal wave function parameters of the corresponding homogeneous system should be used for each subregion, and moreover one must determine the density profile itself.

In the usual simulations with Jastrow or Jastrow plus Triplets wave functions one parametrizes the density profile by imposing an external one-body density. This is necessary for system with one free surface, like clusters or surfaces as the pseudopotentials in the Jastrow factors are purely repulsive and the external one-body density is needed to confine the system. Its parameters are now variational parameters. For this kind of wave function no attempt has been made to use pseudopotentials parameters which are density dependent.

A better procedure is to let the system determine self-consistently the density

profile and to use density dependent correlations that implies a measure of the local density in the simulation. Considering a solid-liquid interface, a SWF with density dependent u_{ss} of the McMillan form can be safely employed; on the contrary, to describe a system with free surfaces one must use the parametrization given in eq. (8.17) in order to have a bounded system.

Following a suggestion by Reatto [36] we have considered a parametrization of the SWF, in which the shadow-shadow pseudopotential u_{ss} depends on the local density and have tested it on the homogeneous system in order to check its feasibility and to refine technical details.

As a first step to a procedure in which all the three parameters are varied we fixed b_p and C to obtain the best compromise in the energy of both the liquid and the solid phase, and examined only the variation of b_s on the Shadow local density (as Shadow particles are responsible for setting the local density profile).

Consider the SWF given by the equations (8.1,8.2) with the factor

$$\varphi_{ss}(\mathbf{S}) = \prod_{i<j} e^{-u_{ss}(ij)}, \qquad (9.2),$$

and the pseudopotential given by the McMillan form

$$u_{ss}(ij) = \left(\frac{b_s(ij)}{|\mathbf{s_i} - \mathbf{s_j}|} \right)^{m_{sh}}, \qquad (9.3),$$

with the shadow variational parameter expressed, like in eq. (9.1) as a function given by

$$b_s(ij) = b_s^{(0)} + b_s^{(1)} \, \rho_{loc}^{(s)}(ij), \qquad (9.4)$$

of the local density of Shadows as defined by the expressions

$$\rho_{loc}^{(s)} = \frac{1}{2} \, [\, c(i) + c(j) \,], \qquad (9.5a)$$

or

$$\rho_{loc}^{(s)} = \frac{c(i)\,c(j)}{\sqrt{c(i)\,c(j)}} \qquad (9.5b),$$

where we the "local density estimator" that is defined through

$$c_{r_c}(i) = \frac{\sum_{l=1}^{N} \nu_{r_c}(|\mathbf{s_i} - \mathbf{s_l}|)}{4\pi \int_0^\infty r^2\, \nu_{r_c}(r)\, dr}, \qquad (9.6)$$

is meant to measure the local density of shadows around a particular shadow i. The function ν_{r_c} is a suitable function used for counting neighbour shadows, which we choose as the Fermi-function

$$\nu_{r_c}(r) = \frac{1}{1 + e^{\mu(r^2 - r_c^2)}}, \qquad (9.7)$$

where r_c is a cutoff parameter and μ describes the steepness of the function. We used a steep function with $\mu\sigma^2 = 3$ that is displayed in figure 9.2. In principle $b_s^{(0)}$,$b_s^{(1)}$, μ are variational parameters and we will require them to be density-independent.

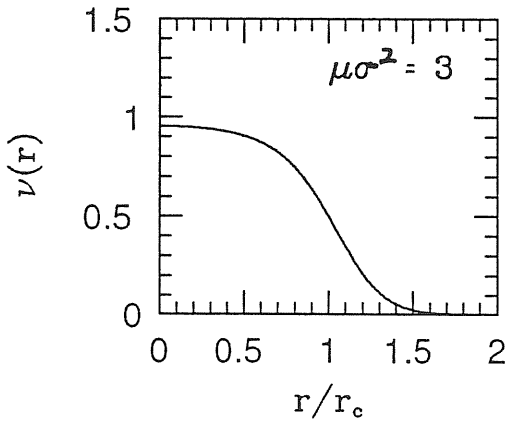

Figure 9.2
Fermi function $\nu(r)$ (9.7) employed in the computation of the local density estimator (9.6). A value $\mu\sigma^2$=3 as been used by us.

The estimator (9.6) is based on the fact that for $r_c \to \infty$ the quantity

$$\frac{N(r_c)}{V} = \frac{4\pi\rho \int_0^{r_c} r^2\, g(r)\, dr}{V}, \qquad (9.8)$$

is proportional to the average density, giving as result $(N-1)/V$ when the g(r) is defined in the canonical ensemble as it is the case for a simulation in a finite volume at constant number of particles.

In order to measure the local density one wants to cutoff after the first or the second shell of neighbours, then one introduces the estimator (9.6); notice that the sum is not restricted to $i \neq l$ to correct for the bias $(N-1)/N$ that would occur in the canonical ensemble.

We verified indeed that the estimator defined as in eq. (9.6) is unbiased and converges correctly to the macroscopic density in an homogeneous system.

The computation of (9.4) (9.6) can be done at each elementary move in the Monte Carlo simulation when we need to compute $|\Psi_t^{inho}|^2$, and if tables are introduced to compute $\nu(r)$ and provided the normalization in (9.6) is stored in a variable, it doesn't introduce a substantial computational overhead, as the distances $|s_i - s_l|^2$ are computed anyway at each step. It is convenient to store the values $c(i)$ in tables that are updated at each elementary move; one can even update only every few steps with a procedure similar to that employed for updating Verlet's neighbour-tables[40].

The estimator defined through (9.6) is the local density at the i-shadow location in a given configuration and it fluctuates even in an homogenous system, around the average macroscopic density at i, and as a consequence if it is used in (9.4) the resulting parameter b_s also fluctuates even in homogeneous systems. To avoid this, since we want to probe the density profile, that is the mean density at location i, one can use in (9.4,9.5) the value of $c(i)$ averaged over some configurations like in

$$\bar{c}(i) = \frac{1}{M} \sum_{t=1}^{M} c(i), \tag{9.9}$$

and maintained in tables, where M is a number of elementary moves equal, let's

say, to ten times the characteristic interval of variation for $c(i)$, which is about $2MCS$ (for 108 particles), so every 20 MCS should be enough.

This should be equivalent to consider a larger cutoff r_c in $\nu(r)$, and allows to reduce of one or two orders of magnitude the variance of $c(i)$ and b_s. As we shall see later, it is recommended to use (9.9) instead of (9.6) with a larger cutoff in the computation of b_s through eq. (9.4).

However, in all the tests we shall report later, we have used the simpler expression (9.6) and we have measured the influence of the fluctuations of $c(i)$ on the energy, and the influence of the cutoff r_c on the determination of the local density.

Dependence of b_s on density.

First we have determined precisely the coefficients $b_s^{(0)}$ and $b_s^{(1)}$ needed in equation (9.4). We fixed $b_p = 1.12$ and $m_p = 5$ to give the best results in the liquid phase and examined three different values for C, namely 4, 4.8, 5.7. For each value of C and each of the three densities

$\rho\sigma^3 = 0.365$ (equilibrium density),

$\rho\sigma^3 = 0.438$ (freezing density),

$\rho\sigma^3 = 0.550$ (solid density),

we performed many Monte Carlo Simulations with the standard SWF of equations (8.1,8.2), changing the parameter b_s.

We employed 108 particles and started always from the FCC lattice as initial condition, running for 10000 MCS (after a suitable equilibration) and monitoring the values of the order parameter for the first Bragg reflection of FCC as defined in eq. (3.34). We obtained the energy curves versus b_s for the standard SWF; the energy curves show a jump near the critical value of b_s predicted in table 8.3 for the crystallization of shadows, except for the freezing density. A remarkable

point is that the energy curve for the solid displays a true minimum only for $C = 5.7$ while in the other cases show a large flat region. This is means that for a better representation of the solid phase a combined variation of C with density is required.

The energy curves were fitted by a 3rd-order polynomial (using points of the same phase near the minimum) and the optimal parameter for each C and each density was determined; their values are summarized in table 9.1.

$\rho\sigma^3$	C	b_s^{opt}	$< E/N >$	*confidence*	*level*
0.365	4.0	1.21	-6.17 (5)	1.09	1.31
"	4.8	1.13	-6.13 (5)	1.04	1.21
"	5.7	1.05	-6.19 (3)	0.99	1.10
0.438	4.0	1.35	-5.46 (5)	1.27	1.43
"	4.8	1.28	-5.51 (4)	1.21	1.34
"	5.7	1.18	-5.33 (3)	1.11	1.25
0.550	4.0	1.70*	-3.30 (3)	1.50	> 2
"	4.8	1.45*	-3.40 (3)	1.35	1.65
"	5.7	1.33	-3.44 (3)	1.28	1.38

Table 9.1
Optimal value for b_s and the minimum energy for SWF at three densities for three fixed values of C. Confidence levels are defined as the variation of b_s which gives an Energy within two standard deviations around the fitted energy curve; the statistical error of the simulation near the minimum is employed in this procedure. The asterisk indicated the mean point of a flat energy region, not a true minimum.

From the values of b_s determined at the equilibrium and freezing densities, the coefficients $b_s^{(0)}$ and $b_s^{(1)}$ in eq. (9.1) are simply found by solving a linear system. If many other density were explored one could have performed a Least Square Fit and could have determined how good is the linear variation hypothesis, and

confidence interval on the parameters. The parameters needed in (9.4) at each value of C are reported in table 9.2.

C	$b_s^{(0)}$	$b_s^{(1)}$
4.0	0.51	1.91
4.8	0.39	2.02
5.7	0.53	1.46

Table 9.2
Fit of the parameters $b_s^{(0)}$ and $b_s^{(1)}$ of equation (9.1) for three different values of C.

In Figures 9.3a, 9.3b, 9.3c we show the relation (9.1) for the three values of C considered; the full symbols mark the optimal parameters found, and the interval shown with error bars indicates the width of the energy curve minimum, which was precisely defined as a confidence interval.

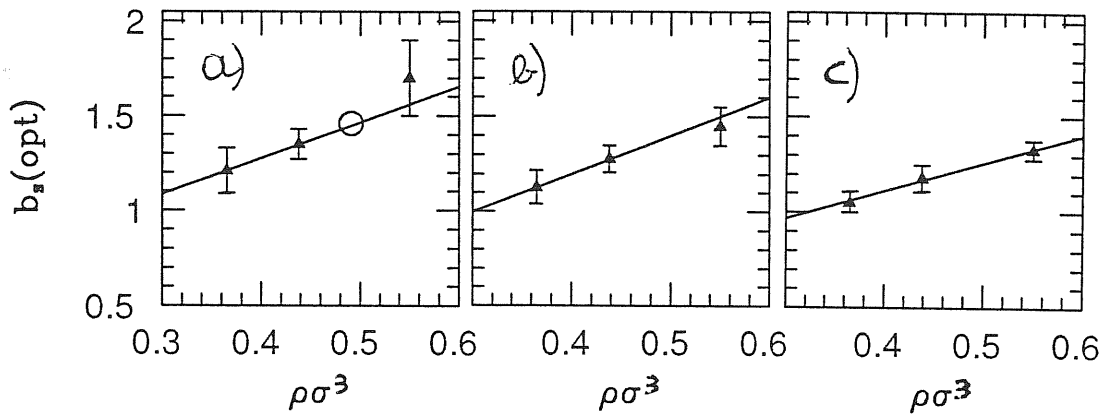

Figure 9.3
Fit of the parameters $b_s^{(0)}$ and $b_s^{(1)}$ from equation (9.1) for three different values of C. a) C=4, b) C=4.8, b) C=5.7. Triangles are the optimal parameters b_s at each density for fixed C, displayed in table 9.1, the error bars are confidence levels (sse text). The circle in a) corresponds to the optimal value at the melting density, not included in the initial fit. Solid lines correspond to the values of $b_s^{(0)}$and $b_s^{(1)}$ reported in table 9.2.

It is the interval of values of b_s that gives an Energy inside two standard deviations $\sigma_{<E>}$ from the optimal one. As one can see the fit for $C = 4$ and $C = 4.8$ gives a value of energy in the "flat region" of the energy curve for the solid. A remarkable event is that for $C = 5.7$ the line passes also through the solid minimum. In fig. 9.3a, for $C = 4$ it is also shown the minimum determined for the melting density, that one see is in good agreement with the linear relation (9.4).

As a final comment the values for the optimal energy in the liquid phase found with this parametrization compare well with the optimal found in ref.[30], while in the solid phase the value is 0.15-0.25 K higher. This could be improved if a combined variation of C and b_p with density is allowed.

Test of the procedure on homogeneous systems

We did a test of the procedure based on the evaluation of the parameter b_s according to the local density on each shadow computed by eq.(9.6). We selected the parametrization at $C = 4$ for our test, as at the freezing density the minimum in the energy curve is about the freezing parameter for shadows, so this density is particularly sensitive to fluctuations in the local density estimator.

During the simulation we monitored the instantaneous value and the fluctuation of the average of $c(i)$ over all the shadow (of the same kind) in a configuration, defined as

$$\bar{c} = \frac{1}{N} \sum_{i=1}^{N} c(i). \tag{9.10}$$

As the system is homogeneous $c(i) \approx N\,\bar{c}$ and $var(c(i)) = N^2 var(\bar{c})$; one can also compute the average value of b_s over the run as

$$< b_s >= b_s^{(0)} + b_s^{(1)} \ < \bar{c} >, \tag{9.11}$$

and the variance of the local instantaneous values of $b_s(ij)$

$$var[\, b_s(ij)\,] = (\, b_s^{(1)}\,)^2 \ var[\, c(i)\,]. \tag{9.12}$$

(It should not be confused with the error on $< b_s >$ which is related to the variance of the average $< \bar{c} >$, not to $var[\, c(i)\,]$.)

The cutoff was fixed at the first minimum in the g(r) at each density, which is the minimal cutoff to obtain a meaningful evaluation of the local density, and for all the densities considered it satisfies the relation

$$r_c \, \rho^{(1/3)} \approx 1.5 \qquad (9.13).$$

We performed simulations at four densities; the results are shown in table 9.3 together with the average value of the parameter $< b_s >$ to which they pertain; in the same table values of the energy obtained with the standard SWF at the same value $b_s =< b_s >$ are displayed for comparison, and the measured average density $< \bar{c} >$ is also shown.

$\rho\sigma^3$	b_s^{opt}	$< b_s >$	σ_{b_s}	E_{rif}	E_{LDO}	$< \bar{c} >$
0.365	1.21	1.21	0.37	-6.17 (5)	-6.23 (5)	0.3671 (6)
0.438	1.35	1.34	0.54	-5.47 (4)	-5.27 (5)	0.4364 (5)
0.491	1.45	1.46	0.24	-4.96 (3)	-4.93 (4)	0.4961 (2)
0.550	1.70	1.53	0.41	-3.28 (3)	-3.20 (4)	0.5313 (6)

Table 9.3
Test of the SWF parametrized with the local density operator (9.5-9.7) by means of the linear dependence (9.4) of b_s on density. The parameters C=4 and b_p=1.12 have been kept fixed. Here we show at each density the results for runs done with this w.f. E_{LDO}, in comparison the values of energy E_{rif} obtained with runs at the same density and a value b_s=$<b_s>$ using the standard SWF. Here we display also the average parameter b_s, the average macroscopic density $< \bar{c} >$ and the standard deviation for the distribution of the local values $b_s(ij)$ (eq. 9.4). The optimal parameter at each density from (9.1) is also shown.

The average parameters $< b_s >$ obtained are close to the optimal one at all densities but the solid one, in which case it falls anyway in the "flat region" of the energy. The values for the energy obtained are in fair agreement with the reference case, within the statistical errors (the worse case being the solid), at all

densities but the freezing density where a serious discrepancy occur. Moreover at this density we observe fluctuations of the order parameters larger than that pertaining to the liquid phase. It seems that fluctuations implying the formation of crystalline regions occur. The average value of the density $< \bar{c} >$ estimated is in reasonable agreement with the macroscopic value. It should be noticed that the variation of the local instantaneous values $b_s(ij)$, indicated by σ_{b_s}, is fairly large. This can be responsible for the failure at the freezing density, as with such a large dispersion of values in the simulation, part of the sample can easily correspond to $b_s(ij)$ in the crystalline region. That this is indeed the case was verified with a simulation with a larger cutoff $R = 3.4\sigma$, corresponding to the second minimum in the $g(r)$, which gives a lower dispersion $\sigma_{b_s} = 0.31$, due to the lower variance of $c(i)$, a good value for the energy $E_{LDO} = -5.36$ (6) and order parameter corresponding strictly to a liquid.

Moreover in all the simulations indicated in the table the "correlation time" for the energy, estimated with the block variance method of Rahman and Jacucci[73], is 2-3 time larger then the reference case with standard SWF. This is again due to the fluctuations of $b_s(ij)$ and could be remedied changing the way to propose moves; insted of an homogeneous distribution in a box of side δ one can try a gaussian probability with a certain width.

The conclusion is that it's advisable to keep the fluctuation of $b_s(ij)$ around its average local value as lower as possible adopting (9.9) instead of (9.6) in the computation of $b_s(ij)$ through eq. (9.4). This corresponds to adapt the value of b_s to the average local density in one point, not to the instantaneous value of the local density, which fluctuates even in a homogeneous system and expecially fluctuates too much in the coexistence region. Too large fluctuations of the estimator ρ_{loc} may be a problem in the coexistence region as they can mask and wash out completely

the spatial variation of the one body density, that actually determine in each point the local value of b_s. The kind of "time" average defined by eq. (9.9) is better than smoothing the fluctuation by increasing the cutoff r_c, that corresponds to a spatial average, as the latter procedure looses information about the spatial variations of the local density inside the simulation cell, for values of cutoff required to obtain the same reduction of fluctuations.

As a second check we verified at the freezing and at the melting density that varying the parameter $b_s^{(0)}$ now in (9.4) one obtains the best energy at the value 0.51 given by the fit. The values showed in table 9.4 confirm that, inside the statistical errors this is the case; all values in this table correspond to a cutoff $r_c\,\rho^{(1/3)} = 1.50$, so all the precedent observations apply to the freezing density case.

The last check regards the sensitivity of the results to the cutoff value r_c. It appears that the optimal choice is at the position of the first or second minimum in g(r), with a lower value of the variance $c(i)$ for the latter choice, and a lower bias in the average value of the density $< \bar{c} >$, expecially in the solid case. One should anyway avoid to put the cutoff in correspondence to the peaks positions.

The results obtained varying the cutoff at the liquid and the solid density are summarized in table 9.5.

9.2 Triplets in the Shadow part

There are essentially two routes one can follow to generalize the SWF when one considers the discussion of cap.7 about the GFMC argument given as a justification of the SWF functional form. One way consists in improving the approximation (8.18) for the propagator present in the convolution integral (8.14); this is the

$\rho\sigma^3$	$b_s^{(0)}$	$< E/N >$	$< \bar{c} >$	$< b_s >$	*phase*
0.438	0.41	-4.79 (7)	0.436	1.24	*liquid*
"	0.46	-5.01 (6)	0.436	1.29	"
"	0.51	-5.27 (5)	0.436	1.34	"
"	0.56	-5.28 (5)	0.435	1.39	"
"	0.61	-5.29 (5)	0.434	1.43	"
"	0.66	-4.14 (4)	0.467	1.55	*solid*
"	0.71	-4.05 (4)	0.465	1.60	"
0.491	0.41	-3.52 (6)	0.477	1.32	*liquid*
"	0.46	-4.95 (5)	0.496	1.41	*solid*
"	0.51	-4.92 (5)	0.496	1.46	"
"	0.56	-4.94 (5)	0.495	1.50	"
"	0.61	-4.86 (5)	0.491	1.55	"

Table 9.4
Energies obtained with the SWF employing the dependence (9.4) of b_s on the local density operator (9.6), when the value $b_s^{(0)}$ has been varied around the value given by the fit.

subject of the next section. The other way we want to discuss here consists in applying the approximate propagator in (8.14) to a better wave function than a simple Jastrow form, using as $\Phi(S,0)$ in (8.14) a Jastrow+Triplet wave function.

The new wave function differs from the standard SWF of eq. (8.1) in that the integrand in eq. (8.2) contains also a Triplet term $\Psi_3(\mathbf{S})$ of the same form as given by eq. (7.16). Now one has also to optimize the variational parameters λ, R_0 and ω, that might be different from the values in table 7.1 as (8.14) is not an exact propagation of the wave function, but a variational argument.

We explored many sets of parameters starting with $b_p = 1.13\sigma$, $n_p = 5$ $C = 4$, the parameters optimal for a McMillan + Triplets wave function $b_s = 1.20\sigma$ $m_s = 5$ and triplet parameters of table 7.1. The Triplet parameters were varied as follows:

$\rho\sigma^3$	$r_c\,\rho^{(1/3)}$	$< E/N >$	$< \bar{c} >$	$var[\,c(i)\,]$	$\sigma_{b_s}(ij)$	*notes*
0.365	1.29	-5.87 (5)	0.3738 (6)	0.0787	0.54	$<$ *I min.*
"	1.50	-6.23 (5)	0.3671 (3)	0.0379	0.37	*I min.*
"	1.86	-6.17 (5)	0.3566 (3)	0.0208	0.28	*II max.*
0.550	1.47	-3.20 (4)	0.5313 (6)	0.1121	0.64	*I min.*
"	1.80	-3.25 (3)	0.4789 (1)	0.0042	0.12	*II min.*
"	2.29	-3.20 (3)	0.5578 (1)	0.0038	0.12	*III min.*

Table 9.5
Influence of the cutoff r_c on the total energy, the measured average density $var[\,c(i)\,]$ the variance of the local density estimator $c(i)$ and the standard deviation for the distribution of local values $b_s(ij)$, at the liquid and solid densities. Last column indicates the cutoff position with respect to the positions of the minima in the pair correlation function $g_{ss}(r)$.

r_t in the range from 0.66σ to 0.93σ, ω from 0.4σ to 0.55σ and $\lambda\sigma^2$ from -1 to -14. The parameters C b_p were also varied and we tried a value $m_s = 9$ and variations of b_s starting from $b_s = 1.20\sigma$. We observed that starting from values of λ greater than 8, the triplet term could interfere in the crystallization properties of shadows, making them crystallize in a structure different from FCC as the preferred lattice. Moreover at these values of λ we in some cases observe an enormous slowing of the shadow "dynamics " in VMC with the appearance of long-lived "metastable" configurations during the Markow-chain sampling, that greatly increases the statistical errors and the computational time. For values less than $\lambda\sigma^2 = 8$ the best result we obtained is $E = -6.38(5)K$ in correspondence of the parameters in the following table

b_p/σ	m_p	b_s/σ	m_s	$C\,\sigma^2$	$\lambda\,\sigma^2$	ω/σ	R_0/σ
1.13	5	1.12	5	4.0	-5.0	0.5	0.8

which is a marginal improvement over the SWF with a McMillan parametrization but it is still worse than the energy obtained by using the attractive pseudopotential (8.17) in standard SWF or than the McMillan+Triplet energy.

In conclusion the insertion of triplets terms in the shadow part is of marginal importance, and in case it should be done in a consistent way by taking the correspondent order in the approximation of the propagator which enters the expression of G_0 and in the dressing terms. This procedure however will introduce also Triplets among particles and will take us to a quite involved form for the wave function.

Triplets term in the Shadow part can be of some use if one wants to study with SWF crystal structures other than the close-packed lattices FCC, BCC or HCP, in which shadows can form a stable crystal structure by means of pseudopotential of the form $(b_s/s_{ij})^{m_s}$. In particular Triplets term might stabilize open structures like the Diamond lattice, which can be studied with a Nosanow wave function that fixes a-priori the lattice structure, but can't be obtained with the standard SWF form.

9.3 Systematic improvements of SFW

It is known from work connected to GFMC and PIMC (see refs.[1,9]), that the short-time approximation form of the propagator G_1 given by (8.18) can be improved. It is our scope here, following an indication by Ceperley[1], to briefly indicate how these improved form reflect on subsequent generalizations of the SWF analytical form. The next approximation, derived from the usage of the

Feynman-Kac formula (see sect 2.2 in ref.[9]), gives

$$G_2(\mathbf{R},\mathbf{S};\tau) = G_1(\mathbf{R},\mathbf{S};\tau)\; e^{-\sum_{i<j} u(r_{ij},s_{ij};\tau)}, \qquad (9.14)$$

where $u(r_{ij},s_{ij};\tau)$ is the exact two particle propagator. The next approximation is

$$G_3(\mathbf{R},\mathbf{S};\tau) = G_2(\mathbf{R},\mathbf{S};\tau)\; e^{-\frac{\lambda\tau}{3}\sum_{i<k<j} \nabla_i u(r_{ik},s_{ik};\tau)\cdot\nabla_i u(r_{ij},s_{ij};\tau)}, \qquad (9.15)$$

We notice that (9.14) is equivalent to take in addition to the gaussian correlation between particle and shadows a pseudopotential $u_{ps}(|\mathbf{r_i}-\mathbf{s_j}|)$ connecting each particle with each shadow (different from its own shadow, i.e $i \neq j$), which heals to zero at large separations. It might be that the form of the exact two-body propagator suggests an analytical form for this pseudopotential. Moreover from (9.15) Triplets terms arise, which are distinct from those employed by us in the preceding section since they now involve Triplets among particle and shadows. Similar terms were also suggested by Reatto *et al.*[31], who analyzed in terms of Fourier representation the usual Triplet term of a Jastrow+Triplet wave function.

9.4 Extended Shadow Wave Functions

The relation (9.14) suggested us some considerations; the wave function corresponding to it is equivalent to a classical system of triatomic molecules, always bounded by harmonic interactions, in which now each Helium atom interacts with all the shadows of the other molecules, and all the shadows interact among them, with the usual restriction that right and left shadows don't interact. Now in classical statistical mechanics one can describe molecules even without the need of a

binding harmonic interaction; it's just a first approximation to a potential going to zero at long distances. We asked whether the same situation is realized here, namely if a particle shadow interaction of the form

$$\Phi_{ps}(\mathbf{R},\mathbf{S}) = e^{-\sum_{i,j} u_{ps}(|\mathbf{r_i}-\mathbf{s_j}|)}, \tag{9.16}$$

where now the sum is not restricted, is able to account for both the "intermolecular" interaction and the "intramolecular" binding interaction, the short range part of the u_{ps} pseudopotential providing the latter. It is not sufficient that this happens for the classical system; also the resulting quantum total energy should behave properly, and our hope was that one could reach a variational minimum of energy as good as (if not better) than the standard SWF. The advantage of this formulation is that now the integral equations greatly simplify with respect to those presented in sect. 8.4. Moreover in principle one is not restricted any more to consider shadows and particles in equal number, and can study systems, i.e. crystals with vacancies, inserting an additional shadow, which is not labelled to any particle and has a finite probability of interaction with other particles so that it could be easily exchanged.

We explored such wave functions by means of VMC; the local energy is still of the form (8.10), but now the pseudoforce acting on a particle is due to all shadows. We employed as a starting point a pseudopotential u_{ps} of the form of a gaussian well, in order to mimic as closely as possible at short range the correlation given by the harmonic term. From an extensive exploration of parameters, mainly in the liquid phase, at equilibrium density, and also some trials in the solid phase, we couldn't find any substantial improvement over the standard SWF form, although we could reach the "molecular " limit previously described. At present we are not in the position to say if this attempt to represent the harmonic interactions of one

shadow with its particle in this way is meaningless or whether the form we tried for the particle-shadow pseudopotential is poor. In particular we still have not fully investigated the effects of the interaction of one shadows with all the other particles, since actually with the pseudopotentials employed in our system, in the limit of particles localized in the wells centered on the shadows, one shadows feels only its own particle.

In an attempt to obtain analytical hints on the form for the optimal pseudopotential to employ in our formulation, we also derived Euler equations for these Extended SWF. We do not report here the explicit form of these equations as they are lengthy and at the end we made little use of them. The cluster diagrams are characterized by only three different types of points p, s^R and s^L (which coincide with p_0,s_0^R,s_0^L of the SWF case).

9.5 Integral Equations for ESWF

Due to the fact that the Extended Shadow form of the wave function is symmetric under the exchange of the shadow variables $\mathbf{s_i}$, irrespective of $\mathbf{r_i}$, there are only four independent HNC quantities, i.e., γ_{pp}, $\gamma_{ps^R} = \gamma_{ps^L}$, $\gamma_{s^Rs^R} = \gamma_{s^Ls^L}$, $\gamma_{s^Rs^L}$ for the Bose case plus four extra quantities γ_{pe}, γ_{se}, γ_{ee}, γ_{cc} for the Fermi case, that is obtained here only antisymmetrizing φ_{ss}, since here on variance with the standard SWF case any Slater determinant inside the convolution integral vanishes. This implies the solution of four (Bose) or eight (Fermi) coupled integral equations, to compute pair correlation functions and the energy expectation value. Now the normalization integral coincides with the partition function of a classical three-component (p,s^R,s^L) system interacting via the (pseudo)potentials $u_{pp} = -lnf_{pp}^2$, $u_{s^Rs^R} = u_{s^Ls^L} = -lnf_{ss}$,

$u_{ps^R} = u_{ps^L} = -lnf_{ps}$, $u_{s^R s^L} = 0$,, where here the f_{ij} stands for the correlations in the Jastrow factors. The integral equations to calculate the distribution functions are well known[74], and has been reported in chap 3. The nodal (3.10) and closure equations (3.12) have a much simpler structure than the corresponding eqns. (8.23-8.28). Similarly, in the Fermi case, one has a mixture of two Bose fluids (s^R, s^L) and one Fermi fluid (p), whose FHNC treatment can be easily derived from that proposed by Fabrocini and Polls[75] for the case of the Boson-Fermion mixture.

The energy per particle

$$\frac{\langle E \rangle}{N} = \frac{\langle T \rangle}{N} + \frac{\langle V \rangle}{N}, \tag{9.17}$$

can be written in terms of the two and three-body distribution functions only. This differs from the case of the Jastrow+Triplet trial wave function, which requires the evaluation of up to the five-body distribution functions if the PB form of kinetic energy is employed. We give in the following the expressions of $< T_{JF} >$, $< T_{PB} >$ and $< V >$ for the Bose case. The potential energy expectation value is given by

$$\frac{\langle V \rangle}{N} = \frac{\rho_p}{2} \int g_{pp}(r) v(r) \mathrm{d}\mathbf{r}, \tag{9.18}$$

where $v(r)$ is the interatomic potential. The kinetic energy expectation value can be split into a two-body plus a three body term

$$\frac{\langle T \rangle}{N} = T_{2B} + T_{3B}, \tag{9.19}$$

where

$$T_{2B} = \int [\rho_p \; t_{pp}(r) g_{pp}(r) + \rho_s \; t_{ps}(r) g_{ps}(r)] \mathrm{d}\mathbf{r}, \tag{9.20}$$

and the two-body kinetic energy operators $t_{pp}(r)$ and $t_{ps}(r)$ are given by

$$t_{pp}^{JF}(r) = \frac{\hbar^2}{8m} \left\{ u''_{pp}(r) + \frac{2}{r} u'_{pp}(r) \right\}, \tag{9.21}$$

$$t_{ps}^{JF}(r) = \frac{\hbar^2}{4m} \left\{ u''_{ps}(r) + \frac{2}{r} u'_{ps}(r) - [u'_{ps}(r)]^2 \right\}, \tag{9.22}$$

in the case of the JF kinetic energy expression, and by

$$t_{pp}^{PB}(r) = \frac{\hbar^2}{4m}\left\{ u\prime\prime_{pp}(r) + \frac{2}{r}u\prime_{pp}(r) - \frac{1}{2}\left[u\prime_{pp}(r)\right]^2 \right\}, \tag{9.23}$$

$$t_{ps}^{PB}(r) = 2\ t_{ps}^{JF}(r), \tag{9.24}$$

for the PB kinetic energy expression. The three-body terms are given by:

$$T_{3B}^{JF} = -\frac{\hbar^2\rho_s^2}{4m}\int \left[\ g^{(3)}_{ps_Ls_R}(\mathbf{r_{12}},\mathbf{r_{13}}) - g^{(3)}_{ps_Rs_R}(\mathbf{r_{12}},\mathbf{r_{13}})\ \right] u\prime_{ps}(r_{12})\ u\prime_{ps}(r_{13})\ \hat{\mathbf{r}}_{12}\cdot\hat{\mathbf{r}}_{13}\mathrm{d}\mathbf{r_{12}}\mathrm{d}\mathbf{r_{13}}, \tag{9.25}$$

$$\begin{aligned} T_{3B}^{PB} = -\frac{\hbar^2}{8m}\int\Big[& \rho_p^2\ g^{(3)}_{ppp}(\mathbf{r_{12}},\mathbf{R_{13}})\ u\prime_{pp}(r_{12})u\prime_{pp}(r_{13}) \\ & + 4\rho_s^2\ g^{(3)}_{pss}(\mathbf{r_{12}},\mathbf{r_{13}})\ u\prime_{ps}(r_{12})u\prime_{ps}(r_{13}) \\ & + 4\rho_s\rho_p\ g^{(3)}_{pps}(\mathbf{r_{12}},\mathbf{r_{13}})\ u\prime_{pp}(r_{12})u\prime_{ps}(r_{13})\ \Big]\ \hat{\mathbf{r}}_{12}\cdot\hat{\mathbf{r}}_{13}\mathrm{d}\mathbf{r_{12}}\mathrm{d}\mathbf{r_{13}}. \end{aligned} \tag{9.26}$$

Similar expressions are found for the Fermi case.

The three-body terms of eqns. (9.25),(9.26) can be integrated directly developing the three particle correlation functions in Abe Diagrams, and retaining the lowest order diagram but could be most conveniently evaluated by first calculating the quantities $\int \hat{\mathbf{r}}_{13}\ u\prime(r_{13})g^{(3)}_{\alpha\beta\gamma}(\mathbf{r_{12}},\mathbf{r_{13}})\mathrm{d}\mathbf{r_{13}}$, and then performing the last integration on $\mathrm{d}\mathbf{r_{12}}$. Such "effective" distribution functions can be obtained by using HNC theory, as shown in ref. [76] or more recently by Lado[77].

Reliable approximations to the elementary diagrams are needed in order to obtain a true variational estimate of the energy; three approaches are the most successfully used for classical liquid-mixtures, that is (i) resorting to some kind of interpolating closure[78], or (ii) parametrizing $E_{\alpha\beta}$ from a suitable reference hard-spheres system[79,80], or, finally, (iii) evaluating directly $E^{(4)}_{\alpha\beta}$ with $g-1$ links and then scaling or correcting them at short range in a proper way [81,82]. The free parameters present in these approaches can be fixed by imposing convenient consistency relations, satisfied by the exact distribution functions, like for instance $< T_{PB} >=< T_{JF} >$.

Chapter 10

Conclusions

Various parametrization recently proposed for SWF have been analyzed in terms of the amount of triplet correlation contained in them. The three body correlation function has been calculated for different geometries in correspondence of the J+T wave, in standard SWF-MM (McMillan form) and SWF-A (attractive pseudopotential). It has been found that the SWF-A provides triplet correlation with an angular dependence very similar to those included in the J+T wave, whereas SWF-(MM) show significative differences.

Several possible extensions of SWF have been studied for the following two purposes: (1) to generalize the SWF to treat inhomogeneous systems; (2) to optimize the SWF type of trial wave functions for homogeneous systems. As far as the first point is concerned, we have verified that the dependence of the optimal variational parameter of SWF on the density for homogeneous systems, is linear to a large extent. In order to study inhomogeneous systems we would like to have a trial function in which the parameters are density-independent. To this aim we have numerically verified the possibility of treating the density ρ in $\alpha = \alpha_0 + \alpha_1 \rho$ as an operator rather then as a number. The results obtained for the parameter b_s in $s - s$ pseudooperator are encouraging.

Possible optimizations of SWF for homogeneous systems may be suggested by the DMC argument employed in a variational fashion. The suggested improvements consist in including triplet correlations between shadows, or between particles, or between particles and shadows.

We have studied SWF with Triplets between shadows, minimizing the energy upper und under variation of the pair - and triplet correlation parameters. It has been found that the of triplet between shadows do not lead to any significative improvement in the energy upper bound. An energy upper bound of 6.38 K was found which is higher than that of SWF-A.

Finally, a HNC scheme for calculating the distribution function and the one-body density matrix with SWF have been presented and discussed. This HNC scheme greatly simplifies if SWF are extended to incorporate correlations between all the particles and the shadows (ESWF). This class of trial functions allow for the use of the HNC previously developed for the quantum mixtures and therefore also for the corresponding Euler equations.

The Bibliography

[1] K.E. Schmidt, D.M. Ceperley: *Monte Carlo Techniques for Quantum Fluids, Solids and Droplets*, in *The Monte Carlo Method in Condensed Matter Physics*, Vol. 71 of *Topics in Applied Physics*, edited by K. Binder (Springer, Berlin, NY 1992), chap. 7.

[2] D.M. Ceperley, M.H. Kalos: *Quantum many-body problems*, in *Monte Carlo Methods in Statistical Physics*, Vol. 7 of *Topics in Current Physics*, edited by K. Binder (Springer, Berlin, NY 1979), chap. 4.

[3] R.A Aziz, V.P.S. Nain, J.S. Carley, W.L. Taylor, G.T. McConville: *J. Chem. Phys.* **70**, 4330 (1979).

[4] R.A Aziz, M.J. Slaman: *Metrologia* **27**, 221 (1990).

[5] R.A Aziz, F.R.W McCourt, C.C.K. Wong: *Mol. Phys.* **61**, 1487 (1987).

[6] M.H Kalos, M.A. Lee, P.A. Withlock, G.V. Chester: *Phys. Rev. B* **24**, 115 (1981).

[7] P.A. Withlock, M.H Kalos, G.V. Chester, D.M. Ceperley: *Phys. Rev. B* **21**, 999 (1980); P.A. Withlock, D.M. Ceperley, G.V. Chester, M.H Kalos: *Phys. Rev. B* **19**, 5598 (1979).

[8] P.A. Withlock, D.M. Ceperley, G.V. Chester, M.H. Kalos: *Phys. Rev. B* **19**, 5598 (1979).

[9] D.M. Ceperley, E.L. Pollock: *Path-integral Computation Techniques for Superfluid* ^{4}*He*, in *Monte Carlo Methods in Theoretical Physics*, edited by S.

Caracciolo, A. Fabrocini (ETS, Pisa 1991), pag. 35.

[10] E.L. Pollock, K.J. Runge: *Phys. Rev. B* **46**, 3535 (1992).

[11] D.M. Ceperley, E.L. Pollock: *Can. J. Phys.* **65**, 1416 (1987).

[12] P.A. Withlock, R.M. Panoff: *Can. J. Phys.* **65**, 1416 (1987).

[13] S. Moroni, G. Senatore: *Europhys. Lett.* **16**, 373 (1991).

[14] J.D. McCoy, S.W. Rick, A.D. Haymet: *J. Chem. Phys.* **92**, 3034 (1990); 3040 (1990); **90**, 4622 (1989).

[15] S. Moroni, D.M. Ceperley, G. Senatore: *Phys. Rev. Lett.* **69**, 1837 (1992).

[16] J.L. Barrat, P. Loubeyre, M.L. Klein: *J. Chem. Phys.* **90**, 5644 (1989).

[17] P. Loubeyre, R. Letoullec, J.P. Pinceaux: *Phys. Rev. Lett.* **69**, 1216 (1992).

[18] M.A. Lee, K.E. Schmidt, M.H. Kalos, G.V. Chester: *Phys. Rev. Lett.* **46**, 728 (1981).

[19] D.M. Ceperley: *Phys. Rev. Lett.* **69**, 331 (1992).

[20] P. Sindzingre, M.L. Klein, D.M. Ceperley: *Phys. Rev. Lett.* **63**, 1601 (1989).

[21] M.V. RamaKrishna, K.B. Whaley: *J. Chem. Phys.* **93**, 6738 (1990); R.N. Barnett, K.B. Whaley: *ibidem* **96**, 2953 (1992).

[22] V.R. Pandharipande: *Phys. Rev. B* **18**, 218 (1978).

[23] Q.N Usmani, S. Fantoni, V.R. Pandharipande: *Phys. Rev. B* **26**, 6123 (1982).

[24] E. Manousakis, S. Fantoni, V.R. Pandharipande, Q.N. Usmani: *Phys. Rev. B* **28**, 3770 (1983); M. Viviani, E. Buendia, S. Fantoni, S. Rosati: *Phys. Rev. B* **38**, 4523 (1988).

[25] K. Schmidt, M.H. Kalos, M.A. Lee, G.V. Chester: *Phys. Rev. Lett.* **45**, 573 (1980); **47**, 807 (1981).

[26] K.E. Schmidt, S.A. Vitiello, in *Condensed Matter Theories* Vol. 5, edited by Anguilera-Navarro (Plenum, NY 1990), pag. 127; *Phys. Rev. B* **46**, 5442 (1992).

[27] R.P. Feynman, M. Cohen: *Phys. Rev.* **102**, 1189 (1956).

[28] L.J. Lantto, P.J. Siemens: *Phys. Lett. B* **68**, 308 (1977); L.J. Lantto, A.D. Jackson, P.J. Siemens: *ibidem*, 311 (1977).

[29] C.J. Umrigar, K.G. Wilson, J.W Wilkins: *Phys. Rev. Lett.* **60**, 1719 (1988); also in *Computer Simulation Studies in Condensed Matter Physics: Recent Developments* Vol. 33 of *Springer Proceedings in Physics*, edited by D.P Landau, K.K. Mon, H.B. Schuttler (Springer, Berlin and NY 1988), pag. 185; C.J. Umrigar: *Int. J. Quantum Chem. Symp.* **23**, (1989).

[30] S. Vitiello, K. Runge, M.H. Kalos: *Phys. Rev. Lett.* **60**, 1970 (1988); S.A. Vitiello, K.J. Runge, G.V Chester, M.H. Kalos: *Phys. Rev. B* **42**, 228 (1990).

[31] L. Reatto, G. L. Masserini: *Phys. Rev. B* **38**, 4516 (1988).

[32] T. MacFarland, S.A. Vitiello, L. Reatto: *J. Low Temp. Physics* (to be published); L. Reatto: *On Shadow Wave Functions for Condensed Phases of Helium*, in *Recent Progress in Many-Body Theories*, edited by C.E. Campbell and E. Krotscheck (Plenum, NY 1992).

[33] W. Wu, S.A. Vitiello, L. Reatto, M.H. Kalos: *Phys. Rev. Lett.* **67**, 1446 (1991).

[34] W. Wu, S.A. Vitiello, L. Reatto, paper in *Monte Carlo Methods in Theoretical Physics*, edited by S. Caracciolo, A. Fabrocini (ETS, Pisa 1991), pag. 197.

[35] A. Ferrante, M. Bernasconi, X.Q.G. Wang, S. Fantoni, E. Tosatti: *HNC Theory for Shadow Wave Functions*, in *Recent Progress in Many-Body Theories*, edited by C.E. Campbell and E. Krotscheck (Plenum NY 1992).

[36] L. Reatto, private communication.

[37] A. Messiah: *Quantum Mechanics* (North Holland, Amsterdam 1975), vol.II, chap.18.

[38] S. Goedecker, K. Maschke: *Phys. Rev. B* **44**, 10365 (1991).

[39] D.S. Lewart W.R. Pandaharipande: *Variational Monte Carlo Studies of many-body Systems* in *Monte Carlo Methods in Theoretical Physics*, edited by S. Caracciolo, A. Fabrocini (ETS, Pisa 1991), pag. 1.

[40] M.P. Allen, D.J. Tildesley: *Computer Simulations of liquids* (Oxford University Press, Oxford 1987).

[41] C. Umrigar: *Accelerated VMC Method for Electronic Structure Simulations*, paper presented at the CECAM Workshop on *QMC for Atoms and Molecules*, held in Orsay, July 1992.

[42] G.M. Torrie, J.P. Valleau: *J. Comp. Phys.* **23**, 187 (1976).

[43] R.L. Coldwell: Int. J. Quantum Chem. Symp. **11**, 215 (1977); S.A. Alexander, R.L. Coldwell, H.J. Monkhorst, J.D. Morgan III: *J. Chem. Phys.* **95**, 6622 (1991), and references therein.

[44] D.M. Ceperley, G.V. Chester, M.H. Kalos: *Phys. Rev. B* **16**, 3081 (1977).

[45] A. Bijl: *Physica* **7**, 869 (1940).

[46] R.B. Dingle: *Phil. Mag.* **40**, 573 (1949).

[47] R. Jastrow: *Phys. Rev.* **98**, 1479 (1955).

[48] N.F. Mott: *Phil. Mag.* **40**, 61 (1949).

[49] W.L. McMillan: *Phys. Rev.* **138A**, 442 (1965).

[50] L. Reatto, G.V. Chester: *Phys. Lett.* **22**, 276 (1966).

[51] K.E. Schmidt, V.R. Pandharipande: *Phys. Rev. B* **19**, 2504 (1979).

[52] R.M. Panoff in *Condensed Matter Theories* vol. 2, edited by P. Vashishta, R.K. Kalia, R.F. Bishop, (Plenum, NY 1987), pag. 173.

[53] V.R. Pandharipande, N. Itoh: *Phys. Rev. A* **8**, 2564 (1973).

[54] J.P. Hansen, E.L. Pollock: *Phys. Rev. A* **5**, 2651 (1972).

[55] L.H. Nosanow: *Phys. Rev. Lett.* **13**, 270 (1964).

[56] E. Saunders: *Phys. Rev.* **126**, 1724 (1962).

[57] J.P. Hansen, D. Levesque: *Phys. Rev.* **165**, 293 (1968).

[58] D.M Ceperley, G.V. Chester, M.H. Kalos: *Phys. Rev. B* **17**, 1070 (1978).

[59] P. Carnevali, E. Tosatti, unpublished results.

[60] D.M. Ceperley, G. Jacucci: *Phys. Rev. Lett.* **58**, 1648 (1987).

[61] K.E. Schmidt, J.W. Moskowitz: *J. Chem. Phys.* **93**, 4172 (1990).

[62] V.R. Pandharipande, H.A. Bethe: *Phys. Rev. C* **7**, 1312 (1973).

[63] G.L. Masserini, L. Reatto, S.A. Vitiello: *Phys. Rev. Lett.* **69**, 2098 (1992).

[64] S.A. Vitiello, P.A. Whitlock: *Phys. Rev. B* **44**, 7373 (1991).

[65] D. Chandler, P.G. Wolynes: *J. Chem. Phys.* **74**, 4078 (1981); K.S. Schweitzer, R.M. Stratt, D. Chandler, P.G. Wolynes: *ibidem* **75**, 1347 (1981); see also the review article by D. Chandler in *Liquids, Freezing and Glass transition*, Les Houches, Session LI, edited by J.P. Hansen, D.Levesque, J. Zinn-Justin (North-Holland, Amsterdam 1991), chap 4.

[66] *Applications of the Monte Carlo Method in Statistical Physics*, Vol. 36 of *Topics in Current Physics*, edited by K. Binder (Springer, Berlin, NY 1984).

[67] W.G. Hoover, S.G. Gray, K.W. Johnson: *J. Chem. Phys.* **55**, 1128 (1971).

[68] D. Chandler in *The Liquid State of Matter*, edited by E.W. Montroll, J.L. Lebowitz (North Holland, Amsterdam, 1982); D. Chandler: *Mol. Phys.* **31**, 1231 (1976).

[69] J. W. Clark: in *Progress in Particle and Nuclear Physics*, edited by D. H. Wilkinson (Pergamon, Oxford, 1979), Vol 2.

[70] A. Fabrocini and S. Fantoni: in *First International Course on Condensed Matter*, edited by D. Prosperi, S. Rosati and G. Violini (World Scientific, Singapore, 1986), ACIF series, Vol. 8.

[71] S.W. Rick, D.L. Lynch, J.D. Doll: *J. Chem. Phys.* **95**, 3506 (1991).

[72] M.V. RamaKrishna, K.B. Whaley: *Z. Phys. D* **20**, 223 (1991).

[73] G. Jacucci, A. Rahman: *Nuovo Cimento D* **4**, 341 (1984).

[74] J. P. Hansen, I. R. McDonald: *Theory of Simple Liquids* (2nd Ed., Academic Press, London, 1986).

[75] A. Fabrocini, A. Polls: *Phys. Rev.* **B 25**, 4533 (1982); *Phys. Rev.* **B 30**, 1200 (1984).

[76] S. Fantoni, S. Rosati: *Phys. Lett.* **B 84**, 23 (1979).

[77] F. Lado: *Mol. Phys.* **72**, 1387 (1991).

[78] J.P. Hansen, G. Zerah: *J. Chem. Phys.* **84**, 2336 (1986).

[79] Y. Rosenfeld, N.W. Ashcroft: *Phys. Rev.* **A 20**, 1208 (1979).

[80] F. Lado: *Phys. Rev. A* **8**, 2548 (1973).

[81] S.Ichimaru, H.Iyetomi: *Phys. Rev.* **A 27**, 3241 (1983).

[82] P. Ballone, G. Pastore, M. P. Tosi: *J. Chem. Phys.* **81**, 3174 (1984).

Ringraziamenti

Vorrei qui ringraziare i miei relatori, prof. Stefano Fantoni e prof. Mario Tosi, che mi hanno seguito durante questi anni. Un caloroso ringraziamento va anche al dott. Giorgio Pastore, per la costante assistenza che mi ha fornito durante tutto il mio lavoro, e al dott. Francesco Pederiva, con cui ho collaborato durante gli ultimi sei mesi. Devo inoltre ringraziare numerose persone per le utili discussioni con loro avute sugli argomenti relativi a questa tesi, fra cui i dott. Ivan Stich, Furio Ercolessi, Saverio Moroni e Guido Chiarotti, il Dr. Cyrus Umrigar e il prof. D.M. Ceperley.

Gran parte dei calcoli relativi a questa tesi sono stati fatti sulle macchine Risc IBM e HP della Sissa, ed una piccola parte sul Cray Y/MP del Cineca, grazie alla collaborazione SISSA-CINECA.

Un ringraziamento collettivo va a tutti i miei amici e colleghi della SISSA, con cui ho condiviso questi anni a Trieste, ed in particolare ai miei due compagni di Stanza degli ultimi anni, il dott. Giorgio Mazzeo ed il dott. Pierluigi Silvestrelli, ed al personale della segreteria, sempre molto gentile e disponibile e a Marina Picek, per la sua pazienza.